Investigations on Drying and Tribocharging Behaviour of Pharmaceutical Powders in a Fluidized Bed Dryer

A Thesis Submitted to the College of Graduate Studies and Research

in partial fulfillment of the requirements for the degree of

Master of Science

in the Department of Chemical and Biological Engineering

University of Saskatchewan

By

Milad Taghavivand

Permission to Use

The author has agreed that the Libraries of the University of Saskatchewan may make this thesis freely available for inspection. Moreover, the author has agreed that permission for extensive copying of this thesis for scholarly purposes may be granted by the professor(s) who supervised the thesis work recorded herein or, in their absence, by the Head of the Department of Chemical and Biological Engineering or the Dean of the College of Graduate Studies and Research. Copying or publication or any other use of the thesis or parts thereof for financial gain without written approval by the University of Saskatchewan is prohibited. It is also understood that due recognition will be given to the author of this thesis and to the University of Saskatchewan in any use of the material of the thesis.

Requests for permission to copy or to make other use of material in this thesis in whole or in part should be addressed to:

Head of the Department of Chemical and Biological Engineering

University of Saskatchewan

57 Campus Drive

Saskatoon, Saskatchewan

S7N 5A9

Canada

Abstract

Among various methods for drying pharmaceutical granules in the pharmaceutical industry, fluidized bed drying is commonly used due to its high rate of moisture removal, excellent performance in solids mixing, and heat and mass transfer. As pharmaceutical powders are typically organic materials with high resistivity, they can easily be charged due to repeated collision and separation of particles, along with particle-wall friction, in a fluidized bed dryer. This phenomenon, called "tribocharging", could adversely affect the process performance. Effects of drying air temperature and drying air velocity on drying performance as well as electrostatic charge generation during the drying process were investigated in this project. In order to elucidate the effect of moisture content (ranging from approximately 30 wt. % to 1.8 wt. %) on tribocharging behaviour, the specific charge of granules was measured in a rotary device and apparent volume resistivity was investigated in a self-designed resistivity testing cell. Limited drying data was available in the literature for drying pharmaceutical granules. Therefore, experimental work also was conducted to investigate drying kinetics under different operating conditions of relevance to industry processes.

Experimental results showed that decreasing the drying air temperature increased the drying time, as expected. The specific charge of pharmaceutical granules was found to be a function of moisture content and drying air velocity rather than drying air temperature. With a decrease in moisture content, the specific charge of pharmaceutical granules increased. There was a sudden increase in measured specific charge when the moisture content decreased to approximately 5 wt. %. The same behaviour was observed in tribocharging experiments

conducted in the rotary device. It also was revealed that the increase in specific charge could be due to an increase in apparent volume resistivity of granules at reduced moisture.

Drying data also indicated that the effective diffusion coefficient could be correlated satisfactorily to drying temperature by the typical Arrhenius equation.

Acknowledgments

First and foremost, I wish to express my sincere gratitude to my supervisor, Dr. Lifeng Zhang, for giving me the opportunity to be part of his fluidization group, and on top of that, for his continuous support and guidance throughout this challenging project.

I also would like to acknowledge Dr. Kwangseok Choi, National Institute of Occupational Safety and Health in Japan, for encouraging me and providing me with valuable advice and suggestions during the research.

And finally, I would like to express my gratitude to all the members of the fluidization and particle characterization group, especially Chao Han, for all of the useful discussions and suggestions.

Table of Contents

List of Figures

List of Tables

Nomenclature

Chapter 2

C_0	Capacitance between two bodies in contact, F
C	Capacitance of a capacitor, F
e	Elementary charge, Coulomb (C)
k_c	Charging efficiency
Δq	Transferred charge, Coulomb (C)
Δq_c	Transferred charge between bodies in contact, Coulomb (C)
S	Contact area, m^2
u_{mb}	Minimum bubbling velocity, m/s
u_{mf}	Minimum fluidization velocity, m/s
V	Total potential difference, V
V_b	Potential difference arising from the space charge, V
V_c	Contact potential difference, V
V_e	Potential difference arising from image charge, V
V_{ex}	Potential difference arising from other electric fields, V
X	Moisture content, $kg_{water}/kg_{dry\text{-}solid}$
X_0	Initial moisture content, $kg_{water}/kg_{dry\text{-}solid}$
X_{cr}	Critical moisture content, $kg_{water}/kg_{dry\text{-}solid}$
X_{eq}	Equilibrium moisture content, $kg_{water}/kg_{dry\text{-}solid}$
Z_0	The gap between contact bodies, m

Greek letters

ϕ_i (i = 1, 2)	Work function of bodies, eV
ϕ_I	Effective work function of insulator, eV

ϕ_M	Work function of metal, eV
ϕ_P	Effective work function of particle, eV
ϕ_W	Work function of metal wall, eV
ε_0	Permittivity of vacuum, F/m
ε	Relative permittivity of air

Abbreviations

CPD	Contact Potential Difference

Chapter 3

D_0	Arrhenius coefficient, m^2/s
D_{eff}	Effective diffusion coefficient, m^2/s
E_a	Activation energy, J/mol
n	Positive integer
R	Universal gas constant, J/mol.K
r	Granule radius, m
T	Temperature, ˚C
t	Time, s
V	Velocity, m/s
X	Local moisture content (dry basis), $kg_{water}/kg_{dry\text{-}solid}$
X_0	Initial moisture content, $kg_{water}/kg_{dry\text{-}solid}$
X_{eq}	Equilibrium moisture content (dry basis), $kg_{water}/kg_{dry\text{-}solid}$

Abbreviations

API	Active Pharmaceutical Ingredient
CCS	Croscarmellose Sodium
HPMC	Hydroxypropyl Methylcellulose
LMH	Lactose Monohydrate
MCC	Microcrystalline Cellulose
MR	Moisture Ratio
RH	Relative Humidity

Chapter 4

I	Electric current, A
k	Cross sectional coefficient, m
L	Electrode thickness, m
m	Mass, kg
Q	Electric charge, Coulomb (C)
q	Specific charge, µC/kg
R	Resistance, ohm (Ω)
r	Electrode radius, m
S	Effective sectional area, m^2
V	Potential difference, V

Greek letters

ρ	Volume resistivity, ohm.meters (Ω.m)

Abbreviations

α-LMH	α-Lactose Monohydrate
API	Active Pharmaceutical Ingredient
CCS	Croscarmellose Sodium
HPMC	Hydroxypropyl Methylcellulose
MCC	Microcrystalline Cellulose
SOD	Solid Oral Dosage

Appendix

a	Parameter in models
c	Parameter in models
g	Parameter in models
k	Parameter in models
N	Number of experimental observations
n	Parameter in models
T	Temperature, ˚C
z	Number of parameters in the models

Greek letters

χ^2	Reduced chi-square

Abbreviations

MR	Moisture Ratio
$MR_{exp,i}$	Experimental Moisture Ratio
$MR_{pre,i}$	Predicted Moisture Ratio
RMSE	Root Mean Square Error

Chapter 1 – Introduction

1.1 Project Motivation and Knowledge Gap

In many gas-solid processes, electrostatic charges are generated by triboelectric charging during particle handling, transport and processing due to particle-particle and particle-container wall contact. In some processes, the charge build-up results in particle-wall adhesion, particle agglomeration and segregation, and generation of high-voltage electrical fields that can cause explosions. The significant negative impact of electrostatic phenomena has been reported in industries such as petrochemicals, oil and gas, and pharmaceuticals.

Drying pharmaceutical granules in a fluidized bed is a process which involves continuous particle-particle and particle-wall contact, hence providing a favorable venue for electrostatic charge generation. Besides, the organic nature of pharmaceutical powders along with their high volume resistivity turn them to insulator materials, making electrostatic charge dissipation quite difficult.

In the literature, studies on tribocharging behaviour of pharmaceutical powders have been conducted mainly on a dry basis and mostly on a vibration feeder. To the best of our knowledge, very limited efforts have been placed on investigating their tribocharging behaviour in a granular form and during a drying process. Moreover, current studies of tribocharging behaviour in a fluidized bed have mainly focused on particles such as polymer

powders or glass beads, which possess quite different particle properties from pharmaceutical powders.

During a typical drying process of pharmaceutical granules in a fluidized bed dryer, their moisture content decreases as drying progresses, which will lead to undesired particle charging. However, there is a dearth of knowledge as to how operating parameters such as fluidizing air temperature, relative humidity and velocity influence the tribocharging of pharmaceutical granules during the drying process.

1.2 Research Objectives

In view of the knowledge gap discussed above, the primary objective of this study was to investigate the tribocharging behaviour of pharmaceutical granules in a fluidized bed dryer under a range of practical operating conditions. The main operating parameters investigated were fluidizing air velocity and fluidizing air temperature. Based on an advanced understanding of tribocharing behaviour of pharmaceutical granules during the drying process, a robust and economic tool was sought to determine the optimal endpoint of the drying process.

Another objective of this project was to understand the drying kinetics of pharmaceutical granules under typical drying conditions employed in the pharmaceutical industry.

Chapter 2 – Literature Review

2.1 Granulation Process in the Pharmaceutical Industry

Tablets are the most applicable solid oral drug form in the pharmaceutical industry as they have high manufacturing efficiency and can carry a wide range of doses [1]. A typical tablet manufacturing process involves various steps, among which mixing and granulation have significant importance, as having a homogenous mixture is equal to ending up with a high quality product with the correct amount of each component. In fact, because of strict regulations in the pharmaceutical industry, hundreds of thousands of dollars worth of single batch products would be discarded if the amount of active pharmaceutical ingredients exceeded the allowable variation [2]. To avoid this, pharmaceutical powders, a combination of active pharmaceutical ingredients (APIs) and excipients, including binders, fillers, disintegrants, lubricants, preservatives, flavours, antiadherents, colours, etc., need to be mixed thoroughly to ensure that each tablet has a sufficient and at the same time the desired amount of each required ingredient [3]. Therefore, ingredients are required to be subjected to granulation processes. In the granulation process, in order to obtain stable larger particles during the whole process, different types of small particles start agglomerating by creating bonds among each other in a way that original particles are still distinguishable [4,5].

"Granulated" material has a Latin origin which is derived from the word "granulatum" meaning grained [5]; in Perry's chemical engineer's handbook, a granulation process is

defined as “any process whereby small particles are gathered into larger, permanent masses in which the original particles can still be identified” [6]. Granulation technology has a wide range of applications in various industries, including the fertilizer, detergent production, mineral processing and pharmaceutical industries [7]. As early as 1843, W. Brockedon invented the tablet press technology and started the development of pharmaceutical granulation [5]. The introduction of high speed tablet and capsule filling machines with automated controls in the 1970s led to further enhancement in granulation technology [5].

The advantages associated with granulation are: i) enhanced flowability and fluidity of granulated particles; ii) improved compressibility of granulated particles; iii) reduction in dust emission; iv) reduction in segregation; v) improved content uniformity of particulate substances; vi) increased bulk density for storage and tableting of feeds; and vii) reduced propensity to caking [7–9].

Depending on the size and type of powder, three conventional methods have been applied to prepare powders for tablet compression: direct compression (DC), wet granulation, and dry granulation.

Direct compression (DC) is used when powders possess great compressibility characteristics and can be mixed well. This method is applicable to crystalline chemicals having good compressible characteristics and flow properties. In such cases, powders are directly placed into a tablet press without the granulation stage [1]. Some of the advantages associated with DC are lower equipment cost, faster process time and efficient operation involving only two process steps [5]. However, when the API and excipient display low

flowability or the final product requires a low dosage where content uniformity is important, DC is not an applicable method [5]. Another method is wet granulation where a non-toxic and volatile granulation liquid solution is added to the well-blended powders [4]. Following this step, wet granulated particles have to undergo a drying stage followed by a tablet compaction process. Dry granulation is another technique where a liquid solution is not used because active ingredients to be granulated are sensitive to either solvent, high temperature or moisture [5]. Binders are added to the powders in dry form, thereby exhibiting high compactibility behaviour and adequate flowability. Dry granulation could be carried out on a tablet press or on a roller compactor [5]. Additionally, nowadays other novel granulation techniques like spray granulation, foam granulation, ultrasonic spray congealing and melt granulation have been developed and introduced to the pharmaceutical industry [10].

Overall, wet granulation is still the most frequently used method in granulation processes. In a typical wet granulation process, adding granulation liquid during the agitation process will facilitate holding the small particles together by forming liquid bridges among them. The typically applied granulation liquids are water, alcohols or mixtures of both. Aqueous solutions of polymeric binders such as polyvinylpyrrolidone (PVP) can be used as granulation liquids as well [11]. In principle, wet granulation takes place in three steps: wetting and nucleation, consolidation and growth, and attrition and breakage [7]. Wetting is a process in which the granulation liquid is introduced and distributed evenly throughout the dry mixture. Once the granulation liquid is introduced to the dry powder mixture, nucleation occurs where nearby particles start to join together in weak structures called nuclei [7,12]. Following nucleation is the coalescence or growth stage, where partially wetted primary

particles and larger nuclei coalesce to form granules composed of several particles. As granules grow, bed agitation exerts compaction forces resulting in their consolidation. It is worth mentioning that internal granule voidage or granule porosity, as well as granule strength, hardness and dissolution are strongly influenced by the consolidation stage [7,12]. Among the formed granules, those inherently weak and poorly formed may be broken up due to attrition during the agitation process [7,12].

After completion of the granulation process, a drying process is required to remove undesired moisture in wet granules. Convective drying methods such as tray drying and fluid-bed drying are the most practical methods in the pharmaceutical industry; however, other methods such as microwave and vacuum drying have recently drawn increasing attention [11].

2.2 The Drying Process

Drying is a process in which the moisture is removed from a wet material in a simultaneous heat and mass transfer operation to yield a solid product. In general, the moisture present in the solid is divided into two categories: bound moisture, that represents the specific moisture amount which is trapped in the microstructure of the solid in a liquid solution form and exerts a vapour pressure less than that of the pure liquid; and unbound moisture, which is in excess of bound moisture [13]. In the case of exposing a wet solid to a thermal drying operation, the two following processes could happen simultaneously [13]:

1. Evapouration of surface moisture via energy transferring from the surrounding environment, which depends very much on the external conditions such as temperature, air humidity and flow, area of exposed surface, and pressure;

2. Evapouration of the internal moisture, which is now transferred to the solid surface due to the previous process, which depends on the physical nature of the solid, its moisture content and the temperature.

Accordingly, the drying kinetics are governed by the rate at which the two aforementioned processes proceed. There are several process parameters determining the drying progress. External conditions, namely temperature, flow and humidity of the drying air, area of exposed surface, and pressure of the drying medium, play notable roles in removal of water in the vapour form, from the surface of the wet material in the first process mentioned above. In contrast, the physical nature of the solid as well as its temperature and moisture content, all known as internal conditions, determine moisture movement inside the solid [13]. Conduction, convection or radiation and in some specific cases combinations of these mechanisms, are denominating heat transfer modes to the wet solid from the surrounding environment [13]. The direction of heat transfer may vary depending on the size and type of industrial dryer. In most cases, heat moves from outside to the surface and subsequently to the interior of the wet solid; however, in some cases where dielectric, radio frequency (RF), or microwave freeze drying are employed, heat moves in the opposite direction, from the interior to the exterior surface [13].

2.2.1 Mechanism of Drying

As noted earlier, the moisture in a wet material is present in two forms, unbound and/or bound. In order to remove the unbound moisture from the wet material, two methods can be applied, evapouration and vapourization [13]. Evapouration occurs when the vapour pressure

of the moisture on the wet material surface is equal to the atmospheric pressure. Increasing the temperature of the moisture to its boiling point would make this happen [13]. It is worth mentioning that if the material to be dried is heat sensitive, vacuum evapouration could be applied. Hence, by lowering the pressure, the boiling point would be decreased, which in turn makes the drying process achievable at a lower temperature [13].

The other method for removal of unbound moisture is vapourization in which warm air passes over the wet material and drying is carried out by convection [13]. In this case, where the saturation vapour pressure of the moisture on the surface of the solid is lower than the atmospheric pressure, the product cools down the air and moisture is transferred to the air from the product and then carried away [13].

External drying conditions are important during the removal of unbound surface moisture at the initial stages of drying [13]. Surface evapouration is controlled by the diffusion of vapour from the surface of the solid to the surrounding atmosphere through a thin film of air in contact with the surface [13].

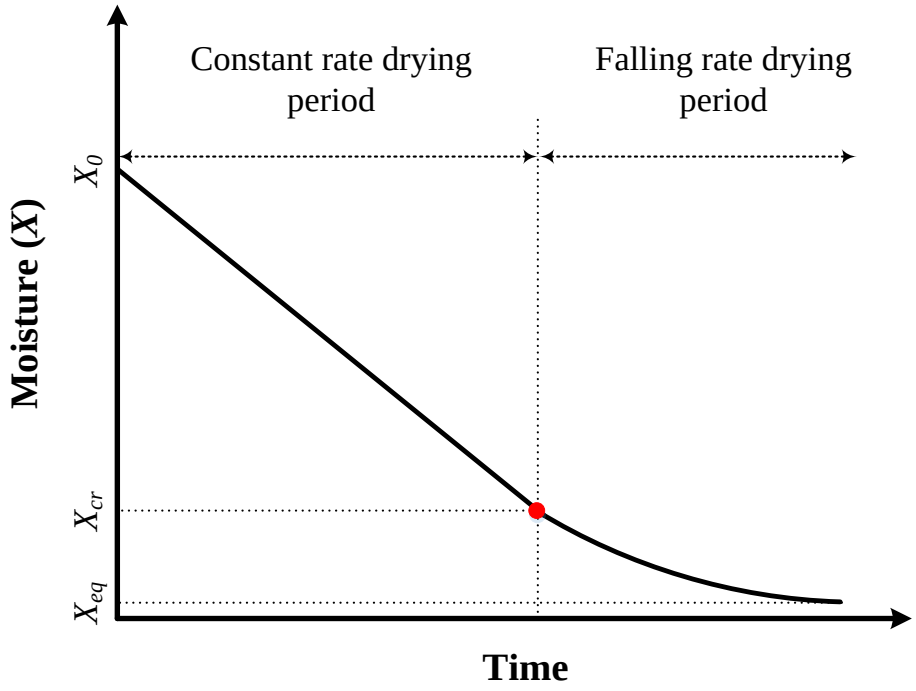

Figure 2.1 Typical drying curve for porous material

Figure 2.1 depicts a typical drying curve for a porous wet material when exposed to an air stream at a constant temperature and humidity. Depending on the moisture content of the material, different behaviours might be observed during a drying process.

During the first stage of the drying process, the drying rate is constant. As long as the moisture on the surface of the material is supplied and removed from the surface at the same rate, the material dries at a constant rate [13]. The rate-controlling step in the constant rate drying period is water vapour diffusion across the interface between air and moisture. As the drying progresses toward the end of the constant rate period, capillary forces enable the moisture transport from the inside of the material to its surface, although the drying rate may still be constant. When the average moisture content has reached the critical moisture content,

X_{cr}, the surface film of moisture has become so thin that further drying causes dry spots to appear upon the surface [13].

In contrast, during the falling rate period, the rate-controlling step becomes the rate of moisture movement through the solid as a result of concentration gradients between the core parts and the surface. Also, heat transfer to the wet solid causes a temperature gradient within the solid while moisture removal occurs from the surface. The overall heat transmission occurs in the form of heat transfer to the surface from the hot gas stream and heat conduction within the product solids [13]. This results in a migration of moisture from within the solid to the surface, which occurs through one or more mechanisms, namely diffusion, capillary flow or internal pressure induced by shrinkage during drying. In this stage, diffusion of moisture from the inside to the surface and then mass transfer from the surface controls the drying rate [13]. As the moisture concentration is reduced, the rate of internal movement of moisture decreases. The drying rate becomes even slower as the moisture content continues to decrease until reaching a point known as the equilibrium moisture content, X_{eq}. At this point the vapour pressure of the moisture in the solid is equal to the partial pressure of the vapour in the gas, and further exposure to this air for prolonged periods will not cause any additional loss of moisture [13]. However, the moisture content in the solid could be reduced further by exposing it to air of lower relative humidity.

2.3 Fluidization

Fluidization is a process in which passing of a fluid (gas or liquid) upward through a static bed of solid particles turns it into a dynamic fluid-like state [15]. Liquid-solid and gas-

solid fluidized beds are two conventional types of fluidized beds used in many industries [16]. In a typical gas-solid fluidization system, depending on the bed dimensions and the type of particles to be fluidized, different types of flow regimes may be observed with increasing gas velocity, as shown in Figure 2.2.

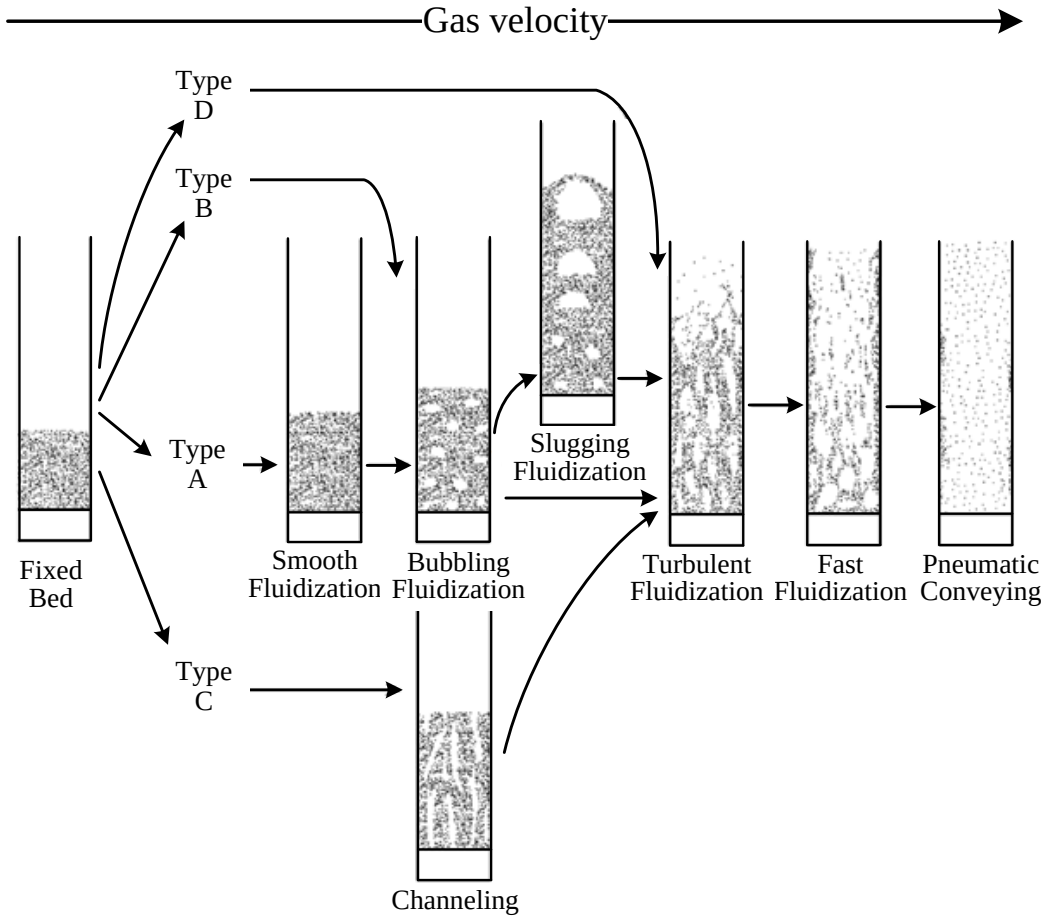

Figure 2.2 The regimes of fluidization (adapted from [17])

As can be seen in Figure 2.2, based on fluidization quality, particles are divided into four types (C, A, B, and D). This classification by Geldart [18] categorizes particles based on their size and density, as shown in Figure 2.3.

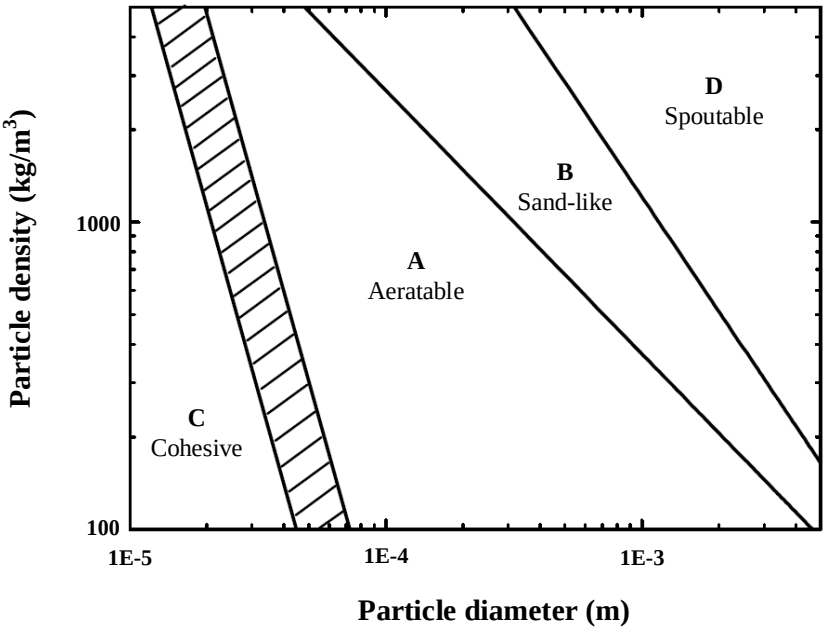

Figure 2.3 The Geldart chart for the classification of particles (adapted from [14])

Particles that belong to group C are fine and ultrafine particles which are difficult to fluidize due to large cohesive forces between particles compared to forces exerted by the fluidizing air. This leads to significant channeling effects [17,19]. The boundary between group C and group A particles is shaded because of variations in interparticle forces caused by differences in particle physical properties [14]. Group A particles are aeratable and easily fluidized in their dry form. By increasing the gas velocity to the minimum fluidization velocity (u_{mf}), the bed of particles will expand and a smooth fluidization regime will be reached. Further increasing the gas velocity leads to occurrences of bubbles. The velocity at which bubbles start to form is noted as the minimum bubbling velocity (u_{mb}) [17,19]. Group B particles are sand-like particles and are easy to fluidize. Group B particles do not exhibit much bed expansion and as soon as the gas velocity exceeds the minimum fluidization velocity, bubbling commences [14,17]. Larger and denser particles are categorized as group D particles,

which exhibit poor fluidization quality and spouted beds might occur as a result of the formation of large bubbles in the bed [14,17,19].

It should be noted that a higher minimum fluidization velocity must be used to fluidize particles with a high initial moisture content than is required for dry particles. Dominant cohesive forces exerted by wetted surfaces keep the bottom layers stationary during the initial stage of drying and only the top layer of the bed of solids is fluidized [17]. However, the liquid bridging forces will become weak toward the end of the drying process with the moisture content of the particles gradually being reduced.

In a typical fluidization process when a low rate gas flow starts passing through a bed of packed solid particles, due to its low velocity, the gas flow can only spread through the void spaces between particles. The drag force being produced as a result of upward gas flow is not strong enough to overcome the downward gravity force. Therefore, the bed remains in the fixed bed state [16]. The only measurable change across the bed, however, is the notable pressure drop. With an increasing gas flow rate, the drag force and subsequently the pressure drop across the bed also will start to increase. Finally, at a point where the drag force and the frictional forces between particles equal the gravity force, the bed becomes fluidized and the pressure drop across the bed will remain constant when further increasing the gas flow [15]. This state is referred as minimum (smooth) fluidization and occurs at a velocity called minimum fluidization velocity. The value of minimum fluidization velocity is a function of several operating parameters, among which the particle physical properties are considered the most important parameters [14].

With further increasing the gas flow rate, the smooth fluidization will change into bubbling fluidization, where the excess gas passes the column in the form of bubbles. In beds with coarse particles or having large height-to-diameter ratios, a slugging regime is expected to occur [15]. In this regime, the size of bubbles grows to as large as the internal diameter of the fluidized bed [15]. The next regime is called turbulent fluidization which may occur right after the bubbling regime without observation of the bubbling regime. In turbulent fluidization, the high shear forces resulting from the fast moving gas cause bubbles to become distorted and eventually disappear [15]. Solid particles start to entrain in this regime, therefore having a cyclone on top of the bed could be useful for capturing and returning the particles to the bed through an external line [14]. Further increasing the gas velocity leads to more entrainment and the so-called fast fluidization regime appears. Finally, all of the solid particles will be suspended in the fluidizing gas and move upward [15]. This regime is known as pneumatic transport.

Selection of the optimum and correct fluidization regime is of great importance in industry and determined mainly by the application. After selection of the appropriate gas-solid contact regime, it is desirable to maximize the mass transfer between these phases [14]. In the case of drying, an increase in mass transfer rate between phases leads to a reduced drying time. Although the turbulent regime is desirable for gas-solid contact due to elimination of the bypassing gas present in the bubbling regime, the vigorous mixing in this regime may result in significant entrainment and attrition of the particles [14]. It is desirable to reduce both of these effects.

Drying of pharmaceutical granules in fluidized beds has some advantages over other conventional methods, namely a high rate of moisture removal, excellent mixing, high thermal efficiency, easy material transport inside the dryer, ease of control, rapid heat and mass transfer between the solid and the gas phases, large capacity of production, and low maintenance costs [8,17].

2.4 Tribocharging Phenomenon

The effects of electrostatic phenomena in gas-solid fluidized beds and their influence on particle adhesion to the vessel wall were first detected in the early 1940s [20]. One common issue associated with gas-solid fluidization processes, and particle handling processes in general, is electrostatic charge generation, i.e. transferring of electrons between materials which are in contact with each other. When two different solid materials are brought into physical contact with each other, electrostatic charges will start to separate from their surfaces and transfer between them until they reach an equilibrium; thereafter, if the materials are separated fast enough so that the existing electrostatic equilibrium is destroyed and charge backflow is disabled, the materials will remain charged and two oppositely charged electrical layers will form on their surfaces [21–24]. It is worth mentioning that in accordance with the charge conservation law, the total amount of charge carried by two materials should remain constant. In the literature, this phenomenon is known as ‘contact electrification’ or ‘contact charging’ [23]. Figure 2.4 demonstrates the contact electrification process.

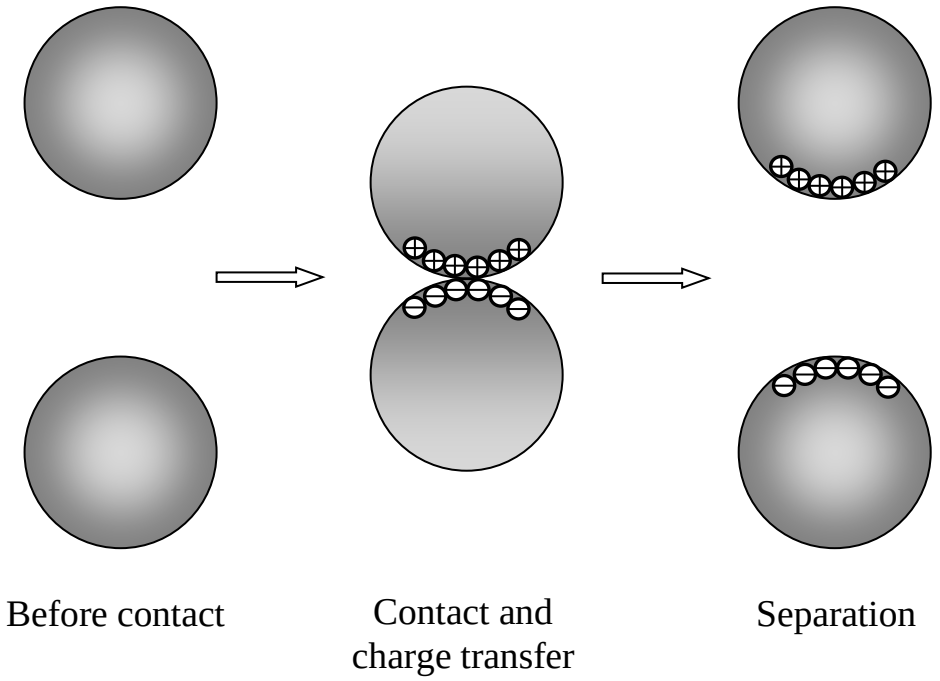

Figure 2.4 Schematic illustration of the contact electrification process

Another more frequently used term is ‘frictional electrification’, which is also known as ‘triboelectrification’ or ‘tribocharging’ and occurs when two materials are rubbed against each other [23]. If only a short contact happens during collision, the term ‘impact charging’ would more suitably describe the phenomenon [23]. However, in the case of dealing with fine particles, due to the fact that it is technically difficult to distinguish these mechanisms, the term ‘triboelectric charging’ or ‘tribocharging’ is widely used in the literature.

Based on the different conductive properties of contacting surfaces, electrostatic charge generation caused by particle-particle contacts can be divided into three different categories: i) metal-metal contact; ii) metal-insulator contact; and iii) insulator-insulator contact [25].

i) Metal-Metal Contact

The cause of electron transferring during a metal-metal contact is the contact potential difference (CPD) which is a result of the difference in work functions of metals in contact [22]. The contact potential difference, V_c, between metals in contact is given by:

$$V_c = -\frac{(\phi_1 - \phi_2)}{e} \tag{2.1}$$

where ϕ_1 and ϕ_2 are the work functions of metals (eV) and e is the elementary charge (C) [25] (Figure 2.5).

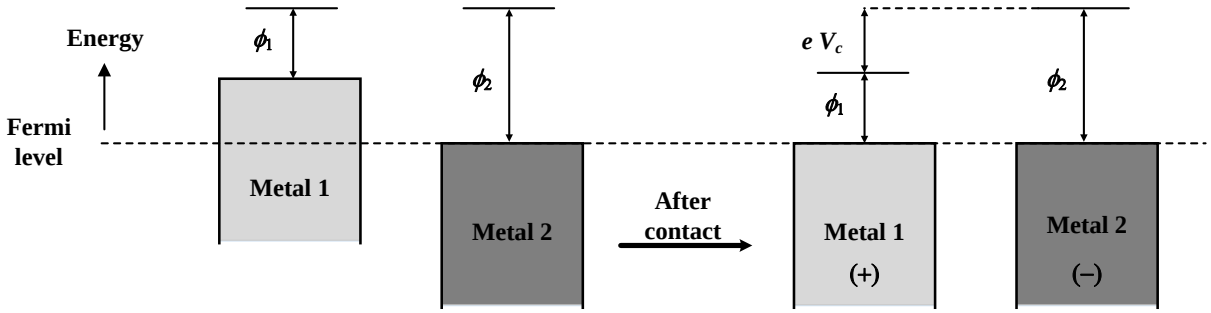

Figure 2.5 Electron potential energy for metal-metal contact

The work function is defined as the minimum energy needed to remove an electron from a solid surface to a point in infinity relative to surface yet not so far away as to be affected by the ambient electric field [2]. According to this theory, the electron transfer from the metal with the lower work function to the metal with the higher work function will continue until the electron energy (chemical potential or Fermi energy level) reaches equilibrium [2]. The Fermi energy level is the occupied energy level at absolute zero temperature [26]. In order to find out the amount of charge being transferred, the condenser (capacitor) model can be applied [23].

This model suggests that the charge accumulation on the surfaces of materials in contact with each other is similar to charge build-up on a capacitor [22]. Therefore, using this model, the transferred charge between materials (Δq_c) can be calculated by:

$$\Delta q_c = C_0 V_c \tag{2.2}$$

where C_0 is the capacitance between two bodies (F) at a distance where charge transfer stops, and V_c is the contact potential difference (V) [23].

ii) Metal-Insulator Contact

Matsusaka and Masuda proposed three possible models for metal-insulator contact [25].

"Electron transfer" is the first model formed based on metal-metal contact and suggests that electron flow is the reason for charging of materials. In order to apply the relations governing the metal-metal contact mechanism, the term effective work function needs to be assigned to the insulator [23]. The following equation could be used to evaluate the net exchanged charge between a metal and an insulator after their energy levels are equalized:

$$\Delta q_c = C_0 \frac{-(\phi_I - \phi_M)}{e} \tag{2.3}$$

where ϕ_I is the effective work function of insulator (eV), ϕ_M is the work function of metal (eV), and C_0 is the capacitance between two bodies (F) at a distance where charge transfer stops [23].

The second model is known as “ion transfer” [25]. Ion transfer could be the dominant effect in the charge exchange process compared to electron transfer if ions exist in excess; otherwise, electron transfer controls the contact charging [25].

“Material transfer” is the last model and is applicable where a material from a body adheres to another body by rubbing them against each other [25]. Charge transfer occurs if the transferred material carries electrical charge.

Although all these three models have practical applications in interparticle contact charging, in the case of pharmaceutical powders the electron transfer model is the most applicable as it can easily describe the charging process caused by surface potential difference [22].

iii) Insulator-Insulator Contact

The main downstream steps involved in tablet processing include sieving, pouring, grinding, mixing, granulation, etc., where continuous particle-particle and particle-wall contacts occur; therefore, pharmaceutical powders experiencing such industrial processes will inevitably acquire electric charges. Mostly, pharmaceutical powders are composed of organic materials which turn them into good electrical insulator materials with electrical resistivity greater than 10^{13} Ω.m; hence, the insulator-insulator contact model could suitably describe the charging process arising from interparticle contact in the pharmaceutical industry [2,22]. However, using the effective work function model alone might not be satisfactory, as an insulator material does not have free electrons available [23]. Therefore, in order to determine the charging tendency and behaviour between insulator materials, the ‘triboelectric series’,

where materials are ranked according to their polarity and its magnitude when they are in contact with other materials, could be used [25]. Materials located higher up in the series have lower work functions and are always inclined to lose electrons and become positively charged when rubbing or contacting with materials located in lower positions with higher work functions [25]. All models that have been proposed so far to better describe contact charging between two insulators are similar to those proposed for metal-insulator contact; however, it should be noted that electron movement in insulator materials is much more restricted compared to metals [23]. One of the models used to describe such contact is the "surface state model" that allocates energy levels, known as the surface state, for electrons and assumes that they are present only on the surface of the insulator material and not in the bulk [23]. When two insulators come into contact with each other, because of the difference in effective work functions of two insulator materials, electrons will transfer from the insulator with the filled surface state to the insulator with the empty surface state until their Fermi levels become equal to each other [23].

Aside from the three aforementioned categories for electrostatic charge generation in a particle-particle contact, the electrostatic charge might also arise from the collision between particles and the wall surface [27]. Particles are always in contact with the surface of the process vessel wall. Thus, it is likely that charge transfer occurs because of the existing total potential difference between particles and the wall [27]. The condenser model should be used in order to determine the exchanged charge as a result of collision between a particle and a wall (Figure 2.6):

$$\Delta q = k_c C V \tag{2.4}$$

where k_c is the charging efficiency, C is the capacitance (F), and V is the total potential difference (V) [23]. The following relation is used to determine the capacitance C:

$$C = \frac{\varepsilon \varepsilon_0 S}{Z_0} \tag{2.5}$$

where ε is the relative permittivity of air, ε_0 is the permittivity of a vacuum (F/m), S is the contact area (m^2) and Z_0 is the gap between the contact bodies (m) [27]. The total potential difference, V (V), is comprised of four parts: i) V_c the contact potential difference based on the surface work function; ii) V_e the potential difference arising from the image charge being induced by an external charge in the wall; iii) V_b is the potential difference arising from the space charge caused by surrounding charged particles; and iv) V_{ex} is the potential difference arising from other electric fields [23]. These terms are related as follows [23]:

$$V = V_c - V_e - V_b + V_{ex} \tag{2.6}$$

The contact potential difference, V_c, is:

$$V_c = \frac{(\phi_P - \phi_W)}{e} \tag{2.7}$$

where ϕ_P is the effective work function of particle (eV), ϕ_W is the work function of the metal wall (eV), and e is the elementary charge (C) [28].

V_e is calculated by:

$$V_e = k_e q \tag{2.8}$$

where q is the initial charge a particle possesses before impact (C) [23].

And V_b is given by [23]:

$$V_b = k_b q \tag{2.9}$$

Figure 2.6 below schematically describes the condenser model.

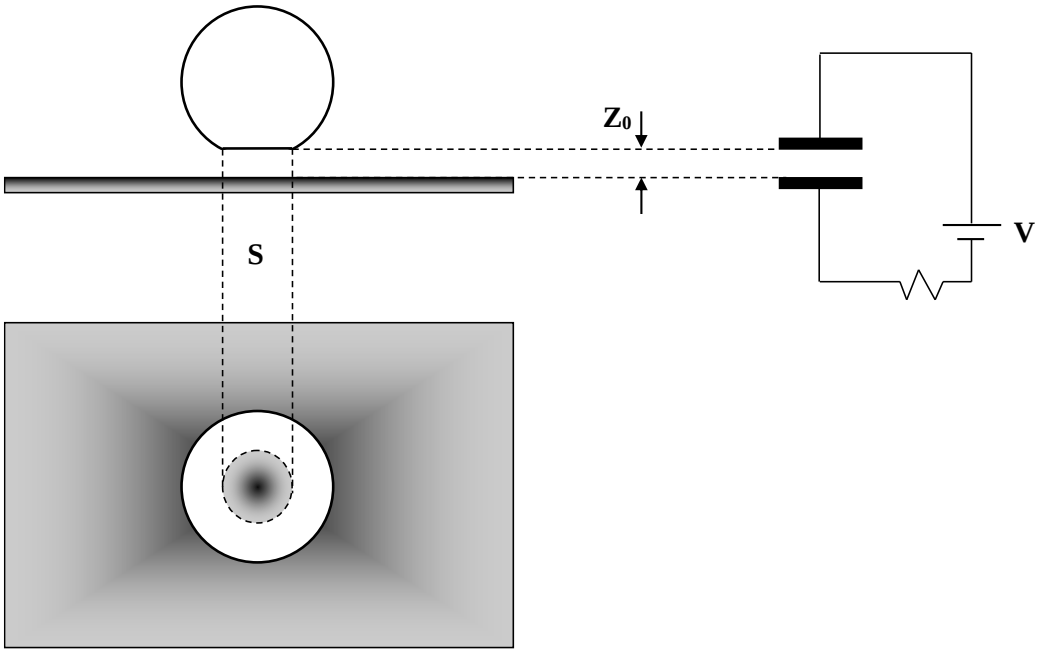

Figure 2.6 Condenser model (adapted from [23])

2.4.1 Tribocharging Phenomenon in Gas-Solid Fluidized Beds

In fluidized beds, repeated particle-particle collision and separation along with rubbing of particles together and particle-wall friction will unavoidably result in electrostatic charge generation [21,29,30]. This phenomenon can typically have significant negative impacts on powder handling processes in the pharmaceutical industry and other industries. Notable changes in gas-solid fluidized bed hydrodynamics, segregation and agglomeration of particles, variability of API and excipients, adhesion of particles to the wall surface known as

"sheeting", and finally electrostatic discharge that can cause explosions are generally the problems associated with tribocharging [1,29,30]. Pharmaceutical powders by their very nature are mainly insulators, as noted earlier, with small size and low bulk density, providing a good condition for electrostatic charge build-up and accumulation which will take quite a long time to decay. Charged particles can attract or repel each other, resulting in segregation or formation of particle agglomerates (chunks), ultimately affecting the fluidization hydrodynamics [1,29,30]. Particles adhering to the wall can break off and cover the distributor plate and cause a long shut down period for clean-up, which results in significant economic losses due to decreased production and higher maintenance costs [29]. Electrostatic discharge which may lead to electrical shocks to operating personnel and fires and explosions are often the result of significant generation of high-voltage electrical fields [30]. Also, studies have revealed that electrostatic discharge was responsible for almost 70% of 153 accidents over a 50-year time span in Japan [31]. Furthermore, according to statistics in Germany, one dust explosion occurs each day and every tenth explosion is caused by static electricity [32]. Therefore, there is a great incentive to reduce or eliminate electrostatic charge build-up from both safety and process standpoints. An essential step is to determine the charging mechanisms, and therefore to accurately quantify electrostatic charge generation and its effects in fluidized bed dryers.

2.4.2 Electrostatic Charge Measurement in Gas-Solid Fluidized Beds

To measure electrostatic charges generated in gas-solid fluidized beds, different techniques have been employed. The Faraday cup method and electrostatic probes are two of the most applicable techniques in measuring generated charges. Depending on the type of

process, the better option can be selected. The Faraday cup is used for measuring the electrostatic charges of particles directly, whereas electrostatic probes are used to determine the cumulative potential generated inside the bed and on the walls of the column [20].

2.4.2.1 The Faraday Cup

The Faraday cup generally consists of concentric vessels of any shape which are insulated from each other (as shown in Figure 2.7). The outer cup is grounded and acts as a shield to prevent external noises from affecting the inner cup and subsequently electrostatic charge measurement. The inner cup, which is used for determining the electrostatic charge, is connected to an electrometer which measures charge by detecting the voltage generated across a known capacitor [26].

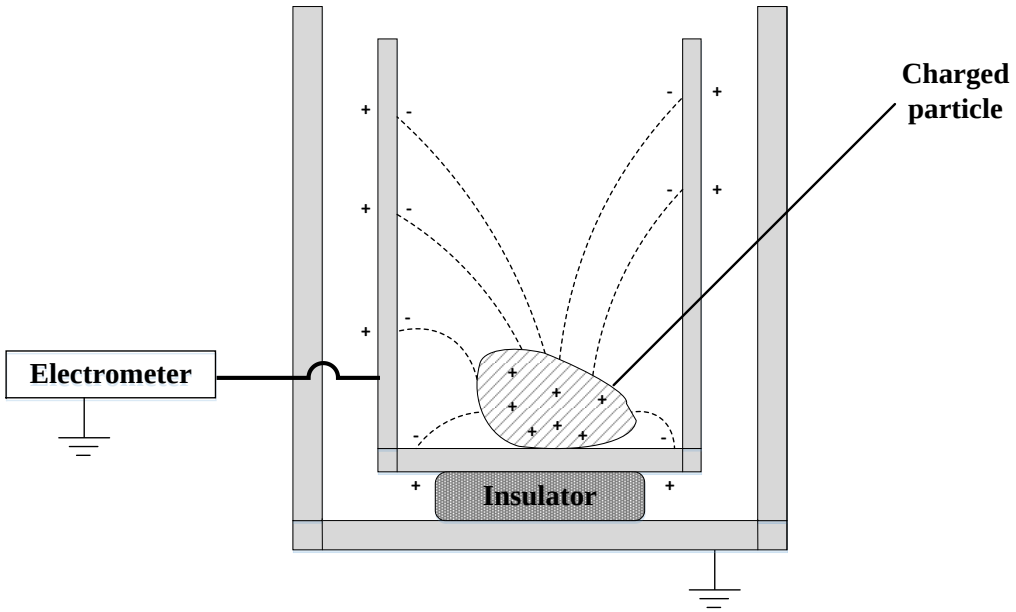

Figure 2.7 Faraday cup for measuring electrostatic charge

As can be seen in Figure 2.7, if a nonconductive particle is placed inside the Faraday cup, equal but opposite charges will accumulate on the inner wall of the inner cup (due to induction between particle and wall) which leads to build up of charge with the same magnitude and polarity of charged particle on the outer wall of the inner cup. However, if the particle is conductive, charges will move directly to the inner cup. These charges are read and measured by the capacitor on the electrometer [26].

However, it is obvious that the Faraday cup cannot be used to measure the charge stored on a moving belt or a large article [26]. Besides, introduction of extra charges on particles before entering them into the Faraday cup and the inability to measure the generated charges *in situ* are some of the drawbacks associated with the Faraday cup method [20,33].

2.4.2.2 Electrostatic Probes

In principle, electrostatic probes measure electrostatic charges by reading the image charge induced on their conductive surfaces [20,33]. In order to measure the electrostatic charge build-up inside a fluidized bed using these probes, they are required to be connected to electrometers and then inserted along the axis of the bed [34].

As for Faraday cups, there are some major issues associated with electrostatic probes. Adhesion of particles to the tip of the probe can significantly influence the charge reading [35]. Moreover, continuous contact between particles and the probe might introduce extra charge and eventually affect the accuracy of charge measurement over time [36]. In addition, inserting any foreign object into the bed can influence hydrodynamics in the fluidized bed [36].

2.4.3 Methods of Charge Reduction in Gas-Solid Fluidized Beds

Several ways have been proposed to reduce electrostatic charge build-up and accumulation in fluidized beds, such as humidification of the fluidizing air, coating particles with conductive materials, reducing the gas flow rate, material selection for the vessel wall, choosing particles which are more conductive, and addition of antistatic agents [24,37]. The use of humidified air as a method to reduce electrostatic charge generation in fluidized beds dates back to the 1960s [20]. Later on, research showed that a relative humidity of 60 – 70% is needed to sufficiently decrease electrostatic charge accumulation; however, one major problem associated with this method is increased cohesive properties of some particles [24]. Coating of particles with conductive materials to facilitate charge leakage from the bed to the ground is considered an alternative way in reducing electrostatic charge accumulation; however, a majority of these materials are incapable of tolerating harsh conditions, especially the high temperatures in fluidized beds and will not last for a long time [24]. Similar to conductive coating, addition of antistatic agents, such as carbon black, by attracting and holding the moisture and subsequently reducing the surface resistance of insulator particles, can cause electrostatic charges to dissipate quickly; however, the effectiveness of these materials depends highly on the relative humidity of the environment so they cannot be expected to last for a long time as they might adsorb on the bed wall in contact with treated particles [2,24,32].

Another method to lower the electrostatic activity of particles in a fluidized bed is to introduce a small amount of fine particles, such as graphite, thereby reducing the number of intimate contacts by acting as a coating agent [24]. In addition, if particles and fines possess

opposite charges, coating the particles with fines will shield their charges and consequently lower their effective specific charges [24].

Additionally, proper bonding and grounding of conductive components and installations in a manufacturing plant can significantly reduce capacitive sparks and ignitions due to electrostatics; however, recent studies have revealed that grounding the facilities might not be as effective as expected [2,24].

Although there are other means, such as lowering the gas velocity coming to the bed or changing the materials of the wall and particles, they may not be considered practical solutions as the fluidization condition is determined by the process and, moreover, it might not be possible to produce desired particles based on electrostatic considerations alone [24].

2.5 References

[1] E. Šupuk, A. Zarrebini, J.P. Reddy, H. Hughes, M.M. Leane, M.J. Tobyn, et al., Tribo-electrification of active pharmaceutical ingredients and excipients, Powder Technol. 217 (2012) 427–434. doi:10.1016/j.powtec.2011.10.059.

[2] J. Wong, P. Chi, L. Kwok, H. Chan, Electrostatics in pharmaceutical solids, Chem. Eng. Sci. 125 (2015) 225–237. doi:10.1016/j.ces.2014.05.037.

[3] T.A.H. Simons, S. Bensmann, S. Zigan, H.J. Feise, H. Zetzener, A. Kwade, Characterization of granular mixing in a helical ribbon blade blender, Powder Technol. (2015). doi:10.1016/j.powtec.2015.11.041.

[4] T. Pugsley, G. Chaplin, P. Khanna, Application of advanced measurement techniques to conical lab-scale fluidized bed dryers containing pharmaceutical granule, Food Bioprod. Process. 85 (2007) 273–283. doi:10.1205/fbp07022.

[5] D.M. Parikh, Introduction, in: Handb. Pharm. Granulation Technol. Third Ed., CRC Press, 2009: pp. 1–5. doi:10.3109/9781616310035-2.

[6] R.H. Perry, D.W. Green, Perry's Chemical Engineers' Handbook, 8th ed., McGraw-Hill, New York, 2008. doi:10.1036/0071422943.

[7] B. Ennis, Theory of granulation, in: Handb. Pharm. Granulation Technol. Third Ed., CRC Press, 2009: pp. 6–58. doi:10.3109/9781616310035-3.

[8] L. Briens, M. Bojarra, Monitoring fluidized bed drying of pharmaceutical granules., AAPS PharmSciTech. 11 (2010) 1612–8. doi:10.1208/s12249-010-9538-1.

[9] S. Srivastava, G. Mishra, Fluid bed technology : Overview and parameters for process selection, Int. J. Pharm. Sci. Drug Res. 2 (2010) 236–246.

[10] D.C.T. Tan, W.W.L. Chin, E.H. Tan, S. Hong, W. Gu, R. Gokhale, Effect of binders on

the release rates of direct molded verapamil tablets using twin-screw extruder in melt granulation, Int. J. Pharm. 463 (2014) 89–97. doi:10.1016/j.ijpharm.2013.12.053.

[11] J. Berggren, Engineering of pharmaceutical particles: modulation of particle structural properties, solid-state stability and tabletting behaviour by the drying process, Uppsala University, 2003.

[12] E.M. Hansuld, L. Briens, A review of monitoring methods for pharmaceutical wet granulation, Int. J. Pharm. 472 (2014) 192–201. doi:10.1016/j.ijpharm.2014.06.027.

[13] A.S. Mujumdar, Principles, classification, and selection of dryers, in: Handb. Ind. Dry., 2009: pp. 3–29.

[14] G. Chaplin, Monitoring fluidized bed dryer hydrodynamics using pressure fluctuations and electrical capacitance tomography, University of Saskatchewan, 2005.

[15] D. Kunii, O. Levenspiel, Fluidization engineering, Elsevier, 1991. doi:10.1016/B978-0-08-050664-7.50007-X.

[16] P. Khanna, Particle tracking in a lab- scale conical fluidized bed dryer, University of Saskatchewan, 2008.

[17] C.L. Law, A.S. Mujumdar, Fluidized bed dryers, in: Handb. Ind. Dry., 2006: pp. 174–201. doi:10.1021/ie50643a003.

[18] D. Geldart, Types of gas fluidization, Powder Technol. 7 (1973) 285–292. doi:10.1016/0032-5910(73)80037-3.

[19] D. Kunii, O. Levenspiel, Fluidization engineering, Elsevier, 1991. doi:10.1016/B978-0-08-050664-7.50009-3.

[20] P. Mehrani, Characterization of electrostatic charges in gas-solid fluidized beds, The University of British Columbia, 2005.

[21] W.O. Moughrabiah, J.R. Grace, X.T. Bi, Effects of pressure , temperature , and gas velocity on electrostatics in gas - solid fluidized beds, Chem. Eng. Sci. 123 (2009) 320–325. doi:10.1021/ie800556y.

[22] S. Karner, N. Anne Urbanetz, The impact of electrostatic charge in pharmaceutical powders with specific focus on inhalation-powders, J. Aerosol Sci. 42 (2011) 428–445. doi:10.1016/j.jaerosci.2011.02.010.

[23] S. Matsusaka, H. Maruyama, T. Matsuyama, M. Ghadiri, Triboelectric charging of powders: A review, Chem. Eng. Sci. 65 (2010) 5781–5807. doi:10.1016/j.ces.2010.07.005.

[24] T.B. Jones, Fluidization, solids handling, and processing, Elsevier, 1998. doi:10.1016/B978-081551427-5.50015-6.

[25] S. Matsusaka, H. Masuda, Electrostatics of particles, Adv. Powder Technol. 14 (2003) 143–166. doi:10.1163/156855203763593958.

[26] J.A. Cross, Electrostatics: principles, problems and applications, Adam Hilger, Bristol, 1987.

[27] S. Matsusaka, M. Ghadiri, H. Masuda, Electrification of an elastic sphere by repeated impacts on a metal plate, J. Phys. D. Appl. Phys. 33 (2000) 2311–2319. doi:10.1088/0022-3727/33/18/316.

[28] L. Zhang, J. Hou, X. Bi, Triboelectric charging behavior of wood particles during pellet handling processes, J. Loss Prev. Process Ind. 26 (2013) 1328–1334. doi:10.1016/j.jlp.2013.08.004.

[29] A. Sowinski, L. Miller, P. Mehrani, Investigation of electrostatic charge distribution in gas-solid fluidized beds, Chem. Eng. Sci. 65 (2010) 2771–2781. doi:10.1016/j.ces.2010.01.008.

[30] P. Mehrani, H.T. Bi, J.R. Grace, Electrostatic charge generation in gas-solid fluidized

beds, J. Electrostat. 63 (2005) 165–173. doi:10.1016/j.elstat.2004.10.003.

[31] A. Ohsawa, Statistical analysis of fires and explosions attributed to static electricity over the last 50 years in Japanese industry, J. Phys. Conf. Ser. 301 (2011) 012033. doi:10.1088/1742-6596/301/1/012033.

[32] M. Glor, Ignition hazard due to static electricity in particulate processes, Powder Technol. 135-136 (2003) 223–233. doi:10.1016/j.powtec.2003.08.017.

[33] C. He, X.T. Bi, J.R. Grace, Simultaneous measurements of particle charge density and bubble properties in gas-solid fluidized beds by dual-tip electrostatic probes, Chem. Eng. Sci. 123 (2015) 11–21. doi:10.1016/j.ces.2014.10.023.

[34] C. He, X.T. Bi, J.R. Grace, A novel dual-material probe for in situ measurement of particle charge densities in gas–solid fluidized beds, Particuology. (2014) 1–12. doi:10.1016/j.partic.2014.11.001.

[35] A. Giffin, P. Mehrani, Comparison of influence of fluidization time on electrostatic charge build-up in the bubbling vs. slugging flow regimes in gas–solid fluidized beds, J. Electrostat. 68 (2010) 492–502. doi:10.1016/j.elstat.2010.06.013.

[36] A. Sowinski, F. Salama, P. Mehrani, New technique for electrostatic charge measurement in gas-solid fluidized beds, J. Electrostat. 67 (2009) 568–573. doi:10.1016/j.elstat.2008.11.005.

[37] Toyota Tsusho receives FDA approval for antistatic agent, Addit. Polym. 2009 (2009) 5. doi:10.1016/S0306-3747(09)70081-8.

Chapter 3 – Investigation on Drying Kinetics and Tribocharging Behaviour of Pharmaceutical Granules in a Fluidized Bed Dryer

The contents of this chapter have been submitted to **Powder Technology**, (Ms. Ref. No.: POWTEC-D-16-00991).

Contribution of the MSc student

Experiments were planned and performed by Milad Taghavivand. Lifeng Zhang supervised and provided consultation during the entire experimental period as well as during thesis preparation. Kwangseok Choi provided consultation for electrostatic charge measurements. All of the writing of the submitted manuscript was done by Milad Taghavivand, with Lifeng Zhang providing editorial guidance regarding the style and content of the paper.

Contribution of this chapter to the overall study

This chapter provides a good understanding of the drying of pharmaceutical granules and the required drying time under different operational conditions inside a fluidized bed dryer. Furthermore, electrostatic charge generation over the course of the drying process has

been investigated. The effects of operating parameters including drying air temperature and velocity on electrostatic charge generation were studied. The electrostatic charge generation was found to closely correlate with moisture content, indicating that monitoring dynamic electrostatic charge could be used to determine the endpoint of the drying process for pharmaceutical powders.

3.1 Abstract

Among various methods for drying of pharmaceutical granules in the pharmaceutical industry, fluidized bed drying is a frequently used method due to its high rate of moisture removal, excellent performance in solids mixing, and heat and mass transfer. As pharmaceutical powders are typically organic materials with high resistivity, they can easily be charged due to repeated collision and separation of particles along with particle-wall friction in a fluidized bed dryer. This phenomenon, also called “tribocharging”, could adversely affect the process performance. In this work, experiments were conducted to investigate the effects of drying air temperature and drying air velocity on drying performance, as well as electrostatic charges generated during the drying process. Experimental results showed that decreasing the drying air temperature increased the drying time, as expected. The drying rate was observed to be lower at lower operating temperatures. The specific charge of pharmaceutical granules was found to be a function of moisture content and drying air velocity, rather than drying air temperature. With a decrease in moisture content, the specific charge of pharmaceutical granules increased. There was a sudden increase in measured

specific charge when the moisture content decreased to approximately 5 wt. %. In addition, regardless of operating conditions, the charge polarity of granules within the bed at the endpoint of the drying process was positive. The current findings indicate that specific charge is directly indicative of moisture content in the fluidized bed dryer, and monitoring its dynamic changes could be used to monitor the drying process in the pharmaceutical industry.

Keywords: Fluidized bed; Drying; Pharmaceutical granules; Tribocharging

3.2 Introduction

Tablets are the most applicable solid oral drug form in the pharmaceutical industry as they have high manufacturing efficiency and can carry a wide range of doses [1]. A typical tablet manufacturing process involves several steps, among which mixing and granulation have significant importance as having a homogenous mixture is equal to ending up with a high quality product with the correct amount of each component. In order to ensure that each tablet has the exact amount of each ingredient, pharmaceutical powders, which are combination of the active pharmaceutical ingredient (API) and excipients need to be mixed and granulated [2]. Granulation processes can be carried out in either wet or dry form and offers several advantages: i) enhanced flowability and fluidity of granulated particles; ii) improved compressibility of granulated particles; iii) reduction in dust emissions; iv) reduction in segregation; and v) improved content uniformity of particulate substances [3–5]. In wet granulation, the most frequently used granulation process, a non-toxic and volatile liquid binder is added to the well-blended powders [6]. When the wet granulation method is chosen, a drying process is required to remove undesired moisture.

Among different conventional drying methods for particles in the range of 50-2000 μm, fluidized beds are considered to be one of the most suitable methods, especially for wet pharmaceutical granules [3,7]. Compared to other drying methods, fluidized bed drying possesses many advantages, including a high rate of moisture removal, excellent mixing media, rapid heat and mass transfer between phases, large capacity of production and low capital cost [3,7]. In order to determine suitable operation conditions and avoid production losses in a fluidized bed dryer, monitoring the drying process and more importantly, determining the drying endpoint, especially in the pharmaceutical industry, is of great importance. Therefore, some online measurement tools have been developed in attempts to meet stringent product quality assurance in fluidized bed drying. For example, Chaplin et al. [8] applied S-statistic analysis to detect the onset of entrainment when the granule moisture content was approximately 11 wt. %; however, this method was not able to measure the bed moisture content during drying. In a related study, Chaplin and Pugsley [9] applied the same analysis to electrical capacitance tomography (ECT) images in the presence of moisture in a fluidized bed dryer. However, this method is costly and difficult to implement in commercial practice. A technique developed by Tsujimoto et al. [10] employed an acoustic emission sensor in a fluidized bed granulator to detect unstable fluidization conditions, such as channelling and blocking, resulting from excessive increases in solids moisture content. However, significant changes in the mean acoustic emission amplitude would require moisture levels higher than 15 wt. %. Therefore, this method could not be used for adequate measurements of solids moisture with a desired endpoint of approximately 2 wt. % for typical pharmaceutical applications. Near-infrared (NIR) spectroscopy has been used to monitor

drying by measuring the moisture content of wet granules in fluidized beds, but this method requires a clear path between NIR sensors and granules to be measured, as particulates can adhere to sensor tips installed in the bed [11]. Recently, Briens and Bojarra [3] used vibration and passive acoustic emission measurements to complement current methods to indicate an endpoint of drying. Again, this method does not directly monitor moisture content and drying profile. Acoustic emissions are also influenced by many other process-related sources. Given the widespread application of fluidized bed dryers in industry, new online monitoring of the drying process is needed to maintain the desired fluidization state and to control the endpoint of the drying process. Once such a new tool is available, fluidizing gas velocities can be optimized to shorten the drying time and product losses associated with attrition and entrainment can be minimized [3].

In gas-solid fluidized beds, charge generation is generally a concern, as it usually has an adverse impact on process performance. In general, electrostatic charges are generated when two different materials are brought into contact and then separated [12]. In fluidized beds, repeated collision and separation of particles along with inter-particle and particle-wall friction will result in unavoidable electrostatic charge generation known as tribocharging [13–15]. Pharmaceutical powders by their very nature are mainly insulators with volume resistivity greater than 10^{13} Ω.m, which prevents the charge transferred in contact from leaking back [16,17]. Notable changes in gas-solid fluidized bed hydrodynamics, segregation of particles, variability in the proportions of API and excipients and subsequent reduction in fill and uniformity, adhesion of particles to the wall surface, and electrostatic discharge are generally the problems associated with tribocharging [1,14,15,18].

In the literature, most studies on tribocharging of pharmaceutical powders have been conducted individually in their dry form and only a few works were carried out in a fluidized bed [1,12,19–21]. A comprehensive understanding of the tribocharging behaviour of pharmaceutical granules in fluidized bed dryers is lacking, and this is impeding the development of a novel economic and robust technique utilizing this feature. Therefore, an advanced understanding of tribocharging behaviour in fluidized bed dryers is required to develop online monitoring of the drying process and to prevent any potential risk of static electrical discharges. In addition, limited drying data on fluidized bed drying having application to the pharmaceutical industry was available. Therefore, the objectives of the present study were to investigate the tribocharging behaviour of pharmaceutical granules in a fluidized bed dryer, and to understand the drying kinetics under various operating conditions of relevance to current pharmaceutical industry operations.

3.3 Materials and Methods

3.3.1 Materials and Wet Granule Preparation

Detailed properties along with the compositions of powders used in the wet granule formulation are shown in Table 3.1. The compositions are provided on their dry basis.

For preparing a batch of 1 kg of wet granules with a moisture content of approximately 30 wt. % (wet basis), dry ingredients were mixed in a 250 W low-shear granulator (Kitchen-Aid classic mixer) for 2 minutes at the lowest speed (setting 1) followed by continuous water addition over a five-minute period at a constant rate of 59.5 mL/min [8]. Afterward, a post-granulation step was carried out for 2 minutes at a higher speed (setting 2 on the mixer) [8].

The granulation product was then sieved through a 3.36 mm screen (mesh No. 6 in US Standard with an opening of 0.132 inches) in order to remove large granules that formed due to poor granulation and also to break up any loosely formed agglomerates. This process was repeated two more times to produce 3 kg of wet particles in total.

Table 3.1
Wet granule formulation along with particle properties [9]

Component	**Percentage by mass (dry basis)**	**Supplier**	**Size (D_{50}) µm***
Lactose Monohydrate (LMH) (filler)	50%	Foremost Farms	55
Microcrystalline Cellulose (MCC) (filler)	44%	FMC BioPolymers	106
Hydroxypropyl Methylcellulose (HPMC) (binder)	4%	DOW Chemical Company	72
Croscarmellose Sodium (disintegrant)	2%	FMC BioPolymers	41
Water (reverse osmosis)	42%		

*Measured by particle size analyzer (Malvern Mastersizer 2000 S Long Bench)

3.3.2 Fluidized Bed Dryer, Instrumentation and Drying Experiments

The fluidized bed drying apparatus is shown in Figure 3.1 with detailed dimensions of the product bowl presented in Figure 3.2. The product bowl was loaded with a batch of 3 kg of wet granules. In order to measure moisture content and the specific charge of granulated particles, samples of approximately 6 g at discrete time intervals (dependent on the drying conditions) were taken via a sample thief as shown in Figure 3.1. Half of the sample was used to determine the moisture content using a drying balance (HB43, Mettler-Toledo, USA), and the rest was used to measure specific charge using a Faraday cup connected to an electrometer (6514, Keithley, USA). Figure 3.2 shows the position of the sample thief as well as the dimensions of the product bowl and bed heights for a 3-kg batch.

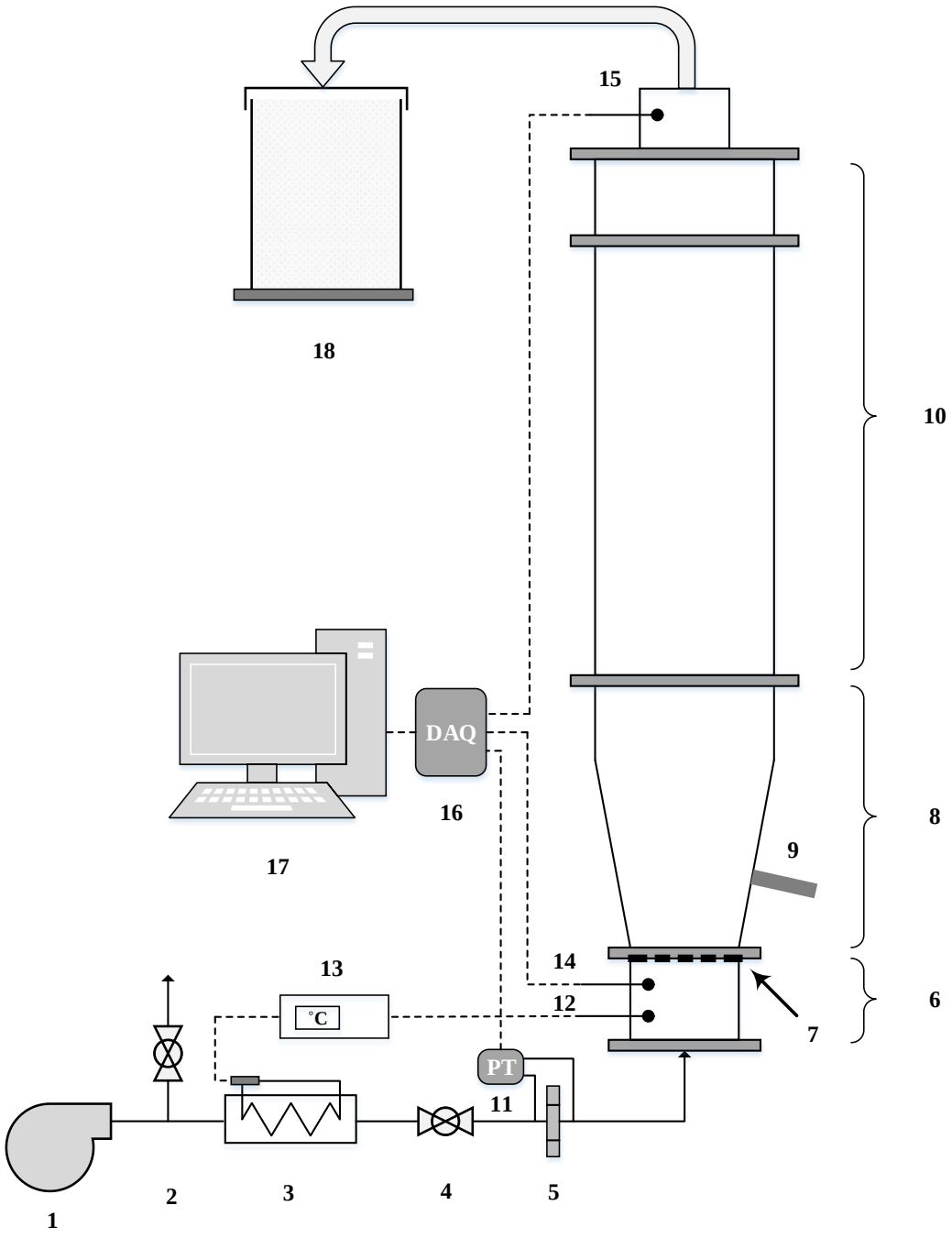

Figure 3.1 Components and instrumentation of the fluidized bed dryer apparatus. (1) Blower, (2) air bypass, (3) air heater, (4) ball valve to control air flow (5) orifice plate, (6) windbox, (7) gas distributor, (8) product bowl, (9) sample thief, (10) freeboard, (11) pressure transducer, (12) inlet air thermocouple, (13) air heater controller, (14) inlet air thermocouple and RH meter, (15) outlet air thermocouple and RH meter, (16) data acquisition card, (17) computer, (18) bucket for collecting entrained fine particles

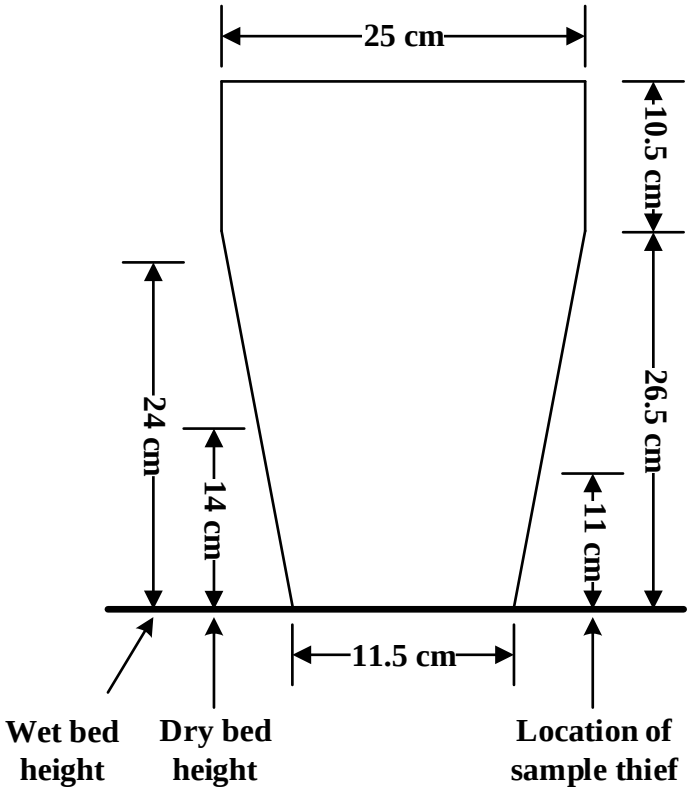

Figure 3.2 Product bowl dimensions along with the location of sample thief and bed height for a 3-kg batch

The distributor plate used in the fluidized bed was constructed of a 1.5 mm thick aluminum plate drilled with 2 mm diameter holes, giving an open area ratio of 5.6 % [8]. A 1.53 m tall cylindrical acrylic freeboard section was flange-connected to the top of the product bowl. Fluidizing air was supplied by a rotary blower (SCL V4, Effepizela, Italy) and heated by an electrical heater (BEN24G6S, Watlow, USA). The air temperature was controlled by a temperature controller (CN7500 series, Omega, USA) with feedback provided by a grounded type-K thermocouple inserted into the windbox. The temperature in the windbox was set at different values ranging from 38 °C to 75 °C. The relative humidity and temperature of the inlet fluidizing air was measured using a humidity and temperature sensor (HTM2500LF, Measurement Specialties, USA). The temperature and relative humidity of the outlet air in the

freeboard was monitored and recorded by a temperature and relative humidity transmitter (HX93BDV2-RP1, Omega, USA).

Metering of the air supply was done using an orifice plate. The pressure drop across the orifice was measured using a differential pressure transducer (PX137-0.3DV, Omega, USA) calibrated with a U-tube manometer. Air velocity could be manually controlled using a bypass valve located immediately downstream of the blower and a ball valve located between the heater and the orifice plate.

Data from all sensors during the test period were recorded at a sampling rate of 160 Hz using a data acquisition card (DT 9829, Data Transformation, USA).

A unique characteristic of the fluidized bed dryer used in this study is its conical geometry. This kind of design promotes solid circulation inside the bed due to the transport of particles by the fluidizing gas in the central region and a return of solids to the bottom of the unit near the walls [22].

3.3.3 Drying Data Analysis

In this study, Fick's second law of diffusion was used to determine the effective moisture diffusion coefficient [23]:

$$\frac{\partial X}{\partial t} = D_{eff} \nabla^2 X \tag{3.1}$$

where X is the local moisture content on a dry basis ($kg_{water}/kg_{dry\text{-}solid}$) and D_{eff} is the effective diffusion coefficient (m^2/s). Assuming that granulated particles are spherical, the mathematical solution of Eq. (3.1) in the spherical coordinate is given by [7,23,24]:

$$MR = \frac{X - X_{eq}}{X_0 - X_{eq}} = \frac{6}{\pi^2} \sum_{n=1}^{\infty} \frac{1}{n^2} \exp\left[-n^2 \frac{\pi^2 D_{eff} t}{r^2}\right] \quad (3.2)$$

where MR is the moisture ratio (dimensionless), X_0 is the initial moisture content, X_{eq} is the equilibrium moisture content, r is radius of granules (m), t is time (s) and n is a positive integer. Eq. (3.2) can be used to calculate D_{eff} when there is negligible shrinkage in particles, uniform initial moisture distribution and constant moisture diffusivity throughout the whole process [25]. At a sufficiently long drying time, Eq. (3.2) can be further simplified to the following equation by taking only the first term in the series expansion into account [22,24,25]:

$$MR = \frac{6}{\pi^2} \exp\left(-\frac{\pi^2 D_{eff} t}{r^2}\right) \quad (3.3)$$

If the geometric mean diameter (2r) of granules is known, D_{eff} can be determined by plotting ln(MR) versus time. Effect of drying temperature on effective moisture diffusion coefficient can be correlated according to the Arrhenius-type equation [25]:

$$D_{eff} = D_0 \exp\left(-\frac{E_a}{RT}\right) \quad (3.4)$$

where D_0 is the pre-exponential factor of the Arrhenius equation (m^2/s), E_a is the activation energy (J/mol), R is the universal gas constant (8.314 J/mol/K), and T is the absolute

temperature (K). Subsequently, activation energy is determined by plotting ln(D_{eff}) against reciprocal of T.

3.4 Results and Discussion

3.4.1 Drying Experiments

It can be seen in Figure 3.3 that when the temperature of the drying air increased, the moisture content of wet granules dropped more rapidly. At a drying air velocity of V=1.0 m/s, it took about 120 minutes to reach a moisture content of approximately 5 wt. % at T=38 ˚C, whereas the drying time was reduced to less than 60 minutes at T=75 ˚C. Similar trends can be found at the two other velocities (V=1.4 m/s and 1.8 m/s) in Figures 3.3(b) and 3.3(c).

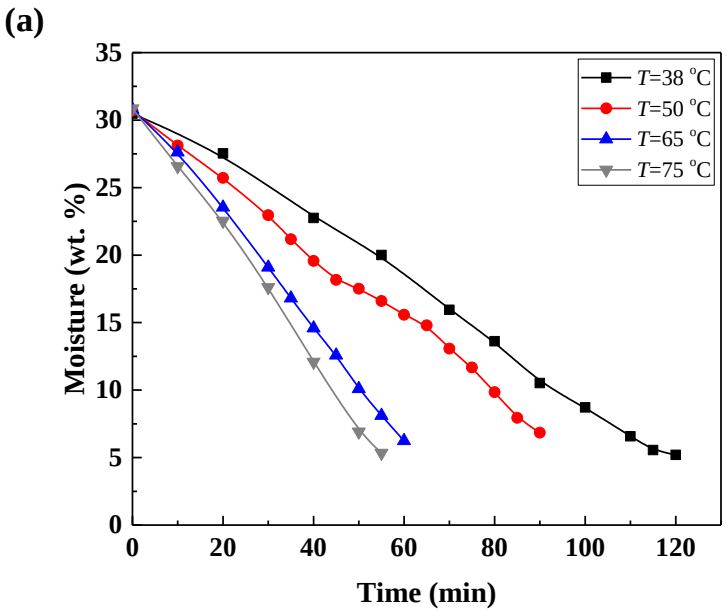

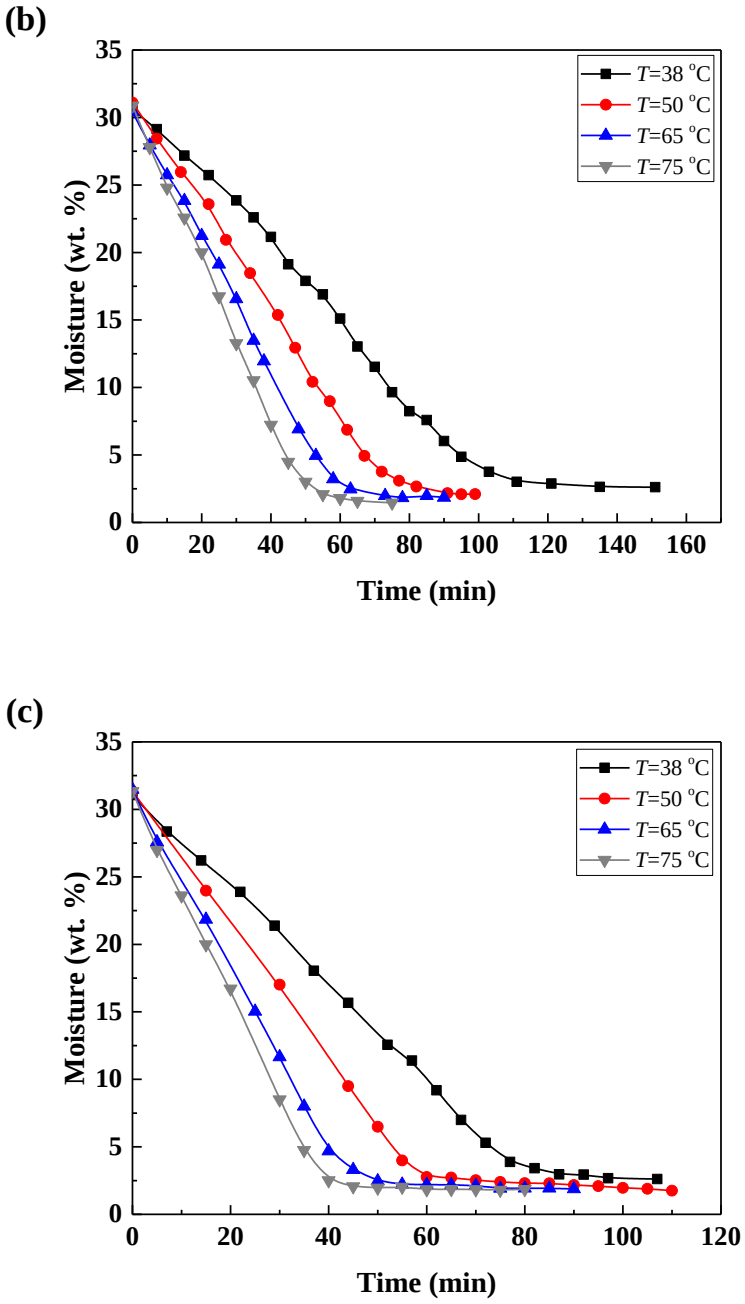

Figure 3.3 Dynamic profiles of granule moisture content for four temperatures at three drying air velocities: (a) V=1.0 m/s, (b) V=1.4 m/s, (c) V=1.8 m/s

The effect of drying air velocity on the moisture content of granules at different temperatures is shown in Figure 3.4.

(a)

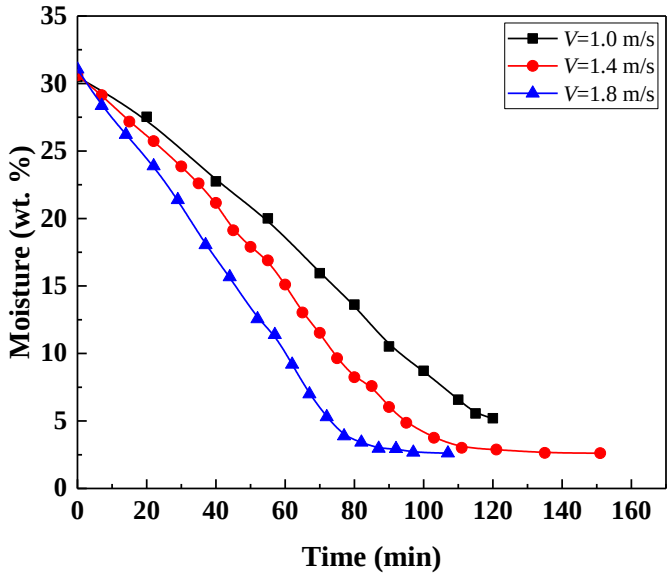
V=1.0 m/s
V=1.4 m/s
V=1.8 m/s
Moisture (wt. %)
Time (min)
0
5
10
15
20
25
30
35
0
20
40
60
80
100
120
140
160

(b)

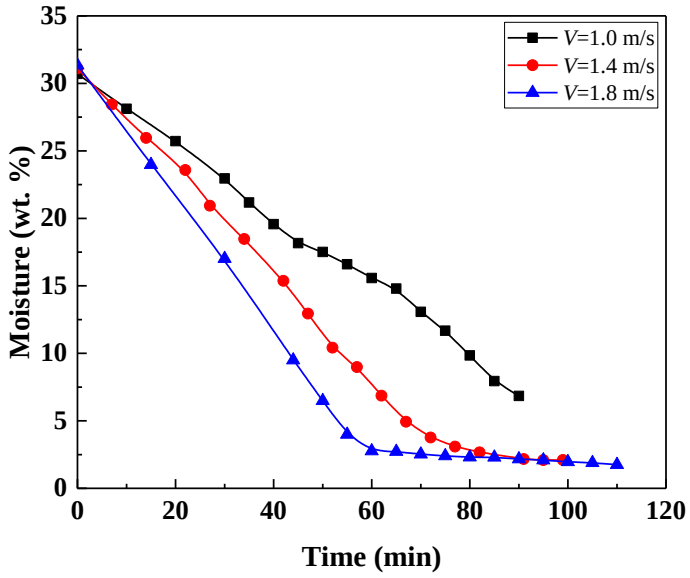
V=1.0 m/s
V=1.4 m/s
V=1.8 m/s
Moisture (wt. %)
Time (min)
0
5
10
15
20
25
30
35
0
20
40
60
80
100
120

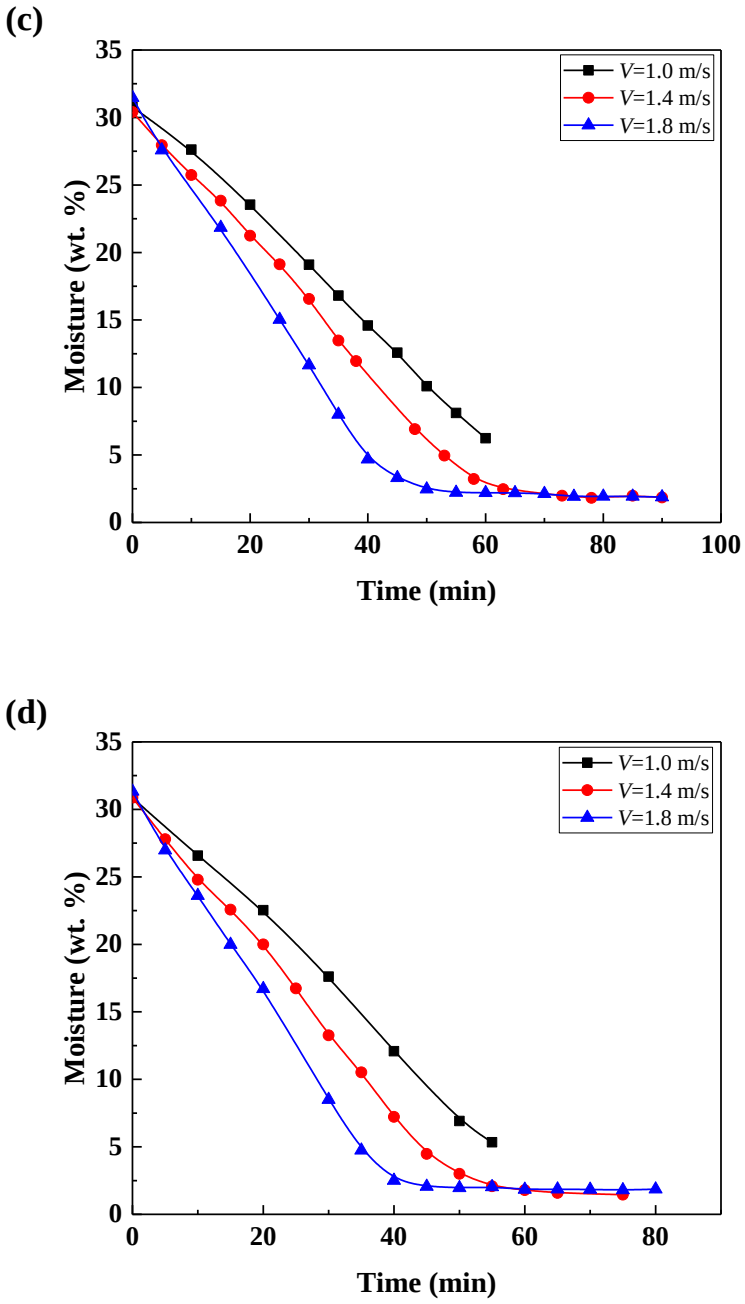

Figure 3.4 Dynamic profiles of granular moisture content for three drying air velocities at four temperatures: (a) T=38 ˚C, (b) T=50 ˚C, (c) T=65 ˚C, (d) T=75 ˚C

It can be clearly seen in Figure 3.4 that increasing the drying air velocity, increases the drying rate and decreases the time required to reach the moisture content of approximately 2 wt. %.

Figures 3.3 and 3.4 clearly illustrate the reduction in the moisture content of granules from an initial moisture content of approximately 30 wt. % to a final moisture content of approximately 2 wt. %. Depending on the application of the final product being produced in the pharmaceutical industry as well as the thermal sensitivity of the API used, the desired final moisture content varies between 2 - 5 wt. % [3,8,27]. As can be seen in Figure 3.3, the rate of moisture removal from granules continuously increased by increasing the drying air temperature. Also, Figure 3.4 indicates a decrease in the drying time with an increase in the drying air velocity. Aside from the reduced drying time as a result of increased drying temperature, there is a slight reduction in the equilibrium moisture content (EMC) of granulated particles (EMC of 2.6, 2, 1.9, and 1.8 wt. % at 38, 50, 65, and 75 ˚C, respectively). However, the increased drying air velocity only reduced the required drying time and did not show any impact on the equilibrium moisture content. This observation could be explained by the fact that the dominant mass transfer mechanism in the falling rate period is molecular diffusion inside the granules, which only drying air temperature influences, with the drying air velocity having a minimal effect. In addition, it can be seen in both Figures 3.3 and 3.4 that the constant rate period (moisture content from approximately 30 wt. % to 5 wt. %) occurs over a significant portion of the whole drying process.

The mean particle diameter of granulated powders was found to be 212 μm for samples collected under different operating conditions. Based on this value, the effective moisture

diffusion coefficient (D_{eff}) can be estimated by a plot of ln(MR) against time. The resultant effective diffusion coefficients under different operating conditions are presented in Table 3.2. The results reveal that both drying air velocity and temperature directly affect the effective moisture diffusion coefficient. Higher air velocity and higher drying temperature led to an increase in D_{eff}. Effect of drying air temperature on D_{eff} at higher drying air velocities was more significant compared to lower air velocities. In practice, the Arrhenius-type equation (Eq. 3.4) is used to correlate the effect of drying air temperature. Figure 3.5 shows that the Arrhenius-type equation can satisfactorily relate the effective moisture diffusion coefficient to the drying air temperature.

A relatively low value for R^2 at the lowest drying air velocity was observed and this might be due to poor fluidization with the occurrence of channeling at this drying air velocity which will result in data with relatively high error. Channeling in fluidized bed drying results from dominant cohesive forces exerted by the wetted surface of granules, especially at the beginning of the drying process, and particularly at low drying velocities [7].

The activation energy (E_a) and the Arrhenius coefficient (D_0) for each drying air velocity also are given in Table 3.2. In drying processes, the E_a value represents how strong the water is bound to the material structure; thus, the higher the E_a, the stronger is the bonding [28]. In this work, activation energy had an average value of 19.5 kJ/mol, although it changed slightly with varying drying air velocities. D_0 can be interpreted as the effect of drying air velocity on D_{eff}. As can be seen in both Table 3.2 and Figure 3.5, D_0 increases as the drying air velocity increases, and there was no linear relationship between these two parameters. Therefore, it can be expected that increasing the drying air velocity further might not have a significant effect

on drying performance, but could cause entrainment of fine particles as well as high charge build-up inside the bed, which will be discussed in the following section.

Table 3.2
Effective moisture diffusion coefficient (D_{eff}) along with Energy of activation E_a and Arrhenius coefficient D_0

Drying air condition		$D_{eff} \times 10^{13}$ (m^2/s)	E_a (kJ/mol)	$D_0 \times 10^{10}$ (m^2/s)	R^2
V **(m/s)**	***T*** **(˚C)**				
1.0	38	2.50	18.27	2.44	0.7289
	50	2.05			
	65	3.64			
	75	4.90			
1.4	38	5.12	19.50	9.02	0.8061
	50	7.06			
	65	8.42			
	75	9.22			
1.8	38	7.06	20.19	17.55	0.9986
	50	9.68			
	65	13.09			
	75	16.39			

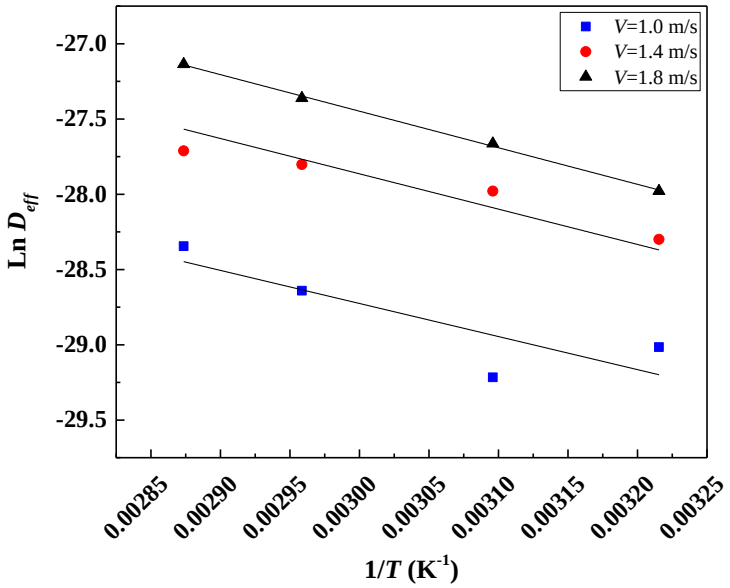

Figure 3.5 Effect of drying air temperature on effective diffusion coefficient

3.4.2 Tribocharging Phenomenon During Drying Processes

As stated earlier, tribocharging is an unavoidable phenomenon in particle handling processes due to repetitive interparticle and particle-wall collisions. Gas-solid fluidization, by its very nature, is categorized in the particle processing which makes tribocharging inevitable. Variations in specific charge as the drying process progressed at drying air velocities of 1.4 m/s and 1.8 m/s are provided in Figures 3.6 and 3.7, respectively. For each drying velocity, experiments were performed at four temperatures. For evaluating experimental error in specific charge measurements, the experiments at the drying air temperature of 65 ˚C were carried out for three times. Error bars are provided in Figures 3.6(c) and 3.7(c), and relative errors are 10.9 % and 14.0 % for V=1.4 m/s and V=1.8 m/s, respectively. It is worth mentioning that drying curves at these experiments were almost identical with relative error of only 2.35 % under the repeated experimental conditions.

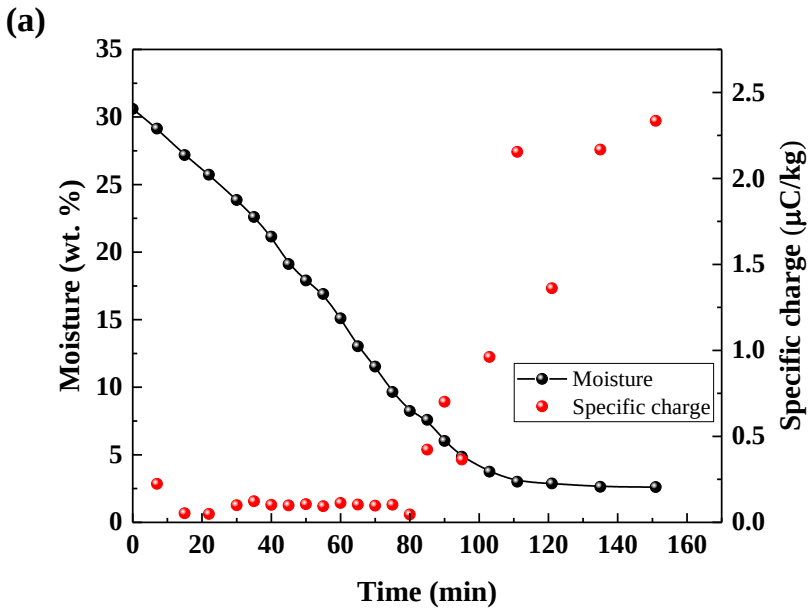

(b)

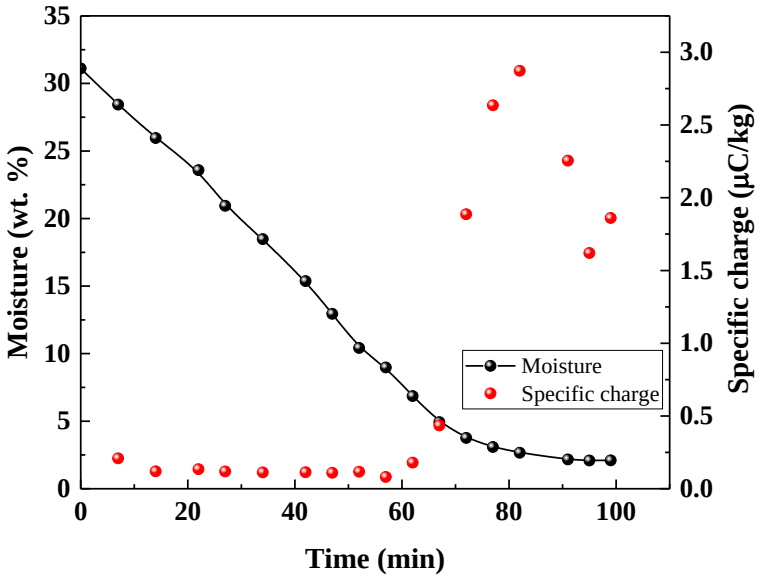
Moisture (wt. %)
Specific charge (μC/kg)
Time (min)
Moisture
Specific charge

(c)

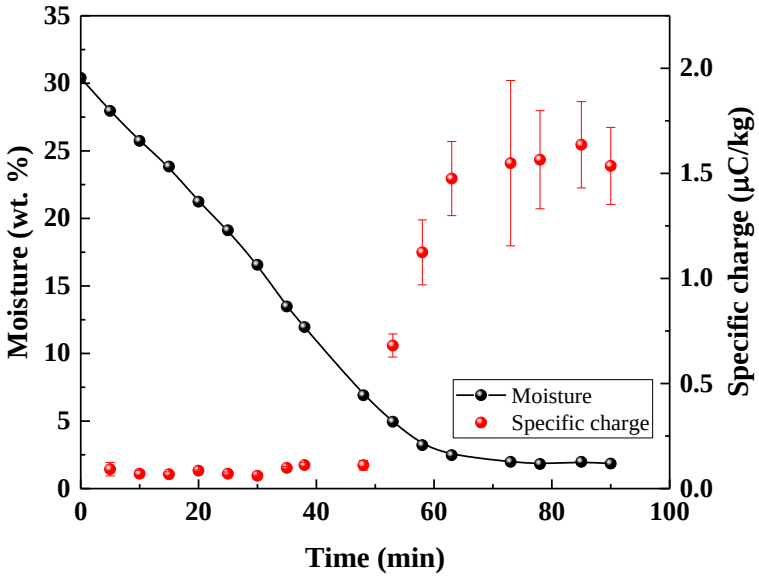
Moisture (wt. %)
Specific charge (μC/kg)
Time (min)
Moisture
Specific charge

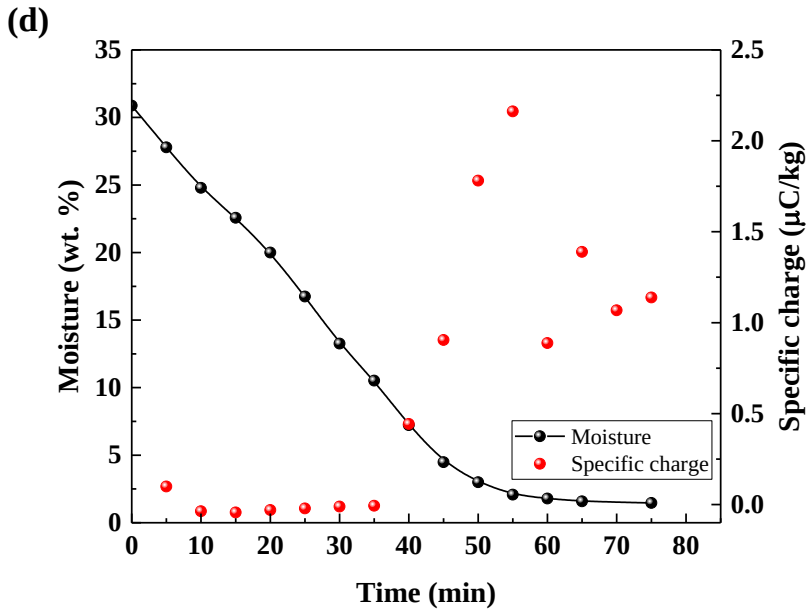

Figure 3.6 Variation of specific charge with drying time at a drying air velocity of 1.4 m/s: (a) *T*=38 ˚C, (b) *T*=50 ˚C, (c) *T*=65 ˚C, (d) *T*=75 ˚C

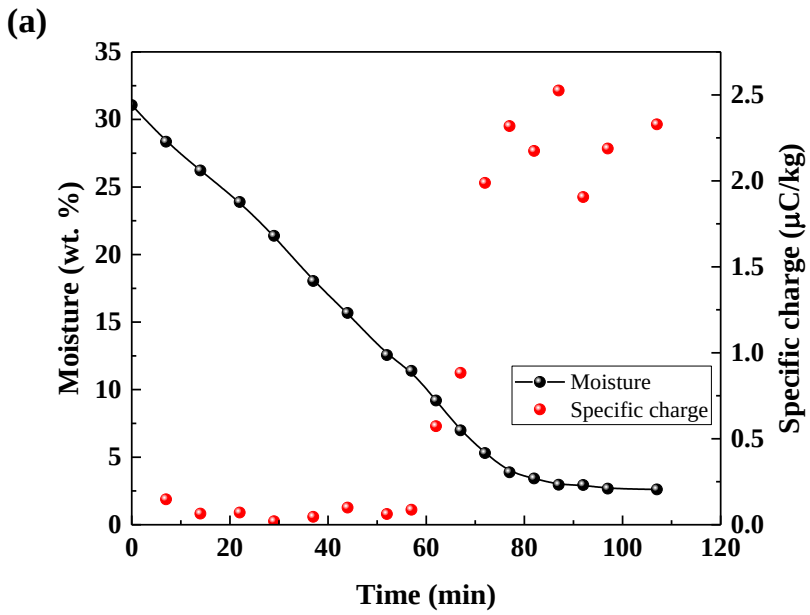

(b)

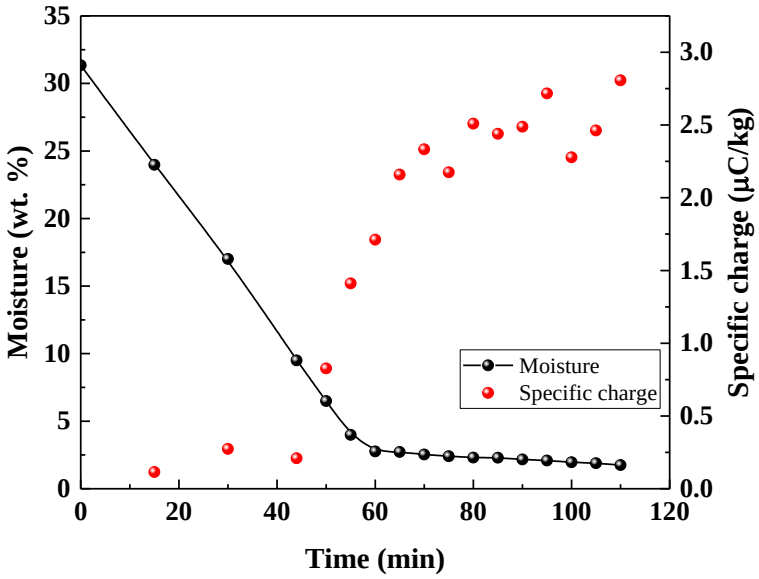
Moisture (wt. %)
Specific charge (μC/kg)
Time (min)
Moisture
Specific charge

(c)

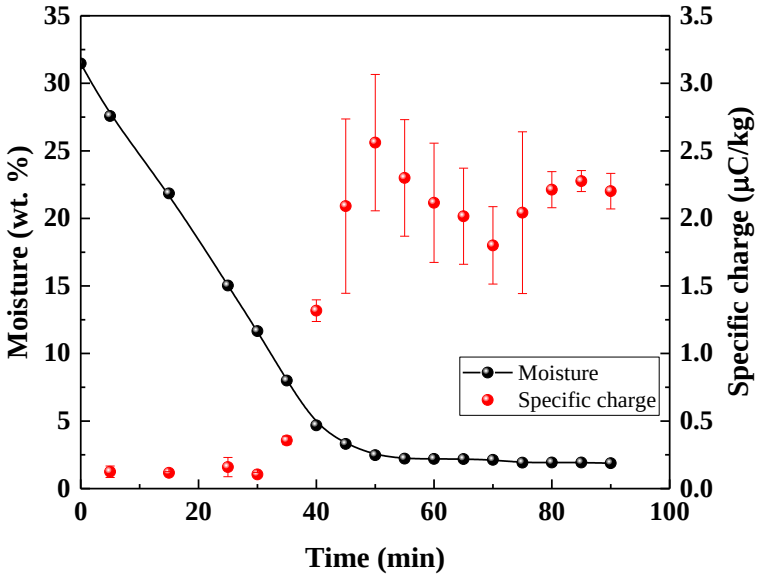
Moisture (wt. %)
Specific charge (μC/kg)
Time (min)
Moisture
Specific charge

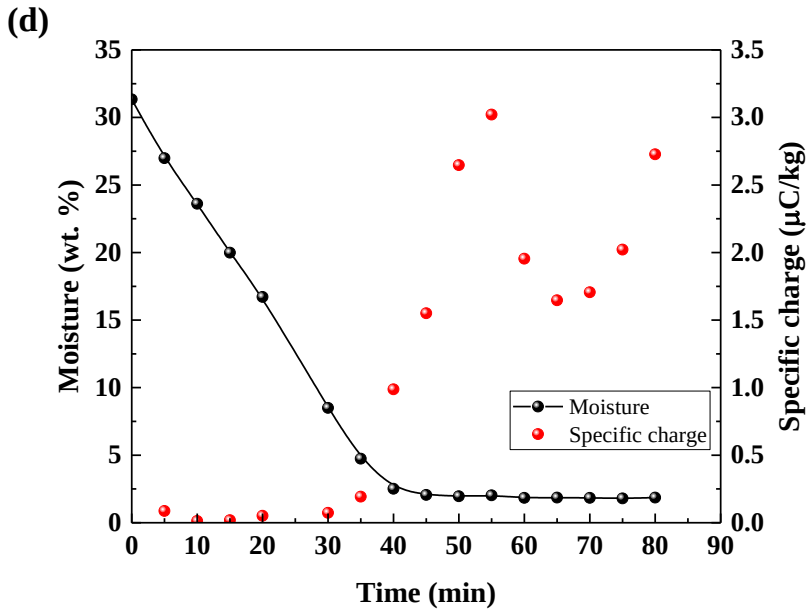

Figure 3.7 Variation of specific charge with drying time at a drying air velocity of 1.8 m/s: (a) *T*=38 ˚C, (b) *T*=50 ˚C, (c) *T*=65 ˚C, (d) *T*=75 ˚C

As can be clearly seen in Figures 3.6 and 3.7, the specific charge did not change at the beginning of the drying process until the moisture content was reduced to the critical moisture content (CMC). Interestingly, under all operational conditions, regardless of drying air velocity and temperature, the specific charge started to increase at a moisture content of approximately 7 wt. %, and reached its highest value at approximately 2 wt. % the moisture content (equilibrium moisture content). This can be explained by that at moisture contents above the CMC where the surfaces of granules are covered with water, there would not be significant charge build-up and all of the generated electrostatic charges would be quickly dissipated due to the low resistivity of water. As the moisture content reached the CMC (approximately 5 – 7 wt. %), granules would start to lose their surface moisture and their surfaces become drier. Therefore, electrostatic charges started to accumulate at the surfaces of granules. After passing the CMC and reaching the equilibrium moisture content

(approximately 2 wt. %) the specific charge reached its equilibrium value. This is because when granules are losing their moisture content and becoming dry, their volume resistivity starts to increase and subsequently reaches the highest value as the granules are considered dry [29,30]. In a separate work, it was found that the volume resistivity of granules increased with a decrease in moisture content. When the moisture content dropped below 5 wt. %, the volume resistivity increased by the order of 10^6 [31]. Detailed discussion on volume resistivity is presented in Chapter 4. This change is consistent with the change observed in specific charge. A clearer relationship between moisture content and specific charge is provided in Figure 3.8. From this figure, it can be seen that a sharp change in the specific charge occurred when the moisture content decreased below 10 wt. %.

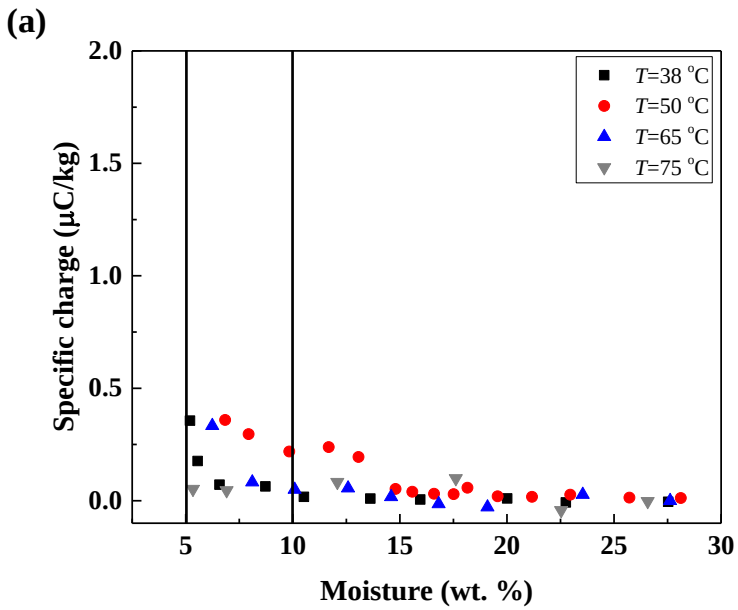

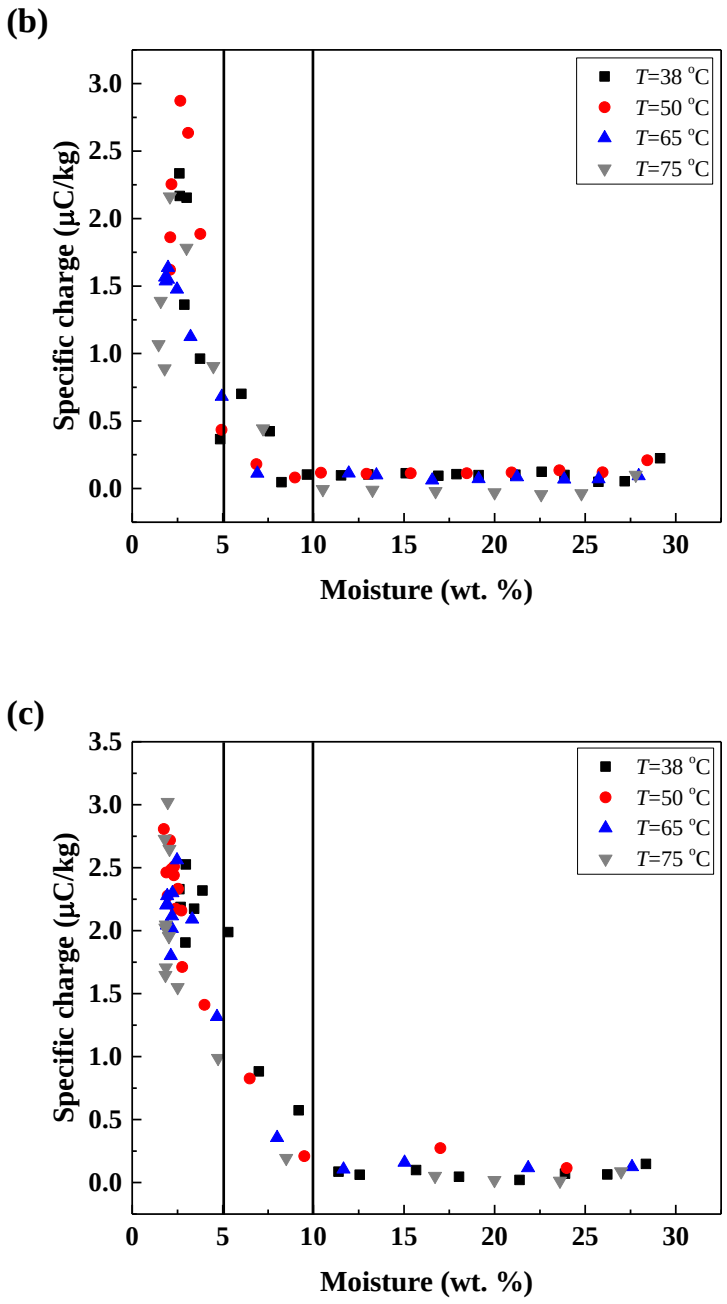

Figure 3.8 Specific charge against moisture content at three drying air velocities: (a) *V*=1.0 m/s, (b) *V*=1.4 m/s, (c) *V*=1.8 m/s

In practice, one of the methods for monitoring the drying process in a fluidized bed dryer is to measure the outlet air temperature or relative humidity (RH) [3]. Figure 3.9

provides representative dynamic profiles of electrostatic charge generation and outlet air temperature and *RH* at a drying air velocity of 1.4 m/s and drying air temperature of 65 ˚C over the course of the drying process. It can be seen from this figure that both the outlet air temperature and *RH* remain constant at the constant rate period of the drying process, indicating a constant rate period. Then, the outlet air *RH* starts to decrease and the outlet air temperature increases, indicating a falling rate period as the surface of the granules becomes dry. Clearly shown in this figure, the specific charge begins to increase at the same time. Therefore, monitoring the electrostatic charge generated in the bed can be considered an accurate alternative method in determining the endpoint of the drying process.

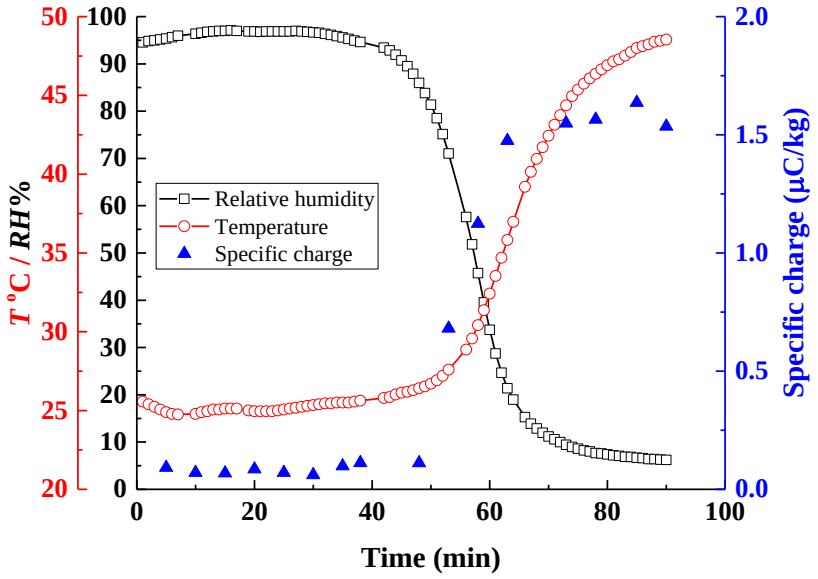

Figure 3.9 Dynamic changes in specific charge, outlet air temperature and relative humidity at a drying air velocity of 1.4 m/s and a drying air temperature of 65 ˚C

3.4.2.1 Effect of Drying Air Velocity on Tribocharging

The effect of fluidizing air velocity on tribocharging behaviour of granules at four temperatures is shown in Figure 3.10. The *RH* of the drying air at the inlet was found to range from 2.2 % to 9.8 %, depending on the inlet air temperature. A comparison of the specific charge of granules at different air velocities is shown in Figure 3.10.

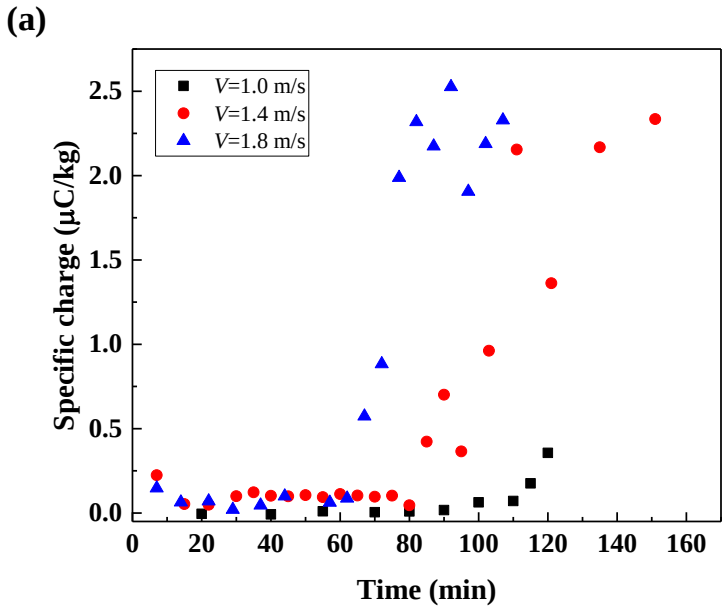

(b)

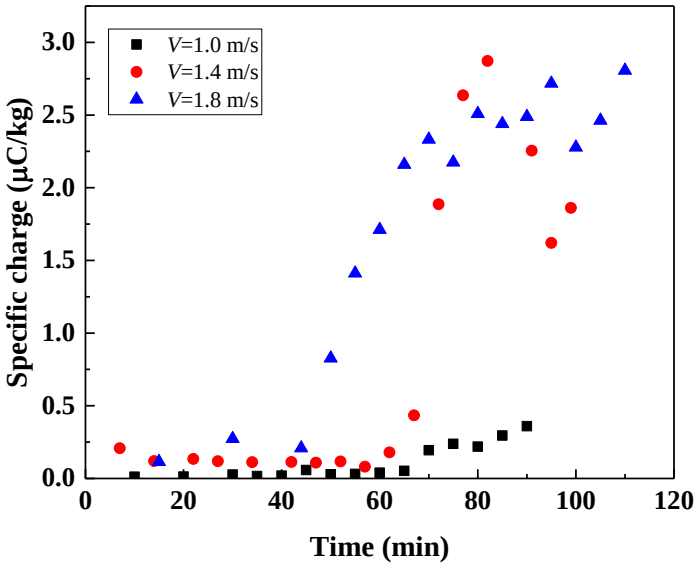
V=1.0 m/s
V=1.4 m/s
V=1.8 m/s
Specific charge (μC/kg)
Time (min)
0.0
0.5
1.0
1.5
2.0
2.5
3.0
0
20
40
60
80
100
120

(c)

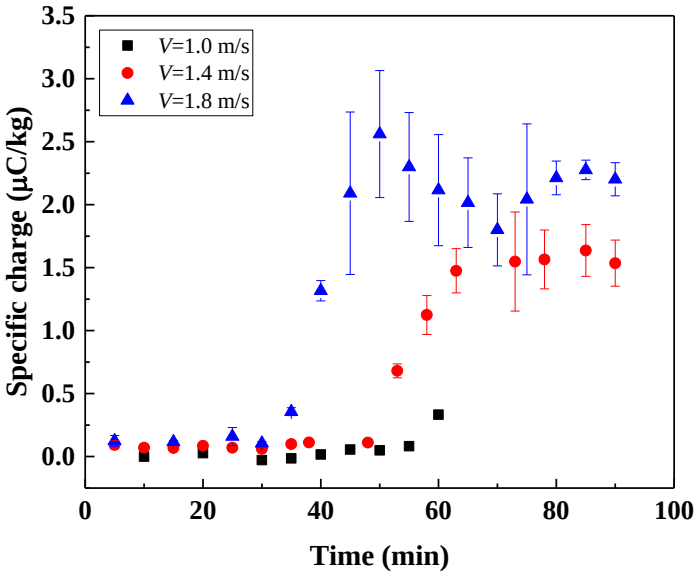
V=1.0 m/s
V=1.4 m/s
V=1.8 m/s
Specific charge (μC/kg)
Time (min)
0.0
0.5
1.0
1.5
2.0
2.5
3.0
3.5
0
20
40
60
80
100

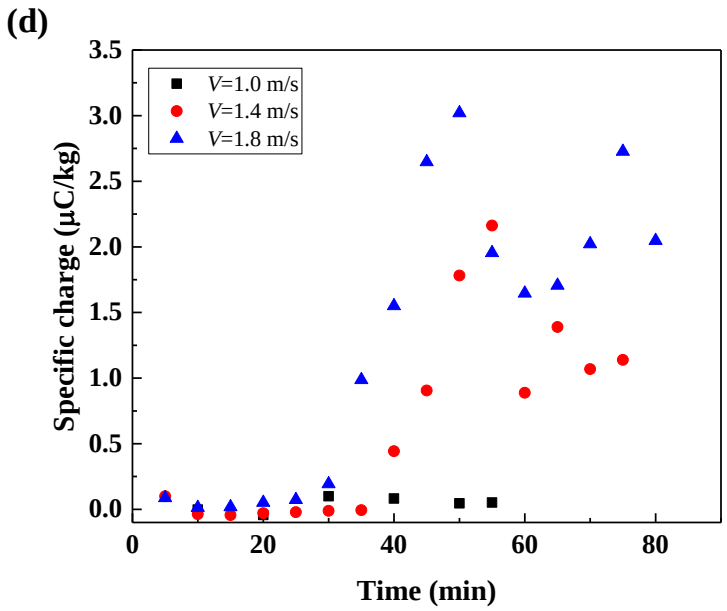

Figure 3.10 Effect of fluidizing air velocity on the specific charge of granules at four temperatures: (a) *T*=38 ˚C, (b) *T*=50 ˚C, (c) *T*=65 ˚C, (d) *T*=75 ˚C

It can be seen that a higher fluidizing velocity resulted in a higher specific charge. This effect was more obvious when the drying process entered the falling rate period (granules became dry on their surface) and the average specific charge of granules in the bed increased markedly as the fluidizing air velocity increased. In contrast, the specific charge of granules was generally low in the constant rate period where moisture at the surface of granules facilitated charge dissipation, preventing charge build-up. As a result, no difference was observed in specific charge at different velocities during this period of the drying process. In general, increasing fluidizing velocities led to an increase in the frequency as well as the intensity of interparticle and particle wall collisions, which resulted in more charges generated [32]. More entrained fine particles in the upper section of the fluidized bed at high velocities could be another contributing factor. At the end of the drying process, fine particles were collected from the wall in the upper section of the bed and their specific charge was measured.

In general, fine particles were found to carry a negative charge, with the specific charge an order of magnitude higher than that of particles from the dense bed. These findings are consistent with those reported in previous works [13,34,35].

3.4.2.2 Effect of Drying Air Temperature on Tribocharging

In principle, electrons transfer between materials because of differences in their Fermi energy levels, which will lead to different work functions (for conductive materials) or ion potentials (for non-conductive materials) [32]. A change in temperature, therefore, can either facilitate or hinder the movement of electrons between material surfaces. Some studies have been done to investigate the effect of temperature on the tribocharging behaviour of materials [13,34,36]. Moughrabiah et al. [13] found that increasing the temperature had a reverse effect on electrostatic charge generation of linear low-density polyethylene (LLDPE) particles in a fluidized bed. It has been found that increasing the fluidizing air temperature led to a decrease in electrostatic charge generation. The same trend was observed in a related study on glass beads [34]. It was found that specific charge decreased and finally its polarity changed as the temperature increased. In another study, Greason [36] found that increasing the temperature resulted in a decreased electrostatic charge of metal spheres. However, based on the work done by Ireland [20,21] on silica particles, Karner and Urbanetz [17] suggested that an increase in the temperature of silica particles can reduce their work function and, subsequently, increase the electrostatic charge.

In this work, a comparison of specific charge at different air temperatures was conducted and the results are shown in Figure 3.11.

(a)

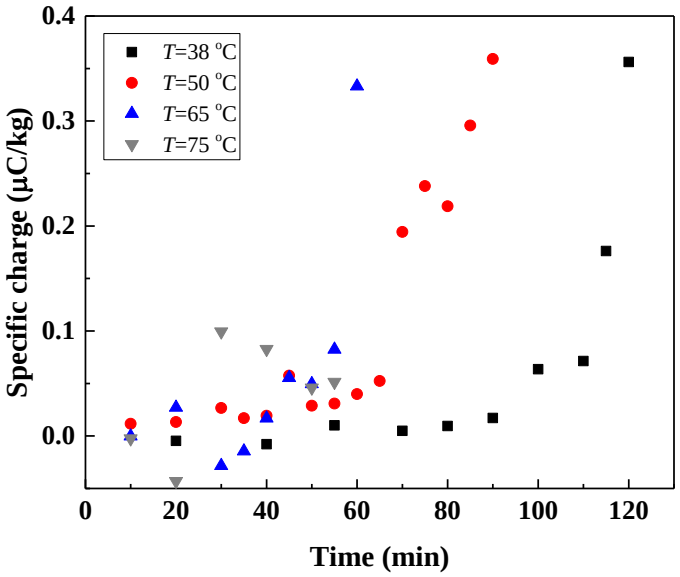
T=38 °C
T=50 °C
T=65 °C
T=75 °C
Specific charge (μC/kg)
Time (min)
0.0
0.1
0.2
0.3
0.4
0
20
40
60
80
100
120

(b)

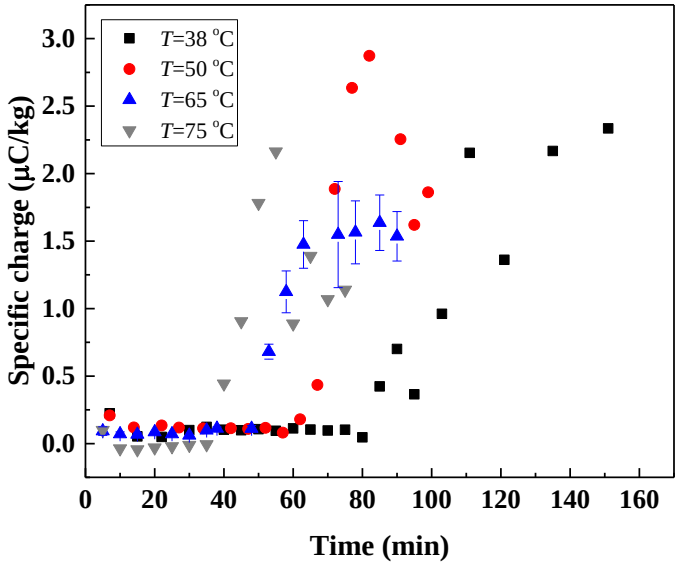
T=38 °C
T=50 °C
T=65 °C
T=75 °C
Specific charge (μC/kg)
Time (min)
0.0
0.5
1.0
1.5
2.0
2.5
3.0
0
20
40
60
80
100
120
140
160

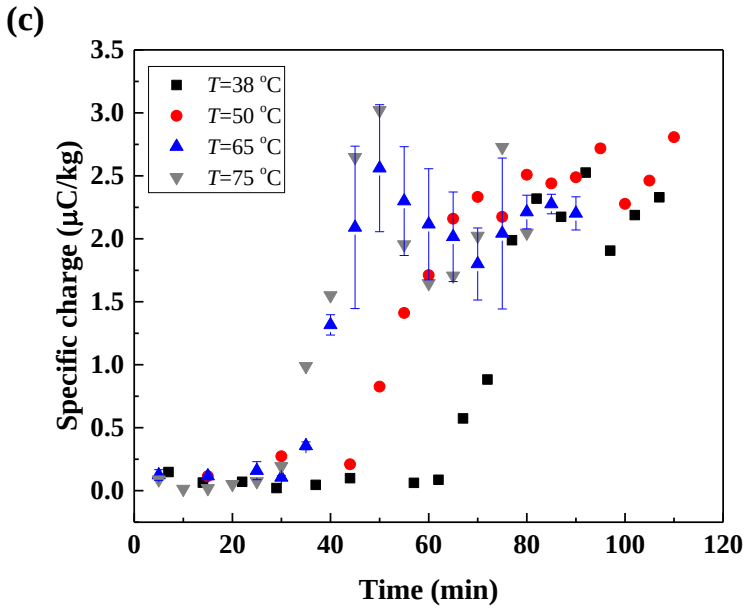

Figure 3.11 Effect of drying air temperature on tribocharging behaviour of granules: (a) V=1.0 m/s, (b) V=1.4 m/s, (c) V=1.8 m/s

In general, the specific charge was not found to be a function of drying air temperature under the studied operating conditions. At the same drying air velocity, granules possessed nearly the same specific charge at the endpoint of the drying process, although some fluctuations were observed. At V=1.4 m/s, the average specific charge was approximately 2.0 μC/kg whereas it increased to approximately 2.5 μC/kg when V=1.8 m/s. Again, this figure also shows that there was no significant charge generated during the constant rate period of the drying process where there is still considerable moisture content at the surface of the granules, and the relative humidity of the air inside the bed also was high.

3.5 Conclusions

In this work, drying performance and tribocharging behaviour of pharmaceutical granules in a conical fluidized bed dryer was studied under various operating conditions.

Experimental results clearly showed that increasing the drying air temperature and velocity shortened the drying time, as expected. The effective diffusion coefficient of moisture in granules was evaluated and the effect of temperature was correlated by the classical Arrhenius equation. A marked increase in effective diffusion coefficient was observed as the drying air velocity or temperature increased.

It also was found that the activation energy was around 19.5 kJ/mol and was not influenced by drying air temperature or drying air velocity under the conditions investigated. However, the Arrhenius constant increased with an increase in drying air velocity, but no linear relationship was observed between the two parameters. In addition, a higher drying velocity would result in more entrained fine particles. Therefore, the optimum drying air velocity needs to be employed in the drying process.

The specific charge of granules was monitored throughout the drying process. It was found that the specific charge of granules started to increase when the moisture content was reduced to approximately 10 wt. % regardless of the drying air temperature and drying air velocity used. This could be attributed to surface moisture changes, i.e. as the surface of granules began to lose moisture, charge accumulation appeared. At the endpoint of the drying process, an equilibrium specific charge was observed. The equilibrium specific charge was a function of drying air velocity, whereas the drying air temperature did not show a significant impact on the specific charge under the experimental conditions investigated. Finally, the current results indicate that charge measurement could be used to determine the endpoint of the drying process for pharmaceutical powders.

3.6 Acknowledgments

The authors gratefully acknowledge financial support from NSERC and the University of Saskatchewan.

3.7 References

[1] E. Šupuk, A. Zarrebini, J.P. Reddy, H. Hughes, M.M. Leane, M.J. Tobyn, et al., Tribo-electrification of active pharmaceutical ingredients and excipients, Powder Technol. 217 (2012) 427–434. doi:10.1016/j.powtec.2011.10.059.

[2] T.A.H. Simons, S. Bensmann, S. Zigan, H.J. Feise, H. Zetzener, A. Kwade, Characterization of granular mixing in a helical ribbon blade blender, Powder Technol. (2015). doi:10.1016/j.powtec.2015.11.041.

[3] L. Briens, M. Bojarra, Monitoring fluidized bed drying of pharmaceutical granules., AAPS PharmSciTech. 11 (2010) 1612–8. doi:10.1208/s12249-010-9538-1.

[4] S. Srivastava, G. Mishra, Fluid bed technology : Overview and parameters for process selection, Int. J. Pharm. Sci. Drug Res. 2 (2010) 236–246.

[5] B. Ennis, Theory of granulation, in: Handb. Pharm. Granulation Technol. Third Ed., CRC Press, 2009: pp. 6–58. doi:10.3109/9781616310035-3.

[6] T. Pugsley, G. Chaplin, P. Khanna, Application of advanced measurement techniques to conical lab-scale fluidized bed dryers containing pharmaceutical granule, Food Bioprod. Process. 85 (2007) 273–283. doi:10.1205/fbp07022.

[7] C.L. Law, A.S. Mujumdar, Fluidized bed dryers, in: Handb. Ind. Dry., 2006: pp. 174–201. doi:10.1021/ie50643a003.

[8] G. Chaplin, T. Pugsley, C. Winters, The S-statistic as an early warning of entrainment in a fluidized bed dryer containing pharmaceutical granule, Powder Technol. 149 (2005) 148–156. doi:10.1016/j.powtec.2004.11.002.

[9] G. Chaplin, T. Pugsley, Application of electrical capacitance tomography to the fluidized bed drying of pharmaceutical granule, Chem. Eng. Sci. 60 (2005) 7022–7033. doi:10.1016/j.ces.2005.06.029.

[10] H. Tsujimoto, T. Yokoyama, C.. Huang, I. Sekiguchi, Monitoring particle fluidization in a fluidized bed granulator with an acoustic emission sensor, Powder Technol. 113 (2000) 88–96. doi:10.1016/S0032-5910(00)00205-9.

[11] J. Rantanen, S. Lehtola, P. Rämet, J.-P. Mannermaa, J. Yliruusi, On-line monitoring of moisture content in an instrumented fluidized bed granulator with a multi-channel NIR moisture sensor, Powder Technol. 99 (1998) 163–170. doi:10.1016/S0032-5910(98)00100-4.

[12] M. Murtomaa, E. Räsänen, J. Rantanen, A. Bailey, E. Laine, J.-P. Mannermaa, et al., Electrostatic measurements on a miniaturized fluidized bed, J. Electrostat. 57 (2003) 91–106. doi:10.1016/S0304-3886(02)00121-3.

[13] W.O. Moughrabiah, J.R. Grace, X.T. Bi, Effects of pressure , temperature , and gas velocity on electrostatics in gas - solid fluidized beds, Chem. Eng. Sci. 123 (2009) 320–325. doi:10.1021/ie800556y.

[14] A. Sowinski, L. Miller, P. Mehrani, Investigation of electrostatic charge distribution in gas-solid fluidized beds, Chem. Eng. Sci. 65 (2010) 2771–2781. doi:10.1016/j.ces.2010.01.008.

[15] P. Mehrani, H.T. Bi, J.R. Grace, Electrostatic charge generation in gas-solid fluidized beds, J. Electrostat. 63 (2005) 165–173. doi:10.1016/j.elstat.2004.10.003.

[16] J. Wong, P. Chi, L. Kwok, H. Chan, Electrostatics in pharmaceutical solids, Chem. Eng. Sci. 125 (2015) 225–237. doi:10.1016/j.ces.2014.05.037.

[17] S. Karner, N. Anne Urbanetz, The impact of electrostatic charge in pharmaceutical powders with specific focus on inhalation-powders, J. Aerosol Sci. 42 (2011) 428–445. doi:10.1016/j.jaerosci.2011.02.010.

[18] M. Murtomaa, V. Mellin, P. Harjunen, T. Lankinen, E. Laine, V.-P. Lehto, Effect of particle morphology on the triboelectrification in dry powder inhalers., Int. J. Pharm.

282 (2004) 107–14. doi:10.1016/j.ijpharm.2004.06.002.

[19] K. Choi, S. Kim, J. Chung, Experimental study on electrostatic field of polymer powders in freeboard region of fluidized bed reactor, Adv. Sci. Lett. 19 (2013) 113–118. doi:10.1166/asl.2013.4705.

[20] P.M. Ireland, Triboelectrification of particulate flows on surfaces: Part I - Experiments, Powder Technol. 198 (2010) 189–198. doi:10.1016/j.powtec.2009.11.008.

[21] P.M. Ireland, Triboelectrification of particulate flows on surfaces: Part II — Mechanisms and models, Powder Technol. 198 (2010) 199–210. doi:10.1016/j.powtec.2009.11.008.

[22] H. Tanfara, T. Pugsley, C. Winters, Effect of particle size distribution on local voidage fluctuations in a bench-scale conical fluidized bed dryer, Dry. Technol. 20 (2002) 1273–1289. doi:10.1081/DRT-120004051.

[23] W. Senadeera, B.R. Bhandari, G. Young, B. Wijesinghe, Influence of shapes of selected vegetable materials on drying kinetics during fluidized bed drying, J. Food Eng. 58 (2003) 277–283. doi:10.1016/S0260-8774(02)00386-2.

[24] C.L. Hii, C.L. Law, M. Cloke, Modeling using a new thin layer drying model and product quality of cocoa, J. Food Eng. 90 (2009) 191–198. doi:10.1016/j.jfoodeng.2008.06.022.

[25] D. Chen, Y. Zheng, X. Zhu, Determination of effective moisture diffusivity and drying kinetics for poplar sawdust by thermogravimetric analysis under isothermal condition., Bioresour. Technol. 107 (2012) 451–455. doi:10.1016/j.biortech.2011.12.032.

[26] S.M. Tasirin, I. Puspasari, A.W. Lun, P.V. Chai, W.T. Lee, Drying of kaffir lime leaves in a fluidized bed dryer with inert particles: Kinetics and quality determination, Ind. Crops Prod. 61 (2014) 193–201. doi:10.1016/j.indcrop.2014.07.004.

[27] M. Wormsbecker, T. Pugsley, The influence of moisture on the fluidization behaviour

of porous pharmaceutical granule, Chem. Eng. Sci. 63 (2008) 4063–4069. doi:10.1016/j.ces.2008.05.023.

[28] C.V. Bezerra, L.H. Meller da Silva, D.F. Corrêa, A.M.C. Rodrigues, A modeling study for moisture diffusivities and moisture transfer coefficients in drying of passion fruit peel, Int. J. Heat Mass Transf. 85 (2015) 750–755. doi:10.1016/j.ijheatmasstransfer.2015.02.027.

[29] M. Murtomaa, J. Peltonen, J. Salonen, One-step measurements of powder resistivity as a function of relative humidity and its effect on charging, J. Electrostat. 76 (2015) 78–82. doi:10.1016/j.elstat.2015.05.016.

[30] M. Murtomaa, E. Mäkilä, J. Salonen, One-step method for measuring the effect of humidity on powder resistivity, J. Electrostat. 71 (2013) 159–164. doi:10.1016/j.elstat.2013.01.010.

[31] K. Choi, M. Taghavivand, L. Zhang, Experimental study on effect of moisture content on electrical properties of pharmaceutical powders in a rotary device, Int. J. Pharm. (under Rev. (2016).

[32] J.A. Cross, Electrostatics: principles, problems and applications, Adam Hilger, Bristol, 1987.

[33] C.F. Gallo, W.L. Lama, Classical electrostatic description of the work function and ionization energy of insulators, IEEE Trans. Ind. Appl. IA-12 (1976) 7–11. doi:10.1109/TIA.1976.349379.

[34] T.A. Alsmari, J.R. Grace, X.T. Bi, Effects of superficial gas velocity and temperature on entrainment and electrostatics in gas–solid fluidized beds, Chem. Eng. Sci. 123 (2015) 49–56. doi:10.1016/j.ces.2014.10.003.

[35] K.S. Choi, K.T. Moon, J.H. Chung, X. Bi, J.R. Grace, Electrostatic hazards of polypropylene powders in the fluidized bed reactor, IEEE Int. Conf. Ind. Eng. Eng.

Manag. (2011) 995–999. doi:10.1109/IEEM.2011.6118065.

[36] W.D. Greason, Investigation of a test methodology for triboelectrification, J. Electrostat. 49 (2000) 245–256. doi:10.1016/S0304-3886(00)00013-9.

Chapter 4 – Experimental Study on the Effect of Moisture Content on the Electrostatic Behaviour of Pharmaceutical Powders in a Rotating Device

Contribution of the MSc student

Experiments were planned by Kwangseok Choi. Samples were prepared by Milad Taghavivand with the assistance of Chao Han. Experiments were performed by both Kwangseok Choi and Milad Taghavivand. Lifeng Zhang supervised and provided consultation during the entire experimental period as well as thesis preparation. Milad Taghavivand and Kwangseok Choi prepared the manuscript with Lifeng Zhang providing editorial guidance regarding the format and content of the paper.

Contribution of this chapter to the overall study

This chapter supports our findings from the previous chapter (chapter 3). The tribocharging behaviour of pharmaceutical granules was studied in a rotating tribocharger device. The volume resistivity of granules with different moisture contents was investigated in a self-designed resistivity test cell. Furthermore, for understanding the effect of each

component on the overall volume resistivity of granules, tests were performed on individual granule components having the same moisture content of granules.

4.1 Abstract

Pharmaceutical powders are mainly organic materials and are likely to be charged during either industrial or clinical processes due to repeated inter-particle and particle-wall contacts. A clear understanding of the tribocharging behaviour of granules is essential for optimal process design. This work experimentally investigated the effect of moisture content (ranging from approximately 1.8 wt. % to 30 wt. %) on the tribocharging behaviour of pharmaceutical granules, as well as their apparent volume resistivity. The tribocharging behaviour was investigated using a rotating device and apparent volume resistivity was measured in a self-designed volume resistivity test cell. Additional measurements were performed on individual components, each having the same moisture content as did the granules, in order to investigate the effect of each single component on the apparent volume resistivity of granules. The individual components used for granules in this study were: α-Lactose Monohydrate (α-LMH), Microcrystalline Cellulose (MCC), Hydroxypropyl Methylcellulose (HPMC) and Croscarmellose Sodium (CCS). The results showed that at moisture contents below 5 wt. % the specific charge of granules begins to increase. It also was revealed that the increase in the specific charge could be due to an increase in apparent volume resistivity of granules, which showed the same behaviour as specific charge. Finally, it was shown that the apparent volume resistivity of granules appeared to be close to that of α-LMH,

which accounted for majority of the granule composition and has a water molecule in its molecular structure.

Keywords: Tribocharging; Volume resistivity; Moisture content; Pharmaceutical granules; Fluidized bed

4.2 Introduction

More than 80 % of the USA and Europe pharmaceutical market is represented by solid oral dosage (SOD) forms due to their relatively easy preparation techniques along with their enhanced physical and therapeutic properties [1]. Among the different types of SOD forms, tablets are the most applicable in the pharmaceutical industry as they have high manufacturing efficiency and can carry a wide range of doses [2]. A typical tablet manufacturing process involves several steps, including sieving, dispensing, mixing, granulation, drying, compression, etc., among which mixing and granulation have significant importance as having a homogenous mixture leads to a high quality product with the correct amount of each component. In order to ensure that each tablet has a sufficient amount of each required component, pharmaceutical powders, which are combinations of the active pharmaceutical ingredients (APIs) and excipients need to be mixed thoroughly in the blending stage [3]. Granulation is a process whereby a homogeneous dispersion of pharmaceutical powders can be achieved in certain size and density [4]. Granulation also can enhance the flowability and fluidity of particles, improve the compressibility of particles, reduce dust emissions and segregation, and improve the content uniformity of particulate substances [5–7]. Granulation can be carried out either in dry or wet form. In wet granulation, which is the most frequently

used granulation method, a non-toxic and volatile liquid binder is added to the well-blended powders [8]. When the wet granulation method is chosen, wet granules need to undergo a drying process to remove undesired moisture. Among different conventional drying methods for particles in the range of 50-2000 μm, fluidized beds are considered to be one of the most successful methods, especially for wet pharmaceutical granules, because of their providing a high rate of moisture removal, excellent mixing, rapid heat and mass transfer between phases, a large capacity of production and low capital cost [5,9].

A common issue associated with the gas-solid fluidized beds, and particle handling processes in general, is electrostatic charge generation. In fluidized beds, repeated collision and separation of particles along with inter-particle and particle-wall friction will result in unavoidable electrostatic charge generation known as "tribocharging" [10–12]. Notable changes in gas-solid fluidized bed hydrodynamics, segregation of particles, variability of API and excipients proportions and subsequent reduction in fill and uniformity leads to a decrease in production efficiency, inter-particle cohesion and particle-wall adhesion, and electrostatic discharge, which may lead to an explosion under some conditions, are generally the problems associated with tribocharging [2,11–13]. Although a few studies have been reported on electrostatic behaviour in fluidized beds [10–13], most were concerned with either polymer particles or glass beads with mono- or polydisperse sizes, hence information on the tribocharging behaviour of pharmaceutical granules in fluidized bed dryers is scarce.

In the previous chapter [14], it was observed that electrostatic charges began to accumulate when the moisture content dropped below a certain value, approximately 5 wt. %, during the drying process in a conical fluidized bed dryer. In the pharmaceutical industry, the

moisture content is typically 2 – 5 wt. % at the endpoint of the drying process. It is already known that several factors, namely surface nature, hygroscopicity and relative humidity, operational and processing conditions, and the physicochemical properties of pharmaceutical powders, may influence their electrostatic charging mechanism [15,16]. Physicochemical properties can be divided into several categories, including resistivity, size distribution, shape distribution and crystallinity. The present study specifically investigated the electrostatic behaviour of pharmaceutical powders in a rotating device in order to better understand their tribocharging behaviour, mimicking frequent particle-wall collision in a drying process inside a fluidized bed dryer, and subsequently their volume resistivity which is a determining factor in electrostatic charge build-up. The newly revealed information on electrostatic charging of pharmaceutical powders will be important to individuals working in the area of production and/or safety management in a manufacturing setting.

The experimental work was conducted in two parts. In the first part, eight different granule samples, each composed of four different components, were prepared possessing different moisture contents (approximately 1.8 wt. % to 30 wt. %) and their tribocharging behaviour was investigated and compared with the results of the previous chapter [14]. Based on the findings in the first part, the volume resistivity of granule samples, along with their individual components were investigated in the second part. Samples of individual components were prepared at four different moisture contents (ranging from 3.5 wt. % to 15 wt. %).

4.3 Materials and Methods

4.3.1 Experimental Set Up for Electrostatic Charge Generation Tests

The experiments for measuring the electrostatic charges generated by simultaneous contact and friction between pharmaceutical granules and a stainless steel container were carried out in a rotating device as shown in Figure 4.1. The experimental set up consisted of a rotating device (AC-1, Asahi-rika corp., Japan) equipped with a speed controller, metal container (stainless steel, 70 mm in diameter, 90 mm in length), a Faraday cup (Figure 2.7) with an internal cup diameter of 100 mm and a height of 100 mm, as well as an outer cup with a diameter of 150 mm and a height of 140 mm, a timer, an electrometer (6514, Keithley, USA), and a DC corona type electrostatic ionizer with an input voltage of 24kV (KD-740B, Kasuga Denki, Japan).

For the tribocharge generation tests, 5 g samples of granule were added to the metal container and agitated on the rotating device with a predetermined rotation speed of 125 rpm. The container was grounded electrically. The specific charge, q (μC/kg), of the granule samples was obtained by dividing the charge, Q (μC), by mass, m (kg), of the granule samples loaded into the Faraday cup:

$$q = \frac{Q}{m} \tag{4.1}$$

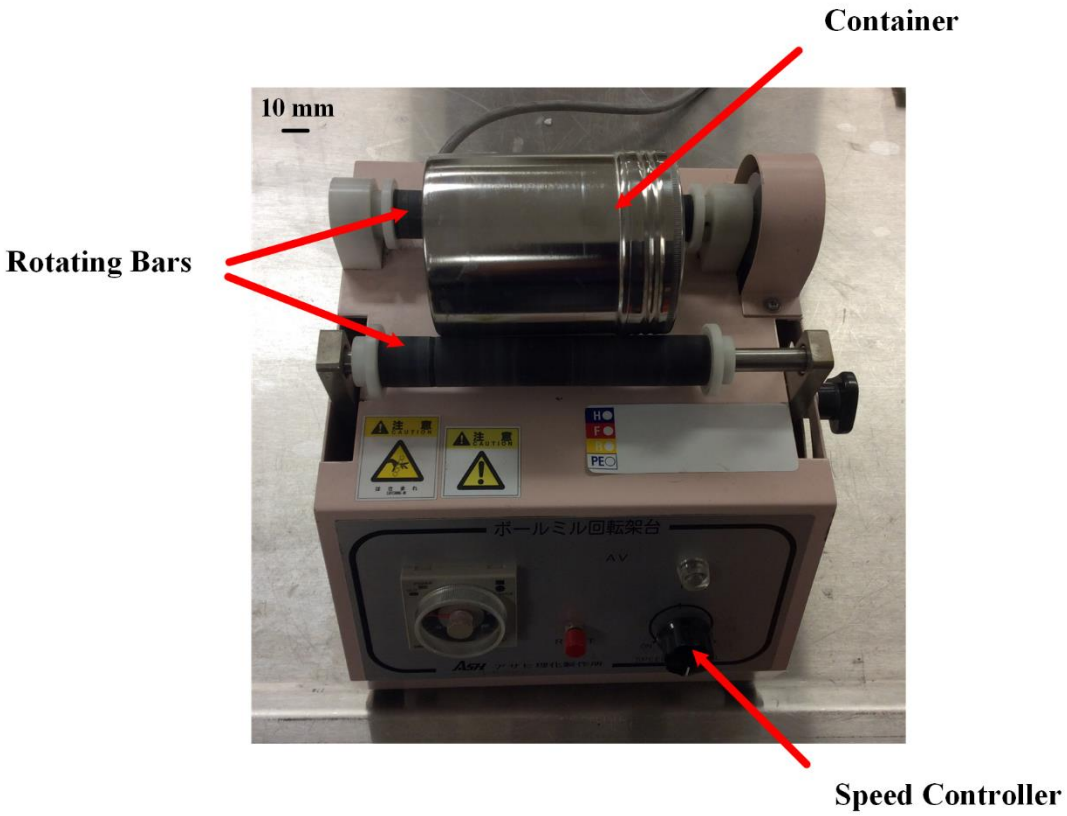

Figure 4.1 The rotating device and the container used in this study

The typical operating procedure for the tribocharge generation test was summarized as follows:

(1) Turning on all the measuring devices half an hour prior to the start of testing.

(2) Checking the level of insulation of the inner Faraday cup and making sure all of the cables were properly connected.

(3) Loading the granule sample into the grounded container.

(4) Removing the initial charge on granule sample using the electrostatic ionizer.

(5) Setting the rotational speed and turning on the power.

(6) Adding the granule sample into the inner Faraday cup after rotating for a definite time.

(7) Determining the charge and mass of granule sample using measuring devices.

All measurements were carried out under the conditions of 20 ± 3 °C and 13 ± 5 % RH.

4.3.2 Experimental Set Up for Apparent Volume Resistivity Tests

The volume resistivity measurements were performed using a self-designed volume resistivity test cell. The experimental set-up also included an electrometer (6514, Keithley, USA), a high-voltage supply (APM-30KIPNX, Max-electronics Co. Ltd, Japan) with a maximum voltage of ±30 kV, a megger insulation tester (MY40, Yokogawa, Japan) with applied voltage ranging between 125 to 1000 V, and a digital data logger (GL200, Graphtec Corp., Japan).

The volume resistivity test cell used for determining the resistivity of the granules is shown in Figure 4.2. The test cell design was based on the standards provided in [17,18] and consisted of an insulator case (polycarbonate) and three electrodes: one main electrode for measuring the electric current passing through the effective sectional area, one counter electrode for applying high voltages, and one guard electrode to ensure that only the current flows through the granule samples [18]. A voltage, V (V), was applied between the electrodes, and the corresponding current, I (A), was measured. The thickness of each electrode, L (m), was 0.01 m, equal to the gap where the specimen was placed. A schematic diagram of the electrical circuit of this cell is presented in Figure 4.3.

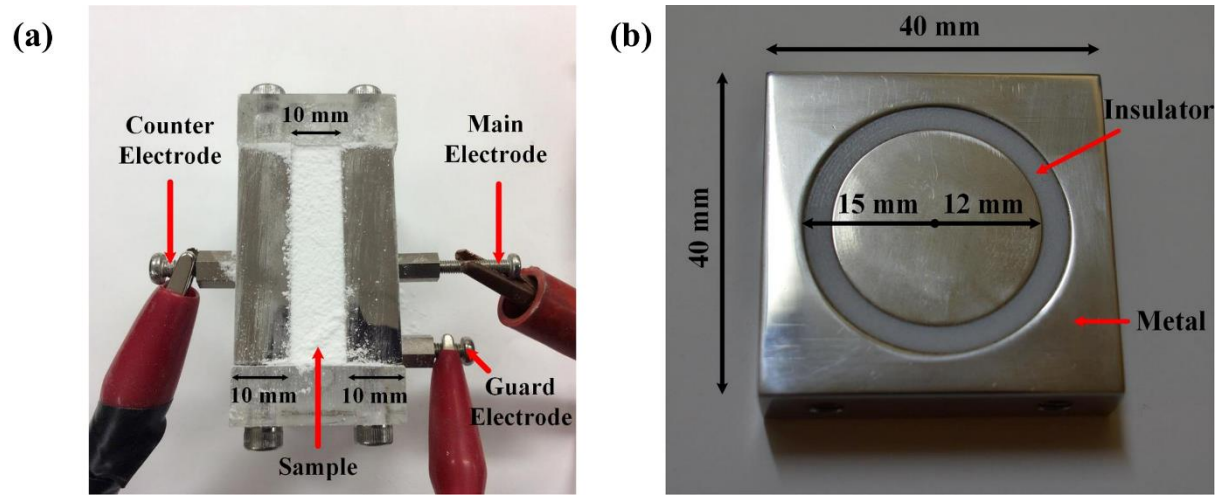

Figure 4.2 Apparent volumetric resistivity test cell. (a) Top view of the volume resistivity test cell, (b) Inner view of the main electrode along with detailed dimensions

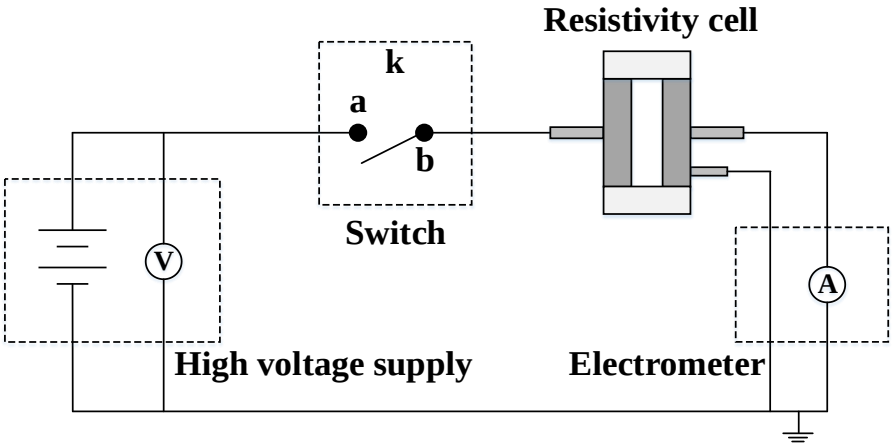

Figure 4.3 Schematic diagram of the electric circuit for electrical volume resistivity of granule samples

The resistance, R (Ω), was then calculated using the Ohm's law relationship, $R = \frac{V}{I}$, and the apparent volume resistivity, ρ (Ω.m), was calculated by:

$$\rho = R\frac{S}{L} \tag{4.2}$$

where S is the effective cross-sectional area of the main electrode (m^2), L is the thickness of the specimen (0.01 m), and R is the resistance (Ω).

The required dimensions to determine the effective cross-sectional area of the main electrode are provided in Figure 4.2(b). The following equation can be used to calculate this value:

$$S = \pi . \left(\frac{r_1 + r_2}{2}\right)^2 \quad (4.3)$$

By replacing $\frac{S}{L}$ in Eq. 4.2 with *k*, it will become:

$$\rho = R . k \quad (4.4)$$

where *k* is a coefficient related to the effective cross-sectional area of the electrode and the thickness of the specimen (m), and equal to 0.057 m in this work.

It should be noted that the megger insulation tester was used for powders having low volume resistivity (below 10^9 Ω.m).

4.3.3 Sample Preparation

Table 4.1 shows the compositions of the pharmaceutical granules. Particle sizes of the individual components were measured by a particle size analyzer (Mastersizer 2000, Malvern Instruments Ltd., UK). Particle morphology was investigated through SEM imaging (JSM 6010, JEOL Ltd., Japan) and is shown in Figure 4.4. Figure 4.4(e) shows a dry granule sample from the previous chapter [14].

Granule samples were prepared having eight different moisture contents: 30.0, 25.0, 20.0, 15.0, 10.0, 5.0, 2.7, and 1.8 wt. % (wet basis) and were stored in sealed glass containers in order to prevent changes in their moisture contents. The moisture content of samples was

confirmed using a drying balance (HB43, Mettler-Toledo, USA). Water used as the granulation liquid in this experiment was purified by reverse osmosis.

Table 4.1
Properties of components and their proportion in granules

Component	Abbreviation	Percentage by mass (dry basis)	Size (μm)		
			D_{10}	D_{50}	D_{90}
α-Lactose Monohydrate	α-LMH	50%	8	55	147
Microcrystalline Cellulose	MCC	44%	33	106	217
Hydroxypropyl Methylcellulose	HPMC	4%	21	72	157
Croscarmellose Sodium	CCS	2%	16	41	105

The procedure to prepare the granule samples was described in the previous chapter [14], with the exception that in this study, the amount of water to be added to the mixture was proportional to the predetermined moisture contents. Dry components, with respect to their compositions presented in Table 4.1, were mixed in a 250 W domestic mixer (Kitchen-Aid classic mixer) for 2 minutes at the lowest speed (setting 1) followed by continuous water addition at a constant rate [19]. Afterward, in order to obtain granules similar to those prepared in Chapter 3 [14], the post-granulation step was carried out for 2 minutes at a higher speed (setting 2 on the mixer). It should be noted that in the wet granulation method, the size and formation of granules depends on the amount of granulation liquid added to the mixture [4]; therefore, samples with moisture contents below 15 wt. % might not be granulated perfectly. The granulation product was then sieved through a 3.36 mm screen (mesh No. 6 in US Standard with an opening of 0.132 inches) in order to remove large granules that were formed due to poor granulation, and also to break up any loosely formed agglomerates.

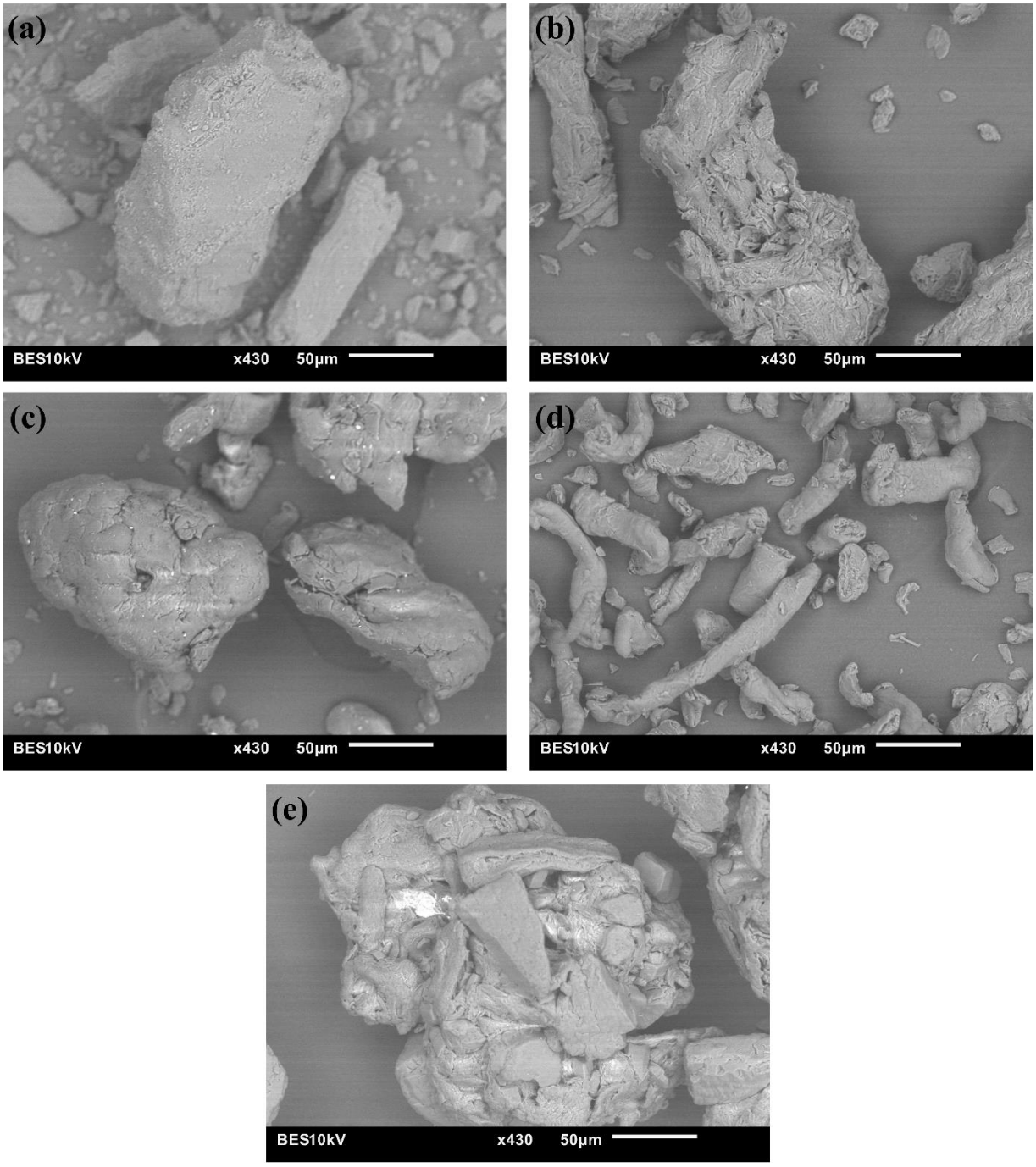

Figure 4.4 Scanning electron micrographs of the pharmaceutical powders. (a) α-Lactose monohydrate (α-LMH), (b) Microcrystalline Cellulose (MCC), (c) Hydroxypropyl Methylcellulose (HPMC), (d) Croscarmellose Sodium (CCS), (e) final dry granule sample taken from fluidized bed dryer

Samples of each component with 15.0, 10.0, 5.0 and 3.5 wt. % moisture content also were prepared in the mixer and stored separately in sealed glass containers.

4.4 Results and Discussion

4.4.1 Influence of Moisture Content on the Specific Charge of Granules

In the tribocharging experiments, the optimum rotational time at which granule samples gained their maximum *q*, needed to be determined first. For this, 5 g of the driest granule sample (1.8 wt. % moisture content) was added to the stainless steel container which was rotated from 30 s to 1200 s at a constant speed of 125 rpm. Figure 4.5 shows the *q* of the studied sample against the rotating time. The reproducibility of the experimental data was tested by three replicates at four different rotating times and the resultant error bars are indicated in Figure 4.5. In general, an average error of 3 % was observed in the experiments. As can be clearly seen in Figure 4.5, the *q* increased considerably as the rotating time increased from 200 s to 300 s and eventually reached a maximum value, which can be referred as the saturated specific charge [20]. The increase in *q* could be explained by the fact that the contact and friction frequencies between the granules and the inner wall of the container increased with an increase in the rotating time, resulting in more charge generation. Granule samples having higher moisture content would be expected to require a shorter time to reach their saturated charges, as the presence of water would turn the granules into more conductive materials by lowering their electrical resistivity and raising their electrical conductivity. Thus, a shorter time would be needed to reach the saturated charge level. Further discussion on the effect of moisture content on resistivity is provided in the next section. Based on the above discussion, a rotating time of 300 s was employed for tribocharging tests of all granule samples.

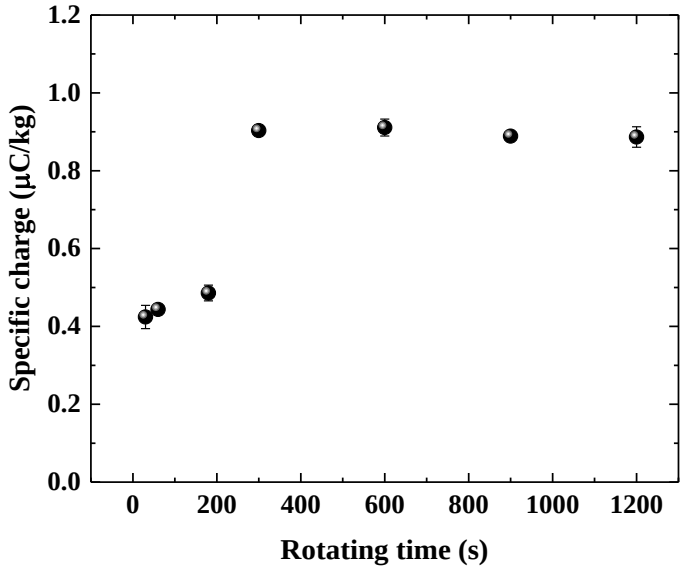

Figure 4.5 Specific charge of the dried granule sample (1.8 wt. % moisture content) as a function of the rotating time

Figure 4.6 shows the obtained values for the *q* of granule samples having eight different moisture contents (1.8 to 30 wt. %) under the aforementioned conditions (5 g of each sample; rotating at 125 rpm for 300 s). For comparison purposes, Figure 4.6 also shows the *q* of the granule sample (in red) with a moisture content of 2.5 wt. % from the fluidized bed dryer [14]. It can be seen in Figure 4.6 that the granule sample taken from the fluidized bed dryer had a higher *q* (1.86 μC/kg) than did the granule sample prepared in the domestic mixer and having a moisture content of 1.8 wt. % (0.9 μC/kg). With an increase in moisture content, the *q* decreased. At a moisture content of 2.7 wt. %, the *q* decreased to 0.48 μC/kg. However, the *q* of granule samples did not change markedly when the moisture content increased above 5 wt. %, with the resultant *q* of 0.01 μC/kg. Therefore, the 5 wt. % moisture content was considered to be a critical value, only below which significant charge accumulation can be observed. This finding is consistent with that observed in the fluidized bed dryer [14]. A typical dynamic

profile of moisture content during the drying process is shown in Figure 4.7. This figure also presents the change in the *q* of granules during the drying process. The drying process in the fluidized bed was operated at a drying air velocity of 1.4 m/s and a drying air temperature of 38 ˚C. The electrostatic charges generated in the present work are of the same order of magnitude as those obtained for organic powders during grinding industrial operations, where electrostatic agglomeration and adhesion may occur [18]. Therefore, it is imperative to develop a method to reduce electrostatic charge build-up for safe handling of powders.

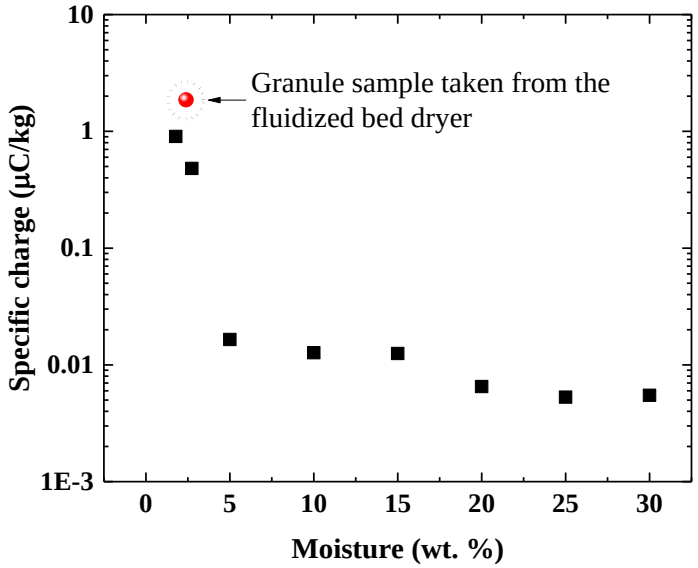

Figure 4.6 Specific charge of granule samples as a function of moisture content

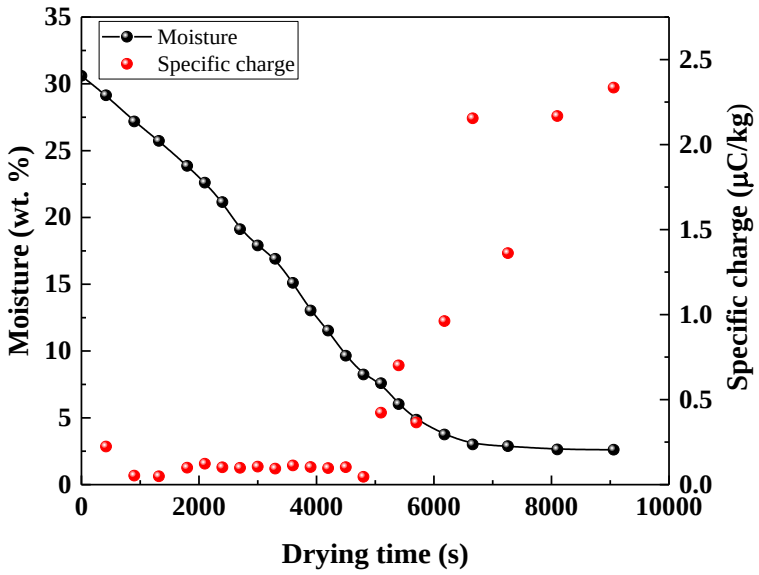

Figure 4.7 Variation of specific charge with drying time at a drying air velocity of 1.4 m/s and a drying air temperature of 38 ˚C [14]

4.4.2 Influence of Moisture Content on the Apparent Volume Resistivity of Granules

In order to better understand and explain the results obtained in the previous section, the effect of moisture content on the apparent volume resistivity of granule samples was measured using the resistivity test cell. Figure 4.8 presents an example of the change in electrical current passing through the granule sample having a moisture content of 1.8 wt. % during the resistivity measurement.

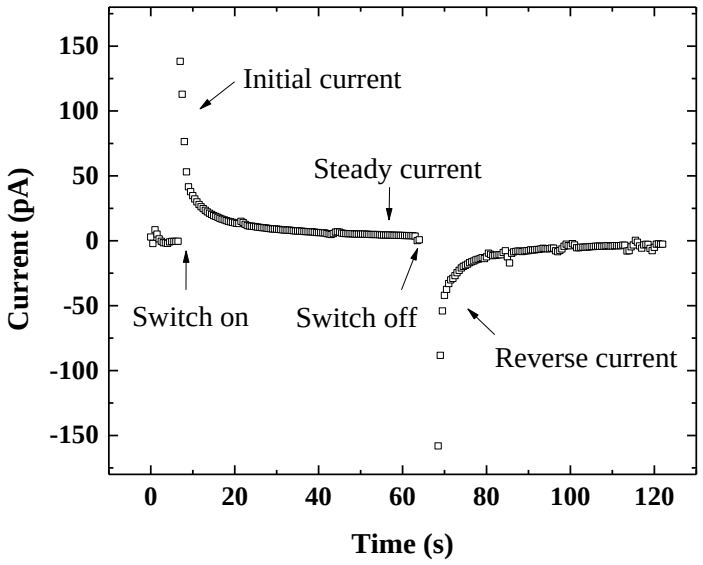

Figure 4.8 Current decay in the granule sample with 1.8 wt. % moisture content as a function of time after applying 500 V (DC) in resistivity measurement

A voltage of 500 V was applied between the electrodes of the test cell. As soon as the high voltage supply was switched on, a high initial current was observed and then it gradually decayed until reaching a steady level of current for the studied sample. The high initial current shown in the figure is the displacement current and represents the energy that must be absorbed to polarize the atoms of the insulator. Sixty seconds was selected to record the electrical current passing through the sample after the current reached its steady level. The measured current value at steady state was approximately 3.5 pA for the granule sample with 1.8 wt. % moisture content. After completing the recording process for one minute, the applied voltage must be stopped with occurrence of a reverse current flow. Once the high voltage supply was switched off, a transient electrical noise occurred, which is not shown in Figure 4.8. The same procedure was applied to the other granule samples. By substituting the required parameters in Eq. 4.4, a ρ of 8.1×10^{12} Ω.m was obtained for the granule sample with

1.8 wt. % moisture content. In principle, powders with 10^{12} Ω.m and above are usually classified as high electrostatic charge materials [17].

Following the same procedure, apparent volume resistivity was measured for granule samples having different moisture content. In order to evaluate the reproducibility of the experimental data, this measurement was carried out in three replicates at three different moisture contents (1.8, 2.7 and 5.0 wt. %) and an average error of 3 % was observed in the experiments. The effect of moisture content on the volume resistivity of granule samples is presented in Figure 4.9.

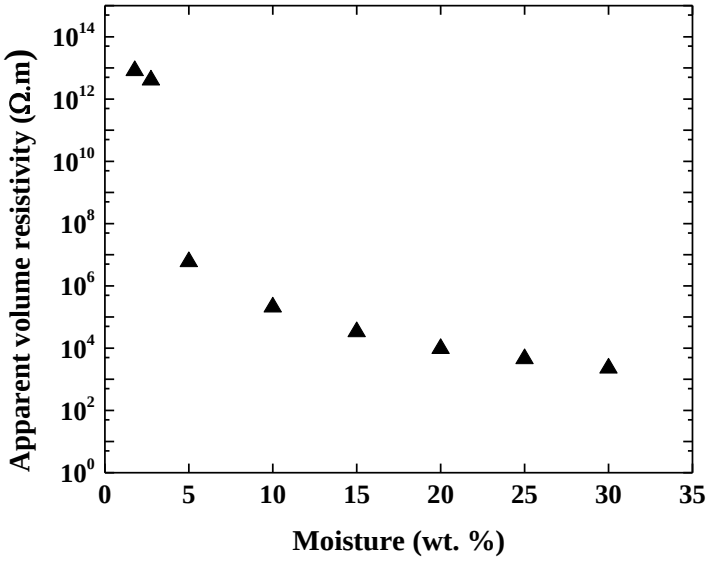

Figure 4.9 Apparent volume resistivity of granule samples as a function of moisture content

It can be seen in Figure 4.9 that the apparent volume resistivity of granule samples increased when the moisture content was reduced. This behaviour is in agreement with the results of other studies [21,22]. This change is most notable at moisture contents below 5 wt.

%. The maximum resistivity value measured in this work was on the order of 10^{12} Ω.m. The sudden change in resistivity at approximately 5 wt. % moisture content explains the trends in electrostatic charging discussed in the previous section and in Chapter 3 [14]. Thus, it can be concluded that the specific charge of granules at moisture contents below 5 wt. % increased considerably because of the significant increase in ρ. This critical value is related to the surface moisture of granules. When the moisture content was above 5 wt. %, a thin layer of water might exist on the surface of granules. However, this layer disappears when the moisture content is reduced below 5 wt. %. During the drying process, this critical value distinguishes two classical drying phases: constant rate and falling rate. During constant rate drying, the evaporation of surface water is dominating, while the rate of moisture diffusion within the granules is responsible for falling rate drying. It can be expected that this critical value would be closely related to the particle characteristics of pharmaceutical powders. Based on the above discussion, it can be concluded that the apparent volume resistivity change is directly linked to tribocharging behaviour. However, other influential factors on apparent volume resistivity such as ambient temperature and relative humidity should not be ignored.

In addition to measurements on granule samples, the apparent volume resistivity of individual component was measured at different moisture contents. The results are shown in Figure 4.10. According to Figure 4.9, at moisture contents above 15 wt. %, granules literally are considered electrically conductive materials with low resistivity; therefore, tests were only performed on components with moisture contents below 15 wt. % for brevity.

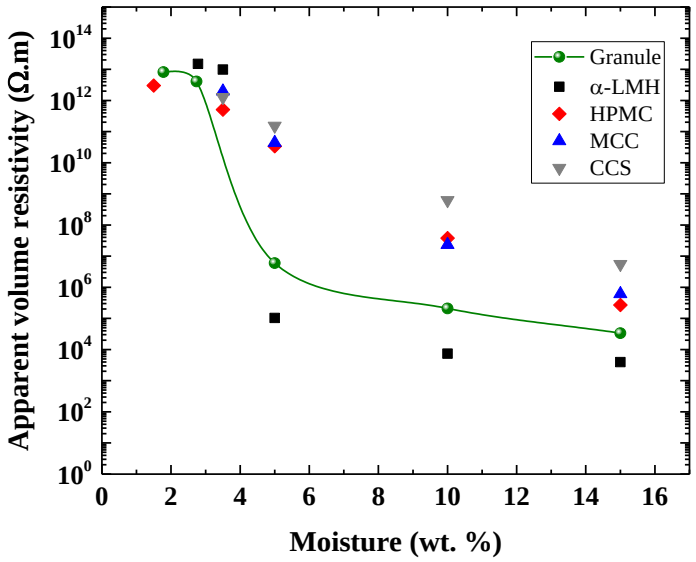

Figure 4.10 Apparent volume resistivity of individual components as a function of moisture content

Figure 4.10 reveals that among the four different components, α-LMH had the lowest volume resistivity at moisture contents of 15.0, 10.0 and 5.0 wt. %. This behaviour could be explained by the fact that α-LMH has a water molecule in its chemical structure, which turns it into a more electrically conductive powder (Figure 4.11). The ρ of other three powders were very similar; however, CCS showed a slightly higher ρ compared to MCC and HPMC. At moisture contents below 5 wt. %, the ρ of all powders became almost the same, with the exception that α- LMH showed relatively higher ρ. In Figure 4.10, the volume resistivity of granules was compared to those of individual components. It can be seen that the magnitude of resistivity of the granules is similar to that of the α-LMH which accounted for over 40 wt. % of the granules composition (wet basis).

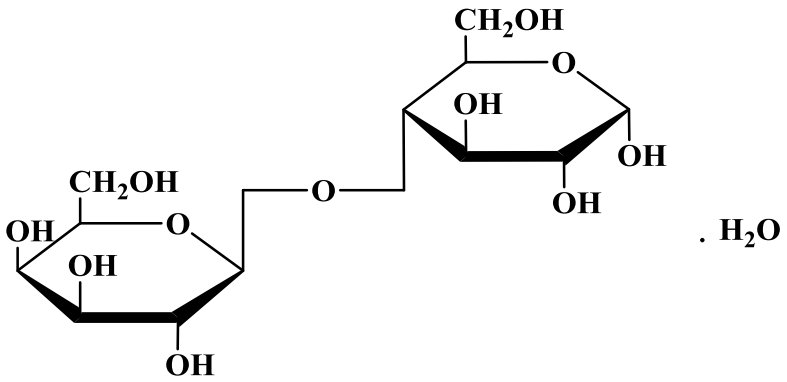

Figure 4.11 Chemical structure of α-Lactose Monohydrate

4.5 Conclusions

In this study, the specific charge and apparent volume resistivity of granules were experimentally investigated to better understand the tribocharging behaviour of pharmaceutical granules at various moisture contents. Conclusions can be drawn from the experimental results as follows:

(1) The specific charge started to increase at a moisture content below 5 wt. %, a critical point related to particle characteristics. The trend found in this work is in good agreement with the tribocharging behaviour observed in a fluidized bed dryer. The generated charges were high enough to cause particle agglomeration and adhesion to dryer walls, which is undesirable.

(2) The apparent volume resistivity of granules increased by several orders of magnitude when the moisture content was reduced to below approximately 5 wt. %. This change became notable at a moisture content below 5 wt. % and a similar trend was observed for the specific charge.

(3) The magnitude of the volume resistivity of granules was similar to that of α-LMH, the major component of the granules accounting for over 40 wt. % of the composition (wet basis).

4.6 Acknowledgments

The authors gratefully acknowledge Chao Han of the University of Saskatchewan for his assistance in making sample powders, and financial support from NSERC and the University of Saskatchewan.

4.7 References

[1] L. Perioli, G. D'Alba, C. Pagano, New oral solid dosage form for furosemide oral administration., Eur. J. Pharm. Biopharm. Off. J. Arbeitsgemeinschaft Für Pharm. Verfahrenstechnik e.V. 80 (2012) 621–9. doi:10.1016/j.ejpb.2011.12.011.

[2] E. Šupuk, A. Zarrebini, J.P. Reddy, H. Hughes, M.M. Leane, M.J. Tobyn, et al., Tribo-electrification of active pharmaceutical ingredients and excipients, Powder Technol. 217 (2012) 427–434. doi:10.1016/j.powtec.2011.10.059.

[3] T.A.H. Simons, S. Bensmann, S. Zigan, H.J. Feise, H. Zetzener, A. Kwade, Characterization of granular mixing in a helical ribbon blade blender, Powder Technol. (2015). doi:10.1016/j.powtec.2015.11.041.

[4] N. Kivikero, M. Murtomaa, B. Ingelbeen, O. Antikainen, E. Räsänen, J.-P. Mannermaa, et al., Microscale granulation in a fluid bed powder processor using electrostatic atomisation., Eur. J. Pharm. Biopharm. Off. J. Arbeitsgemeinschaft Für Pharm. Verfahrenstechnik e.V. 71 (2009) 130–7. doi:10.1016/j.ejpb.2008.07.009.

[5] L. Briens, M. Bojarra, Monitoring fluidized bed drying of pharmaceutical granules., AAPS PharmSciTech. 11 (2010) 1612–8. doi:10.1208/s12249-010-9538-1.

[6] S. Srivastava, G. Mishra, Fluid bed technology : Overview and parameters for process selection, Int. J. Pharm. Sci. Drug Res. 2 (2010) 236–246.

[7] B. Ennis, Theory of granulation, in: Handb. Pharm. Granulation Technol. Third Ed., CRC Press, 2009: pp. 6–58. doi:10.3109/9781616310035-3.

[8] T. Pugsley, G. Chaplin, P. Khanna, Application of advanced measurement techniques to conical lab-scale fluidized bed dryers containing pharmaceutical granule, Food Bioprod. Process. 85 (2007) 273–283. doi:10.1205/fbp07022.

[9] C.L. Law, A.S. Mujumdar, Fluidized bed dryers, in: Handb. Ind. Dry., 2006: pp. 174–

201. doi:10.1021/ie50643a003.

[10] W.O. Moughrabiah, J.R. Grace, X.T. Bi, Effects of pressure , temperature , and gas velocity on electrostatics in gas - solid fluidized beds, Chem. Eng. Sci. 123 (2009) 320–325. doi:10.1021/ie800556y.

[11] A. Sowinski, L. Miller, P. Mehrani, Investigation of electrostatic charge distribution in gas-solid fluidized beds, Chem. Eng. Sci. 65 (2010) 2771–2781. doi:10.1016/j.ces.2010.01.008.

[12] P. Mehrani, H.T. Bi, J.R. Grace, Electrostatic charge generation in gas-solid fluidized beds, J. Electrostat. 63 (2005) 165–173. doi:10.1016/j.elstat.2004.10.003.

[13] M. Murtomaa, V. Mellin, P. Harjunen, T. Lankinen, E. Laine, V.-P. Lehto, Effect of particle morphology on the triboelectrification in dry powder inhalers., Int. J. Pharm. 282 (2004) 107–14. doi:10.1016/j.ijpharm.2004.06.002.

[14] M. Taghavivand, K. Choi, L. Zhang, Investigation on drying kinetics and tribocharging behaviour of pharmaceutical granules in a fluidized bed dryer, J. Powder Technol. under review (2016).

[15] W. Kaialy, A review of factors affecting electrostatic charging of pharmaceuticals and adhesive mixtures for inhalation, Int. J. Pharm. 503 (2016) 262–276. doi:10.1016/j.ijpharm.2016.01.076.

[16] J. Wong, P. Chi, L. Kwok, H. Chan, Electrostatics in pharmaceutical solids, Chem. Eng. Sci. 125 (2015) 225–237. doi:10.1016/j.ces.2014.05.037.

[17] JNIOSH, Technical recommendations of national institute of occupational safety and health (TR-No.42), Recommendationa for requirements for avoiding electrostatic hazards in industry, 2007.

[18] M. Glor, Electrostatic hazards in powder handling, Research studies press LTD. and John Wiley & Sons, 1988.

[19] G. Chaplin, T. Pugsley, C. Winters, The S-statistic as an early warning of entrainment in a fluidized bed dryer containing pharmaceutical granule, Powder Technol. 149 (2005) 148–156. doi:10.1016/j.powtec.2004.11.002.

[20] E. Šupuk, C. Seiler, M. Ghadiri, Analysis of a simple test device for tribo-electric charging of bulk powders, Part. Part. Syst. Charact. 26 (2009) 7–16. doi:10.1002/ppsc.200800015.

[21] M. Murtomaa, E. Mäkilä, J. Salonen, One-step method for measuring the effect of humidity on powder resistivity, J. Electrostat. 71 (2013) 159–164. doi:10.1016/j.elstat.2013.01.010.

[22] M. Murtomaa, J. Peltonen, J. Salonen, One-step measurements of powder resistivity as a function of relative humidity and its effect on charging, J. Electrostat. 76 (2015) 78–82. doi:10.1016/j.elstat.2015.05.016.

Chapter 5 – Conclusions and Recommendations

5.1 Summary of Results

The experimental results clearly demonstrated that increasing the drying air temperature and velocity shortened the drying time as expected. Fick's second law of diffusion was used to describe the drying kinetics and an Arrenhius-type equation was used to describe the effect of air temperature on the effective diffusion coefficient of moisture. It was revealed that the Arrhenius constant increased with an increase in drying air velocity, but no linear relationship was found between the two parameters. Besides, operating at higher velocities increases the risk of fine particles entrainment. It also was found that the effect of drying air temperature became more significant at higher drying air velocities. However, there is a possibility that higher temperatures might denature the chemical structure of some or all of the components. Also, the activation energy was discovered to be approximately 19.5 kJ/mol. Neither drying air temperature nor drying air velocity showed an impact on the activation energy.

From experiments on specific charge during the drying process, it was found that the specific charge of granules started to increase when the moisture content was reduced to a critical value (approximately 5 wt. % to 10 wt. %), regardless of drying air temperature or drying air velocity. This could be attributed to surface moisture changes over the course of the drying process. Initially, the surfaces of granules would be covered by a thin layer of liquid water. This surface water made granules more electrical conductive and facilitated charge

dissipation. Therefore, no charge accumulation was observed. With time, granules gradually lost surface moisture and charge accumulation occurred. The effect of moisture content on electrostatic charge generation can be explained by the apparent volume resistivity of granules. In fact, the apparent volume resistivity of granules increased by several orders of magnitude when the moisture content was reduced. This change became notable at moisture contents below 5 wt. %.

At the endpoint of the drying process, an equilibrium specific charge was observed. The equilibrium specific charge appeared to be a function of drying air velocity and the drying air temperature, which didn't show a significant impact on the specific charge under the experimental conditions investigated in this work. A higher drying air velocity resulted in a higher equilibrium specific charge.

The tribocharging behaviour of pharmaceutical granules against moisture content discovered in the present work could be utilized for monitoring the endpoint of the drying process. In addition, fine particles entrained in the freeboard of the fluidized bed were found to carry charges with opposite polarity to that observed in the dense bed. This observation was consistent with charge separation theory.

5.2 Conclusions

- The specific charge of granules increased as their surface became dry and the moisture content decreased below 5 wt. %. This was mainly because of a significant increase in volume resistivity of granules.

- Increasing the drying air velocity increased the electrostatic charge generation in the fluidized bed dryer. This was mainly due to increase in particle-particle collisions and bi-polar charging at higher drying air velocities.
- The drying air temperature did not show any impact on the specific charge of the granules under experimental conditions investigated in this study.

5.3 Recommendations

This study has shown that a significant amount of electrostatic charge was generated inside the fluidized bed dryer at moisture contents below 5 wt. %. The components studied in this project were excipients, and the effect of APIs on electrostatic charge and volume resistivity were not explored. Therefore, the tribocharging behaviour of the granules after addition of APIs should be investigated in the future work.

The parameters studied in this project included drying air temperature and drying air velocity. The effects of other parameters, such as relative humidity, on drying kinetics and tribocharging behaviour should be explored.

Charge distribution of poly-dispersed powders also would be expected in the current study. A detailed understanding of charge distribution and how charge distribution is related to mixing and segregation is needed.

This project used a conventional Faraday cup technique to measure specific charge offline. No effect on hydrodynamics inside the fluidized bed dryer was expected due to the

small number of samples withdrawn. However, developing a method which can measure the electrostatic charge *in situ* would be desirable from process control point of view.

In view of the significant charge build-up at the endpoint of the drying process, suitable mitigation approaches should be sought to prevent charge build-up and possible undesirable resultant consequences such as variations in API content and sheeting on dryer walls.

Appendix – Comparison of Drying Models

An attempt was made to fit the drying curves achieved from experiments with the commonly used mathematical models listed in Table A.1 for drying process in agriculture and food industries [1–7].

The models listed in Table A.1 are categorized based on thin-layer drying equations [8]. Thin-layer drying means drying of sample particles as one layer and it assumes no temperature gradient in the material to be dried [8]. In fact, by using the thin-layer drying model, it is assumed that the temperature of the material is equivalent to that of the ambient air [8].

Thin layer drying equations could be either theoretical, semi-theoretical, or empirical [8]. Considering the following assumptions, the theoretical model would result finally in Eq. 3.2 for sphere particles.

- the particle is homogenous and isotropic;
- the material characteristics are constant, and the shrinkage is neglected;
- the pressure variations are neglected;
- evapouration occurs only at the surface;
- initially moisture distribution is uniform and symmetrical during the process;
- surface diffusion is ended, so moisture equilibrium arises on the surface;
- temperature distribution is uniform and equals the ambient drying air temperature, namely the lumped system;
- heat transfer is by conduction within the product, and by convection outside of the product;
- effective moisture diffusivity is constant versus moisture content during drying.

Semi-theoretical models can be divided into two types based the derivation method, which are Newton's law of cooling and Fick's second law of diffusion [8]. Among the models listed in Table A.1, Newton and Page models were derived from Newton's law of cooling and others were derived from Fick's second law of equation [8,9].

Table A.1
Drying models used for fitting drying curves

No.	Model	Equation	Parameters
1	Newton [1]	*MR=exp(-k.t)*	k
2	Henderson and Pabis [1]	*MR=a.exp(-k.t)*	a, k
3	Logarithmic [9]	*MR=a.exp(-k.t) + c*	a, k, c
4	Two term model [9]	*MR=a.exp(-k.t) + c.exp(-g.t)*	a, k, c, g
5	Two-term exponential [9]	*MR=a.exp(-k.t) + (1-a).exp(-k.a.t)*	a, k
6	Verma et al. [1]	*MR=a.exp(-k.t) + (1-a).exp(-g.t)*	a, k, g
7	Page [9]	$MR=exp(-k.t^n)$	k, n
8	Midilli–Kucuk [9]	$MR=a.exp(-k.t^n) + c.t$	a, k, c, n
9	Hii et al. [1]	$MR=a.exp(-k.t^n) + c.exp(-g.t^n)$	a, k, c, g, n

Two statistical parameters, reduced chi-square (χ^2) and root mean square error (*RMSE)* were used to assess the goodness of the curve fitting.

Reduced chi-square was calculated by:

$$\chi^2 = \frac{\sum_{i=1}^{N}\left(MR_{exp,i}-MR_{pre,i}\right)^2}{N-z} \quad \text{(A.1)}$$

And root mean square error (*RMSE*) was estimated by:

$$RMSE = \left[\frac{1}{N}\sum_{i=1}^{N}\left(MR_{exp,i} - MR_{pre,i}\right)^2\right]^{1/2} \quad \text{(A.2)}$$

where $MR_{exp,i}$ and $MR_{pre,i}$ are the experimental and predicted moisture ratio, respectively, N is the number of experimental observations and z is the number of parameters in the models [1,2,5,8].

Tables A.2 – A.4 present the statistical analysis results for the nine models employed in this project. The statistical analysis was conducted using the Solver function in Excel with minimizing chi-square. The model with the lowest RMSE and $\chi 2$ was considered the best model to predict the drying curve of pharmaceutical granules under the experimental conditions.

As can be seen in Tables A.2 – A.4, the models of Page, Midilli-Kucuk, and Hii et al. present very good curve fitting. Among the three models, the Hii et al. model (model # 9) had the lowest *RMSE* and χ^2 values, indicating that it was the best-fitted model to describe the drying curves under the conditions investigated. Results in Tables A.2 – A.4 also reveal that the "c" parameter in models # 3 and # 4 was zero under all circumstances, which makes them similar to model # 2.

Figures A.1 – A.3 show comparisons between the drying data obtained from experiments and the values predicted by the models used. It is evident from these figures that the Page, Midilli-Kucuk, and Hii et al. models all can predict the drying curves of pharmaceutical granules with the fitted parameters.

Table A.2
Statistical results obtained from all drying models at a drying air velocity of V=1.0 m/s

T (˚C)	Model No.	*RMSE*	χ^2	*a*	*k*	*n*	*c*	*g*
	1	0.0791	0.0069	-	0.0150	-	-	-
	2	0.0716	0.0063	1.0923	0.0162	-	-	-
	3	0.0716	0.0070	1.0923	0.0162	-	0	-
	4	0.0716	0.0081	1.0923	0.0162	-	0	0.0641
38	5	0.0346	0.0015	2.0906	0.0240	-	-	-
	6	0.0310	0.0013	20.5028	0.0314	-	-	0.0332
	7	0.0210	0.0005	-	0.0008	1.6755	-	-
	8	0.0200	0.0006	0.9842	0.0007	1.7141	0	-
	9	0.0142	0.0004	0.9047	0.0002	1.9871	0.0953	1.1758
	1	0.0430	0.0020	-	0.0167	-	-	-
	2	0.0390	0.0017	1.0528	0.0178	-	-	-
	3	0.0390	0.0019	1.0528	0.0178	-	0	-
	4	0.0390	0.0020	1.0528	0.0178	-	0	0.0641
50	5	0.0259	0.0008	1.8143	0.0247	-	-	-
	6	0.0252	0.0013	19.8962	0.0308	-	-	0.0320
	7	0.0252	0.0007	-	0.0053	1.2860	-	-
	8	0.0246	0.0008	0.9818	0.0044	1.3291	0	-
	9	0.0228	0.0008	0.9264	0.0022	1.4766	0.0736	1.1758
	1	0.0596	0.0039	-	0.0263	-	-	-
	2	0.0535	0.0036	1.0685	0.0281	-	-	-
	3	0.0535	0.0041	1.0685	0.0281	-	0	-
	4	0.0535	0.0048	1.0685	0.0281	-	0	0.0590
65	5	0.0226	0.0006	1.9863	0.0416	-	-	-
	6	0.0201	0.0005	31.1994	0.0542	-	-	0.0559
	7	0.0152	0.0003	-	0.0040	1.5132	-	-
	8	0.0144	0.0003	0.9854	0.0034	1.5545	0	-
	9	0.0086	0.0001	0.9178	0.0014	1.7725	0.0819	1.1759
	1	0.0694	0.0056	-	0.0305	-	-	-
	2	0.0646	0.0058	1.0570	0.0323	-	-	-
	3	0.0646	0.0073	1.0570	0.0323	-	0	-
	4	0.0646	0.0097	1.0570	0.0323	-	0	0.0583
75	5	0.0694	0.0067	0.9986	0.0305	-	-	-
	6	0.0319	0.0009	35.1739	0.0623	-	-	0.0640
	7	0.0265	0.0010	-	0.0049	1.5169	-	-
	8	0.0251	0.0015	0.9778	0.0038	1.5820	0	-
	9	0.0065	0.0001	0.8523	0.0006	2.0681	0.1478	1.1758

Table A.3
Statistical results obtained from all drying models at a drying air velocity of *V*=1.4 m/s

T (˚C)	Model No.	*RMSE*	χ^2	*a*	*k*	*n*	*c*	*g*
	1	0.0842	0.0074	-	0.0185	-	-	-
	2	0.0738	0.0060	1.1221	0.0206	-	-	-
	3	0.0738	0.0063	1.1220	0.0206	-	0	-
	4	0.0738	0.0067	1.1221	0.0206	-	0	0.0641
38	5	0.0427	0.0020	2.0542	0.0295	-	-	-
	6	0.0384	0.0041	21.9736	0.0386	-	-	0.0406
	7	0.0271	0.0008	-	0.0012	1.6719	-	-
	8	0.0224	0.0006	0.9493	0.0006	1.8213	0	-
	9	0.0162	0.0003	0.9034	0.0003	2.0031	0.0966	1.1758
	1	0.0735	0.0057	-	0.0273	-	-	-
	2	0.0664	0.0050	1.0936	0.0296	-	-	-
	3	0.0664	0.0054	1.0936	0.0296	-	0	-
	4	0.0664	0.0058	1.0936	0.0296	-	0	0.0619
50	5	0.0397	0.0018	1.9828	0.0411	-	-	-
	6	0.0362	0.0028	17.6898	0.0528	-	-	0.0558
	7	0.0292	0.0010	-	0.0035	1.5418	-	-
	8	0.0253	0.0009	0.9497	0.0019	1.6867	0	-
	9	0.0155	0.0003	0.8728	0.0006	1.9533	0.1272	1.1758
	1	0.0737	0.0058	-	0.0333	-	-	-
	2	0.0668	0.0051	1.0843	0.0360	-	-	-
	3	0.0668	0.0056	1.0843	0.0360	-	0	-
	4	0.0668	0.0061	1.0843	0.0360	-	0	0.0619
65	5	0.0409	0.0019	1.9544	0.0508	-	-	-
	6	0.0376	0.0026	15.7888	0.0649	-	-	0.0689
	7	0.0313	0.0011	-	0.0054	1.5161	-	-
	8	0.0267	0.0010	0.9420	0.0025	1.7161	0	-
	9	0.0154	0.0004	0.8743	0.0010	1.9580	0.1257	1.1758
	1	0.0717	0.0070	-	0.0413	-	-	-
	2	0.0661	0.0066	1.0794	0.0442	-	-	-
	3	0.0661	0.0073	1.0794	0.0442	-	0	-
	4	0.0661	0.0082	1.0794	0.0442	-	0	0.0620
75	5	0.0428	0.0027	1.9386	0.0612	-	-	-
	6	0.0396	0.0029	20.3188	0.0782	-	-	0.0818
	7	0.0341	0.0017	-	0.0078	1.4925	-	-
	8	0.0303	0.0017	0.9496	0.0049	1.6145	0	-
	9	0.0173	0.0006	0.8465	0.0011	2.0231	0.1535	1.1758

Table A.4
Statistical results obtained from all drying models at a drying air velocity of V=1.8 m/s

T (˚C)	Model No.	*RMSE*	χ^2	*a*	*k*	*n*	*c*	*g*
38	1	0.0750	0.0060	-	0.0260	-	-	-
	2	0.0685	0.0053	1.0888	0.0280	-	-	-
	3	0.0685	0.0057	1.0888	0.0280	-	0	-
	4	0.0685	0.0061	1.0888	0.0280	-	0	0.0619
	5	0.0439	0.0022	1.9661	0.0386	-	-	-
	6	0.0405	0.0035	24.8758	0.0497	-	-	0.0516
	7	0.0340	0.0013	-	0.0033	1.5314	-	-
	8	0.0294	0.0011	0.9415	0.0016	1.7061	0	-
	9	0.0191	0.0005	0.8626	0.0005	1.9914	0.1374	1.1758
50	1	0.0598	0.0039	-	0.0389	-	-	-
	2	0.0573	0.0038	1.0586	0.0403	-	-	-
	3	0.0573	0.0042	1.0586	0.0403	-	0	-
	4	0.0573	0.0046	1.0586	0.0403	-	0	0.0618
	5	0.0315	0.0012	2.0876	0.0569	-	-	-
	6	0.0288	0.0014	33.5460	0.0735	-	-	0.0759
	7	0.0231	0.0006	-	0.0046	1.5756	-	-
	8	0.0228	0.0007	0.9845	0.0040	1.6102	0	-
	9	0.0082	0.0001	0.7426	0.0001	2.4968	0.2574	1.1758
65	1	0.0523	0.0027	-	0.0495	-	-	-
	2	0.0498	0.0026	1.0511	0.0514	-	-	-
	3	0.0498	0.0028	1.0511	0.0514	-	0	-
	4	0.0498	0.0031	1.0511	0.0514	-	0	0.0598
	5	0.0332	0.0012	1.9020	0.0689	-	-	-
	6	0.0307	0.0019	35.3623	0.0881	-	-	0.0902
	7	0.0272	0.0008	-	0.0103	1.4613	-	-
	8	0.0245	0.0007	0.9563	0.0064	1.5917	0	-
	9	0.0107	0.0002	0.8418	0.0014	2.0096	0.1581	1.1758
75	1	0.0630	0.0043	-	0.0543	-	-	-
	2	0.0591	0.0041	1.0633	0.0574	-	-	-
	3	0.0591	0.0045	1.0633	0.0574	-	0	-
	4	0.0591	0.0050	1.0633	0.0574	-	0	0.0600
	5	0.0381	0.0017	1.9062	0.0792	-	-	-
	6	0.0354	0.0020	33.2926	0.1013	-	-	0.1039
	7	0.0318	0.0012	-	0.0141	1.4334	-	-
	8	0.0296	0.0013	0.9567	0.0090	1.5616	0	-
	9	0.0143	0.0003	0.8201	0.0017	2.0320	0.1800	1.1758

(a)

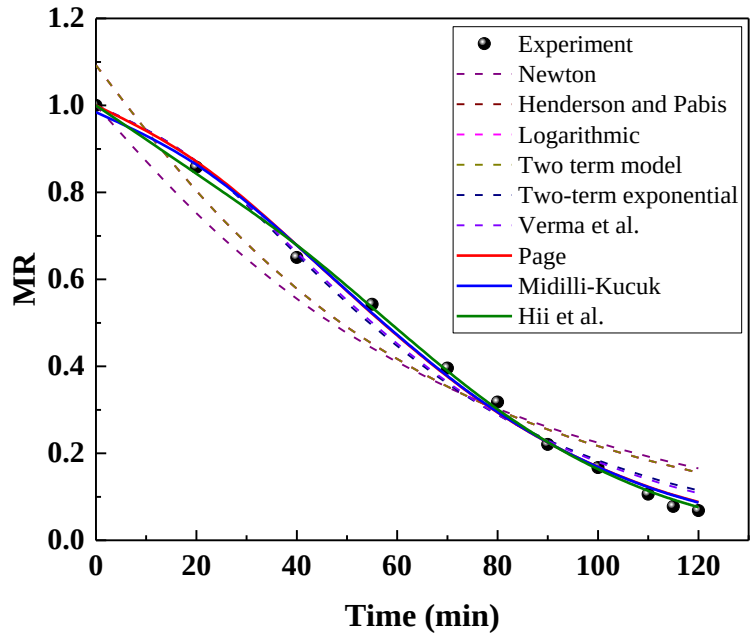
MR
Time (min)
Experiment
Newton
Henderson and Pabis
Logarithmic
Two term model
Two-term exponential
Verma et al.
Page
Midilli-Kucuk
Hii et al.

(b)

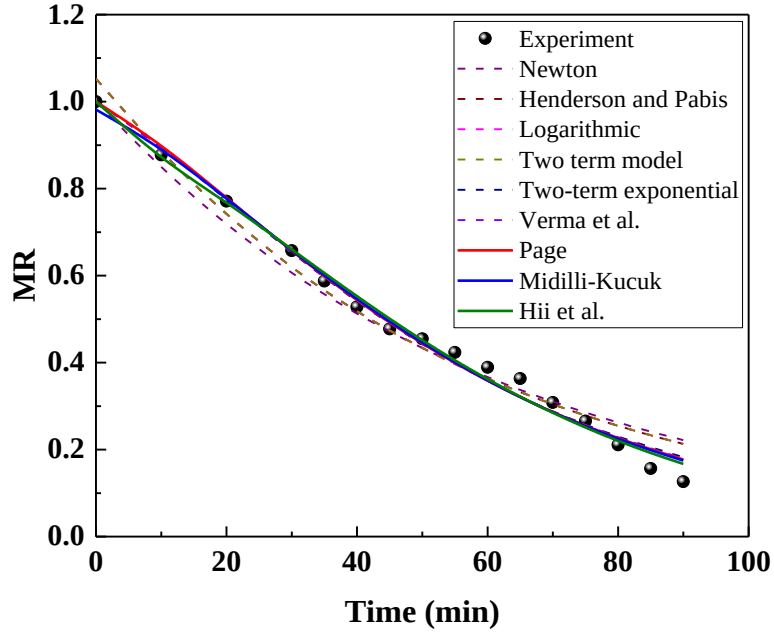
MR
Time (min)
Experiment
Newton
Henderson and Pabis
Logarithmic
Two term model
Two-term exponential
Verma et al.
Page
Midilli-Kucuk
Hii et al.

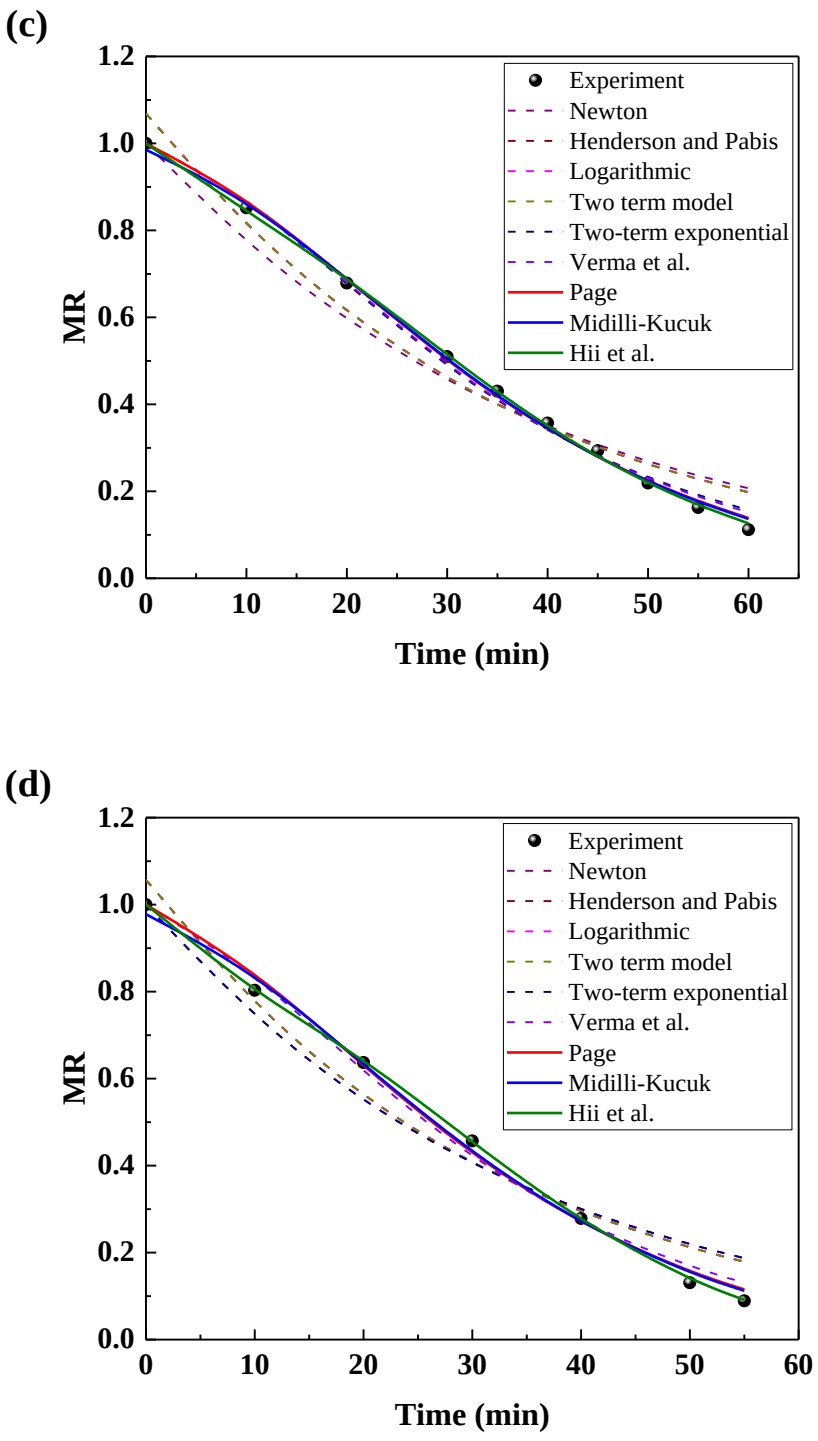

Figure A.1 Comparison between experimental drying data and model predicted data at a drying air velocity of 1.0 m/s: (a) *T*=38 ˚C, (b) *T*=50 ˚C, (c) *T*=65 ˚C, (d) *T*=75 ˚C

(a)

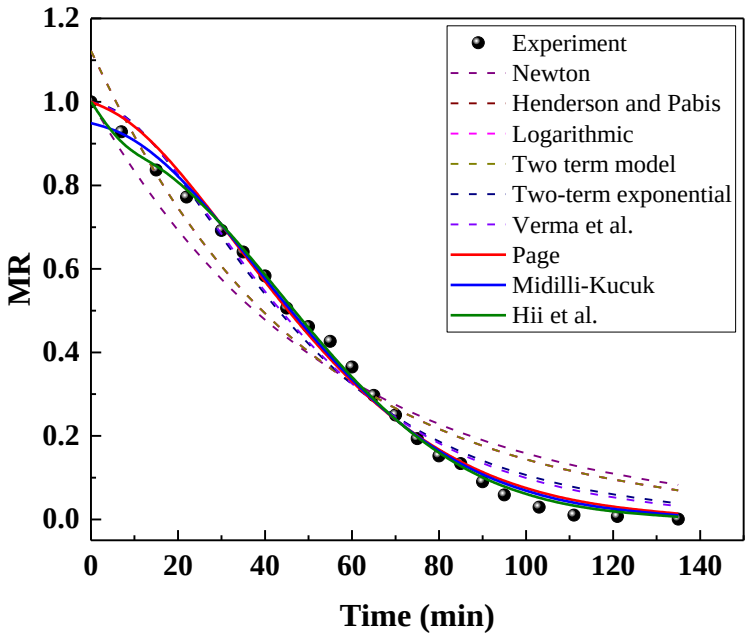
MR
Time (min)
Experiment
Newton
Henderson and Pabis
Logarithmic
Two term model
Two-term exponential
Verma et al.
Page
Midilli-Kucuk
Hii et al.

(b)

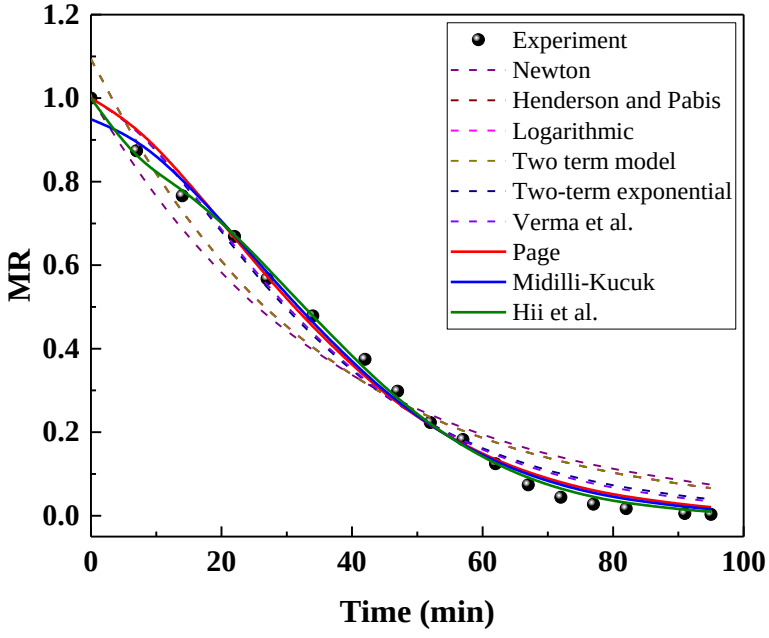
MR
Time (min)
Experiment
Newton
Henderson and Pabis
Logarithmic
Two term model
Two-term exponential
Verma et al.
Page
Midilli-Kucuk
Hii et al.

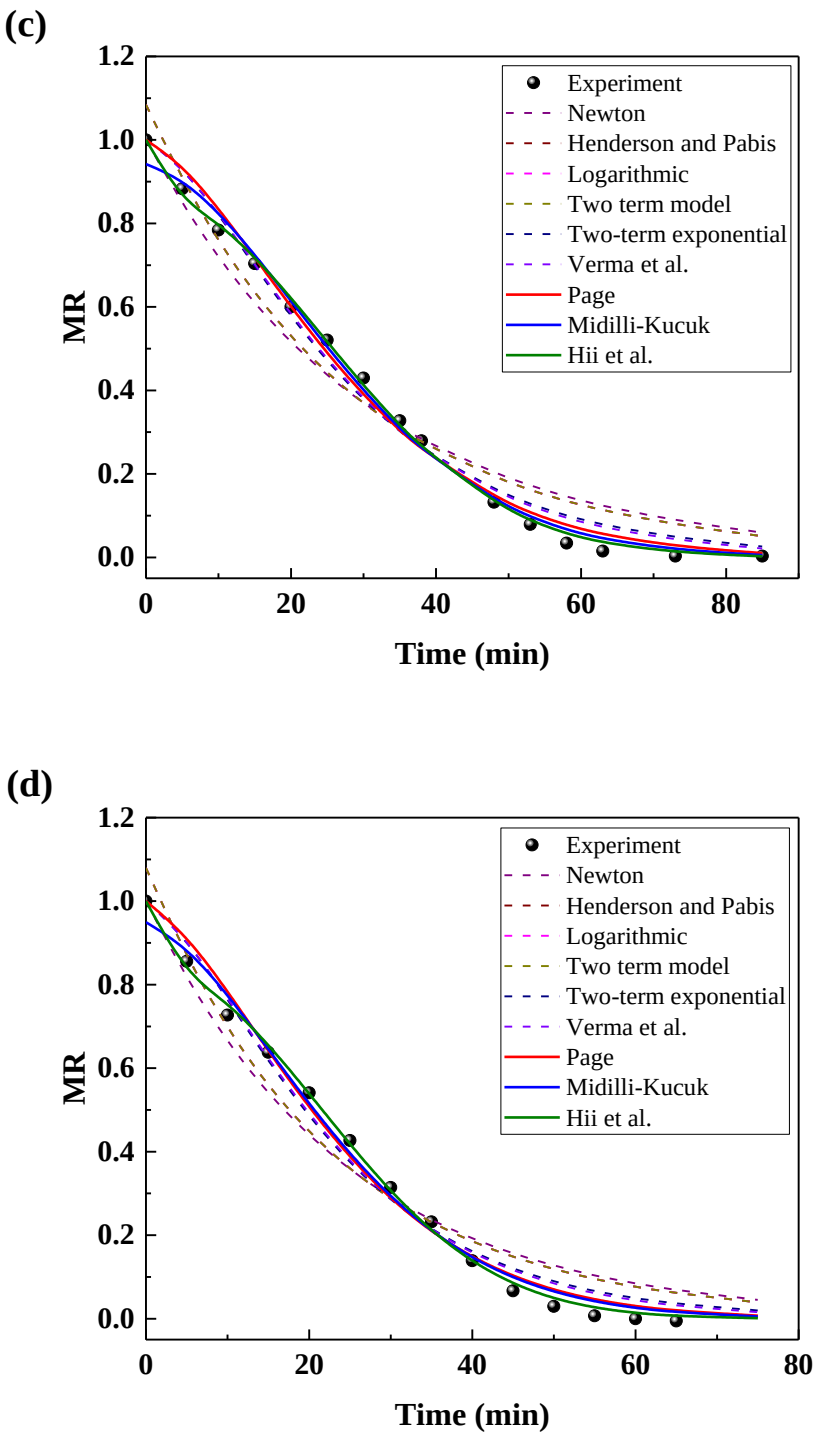

Figure A.2 Comparison between experimental drying data and model predicted data at a drying air velocity of 1.4 m/s: (a) *T*=38 ˚C, (b) *T*=50 ˚C, (c) *T*=65 ˚C, (d) *T*=75 ˚C

(a)

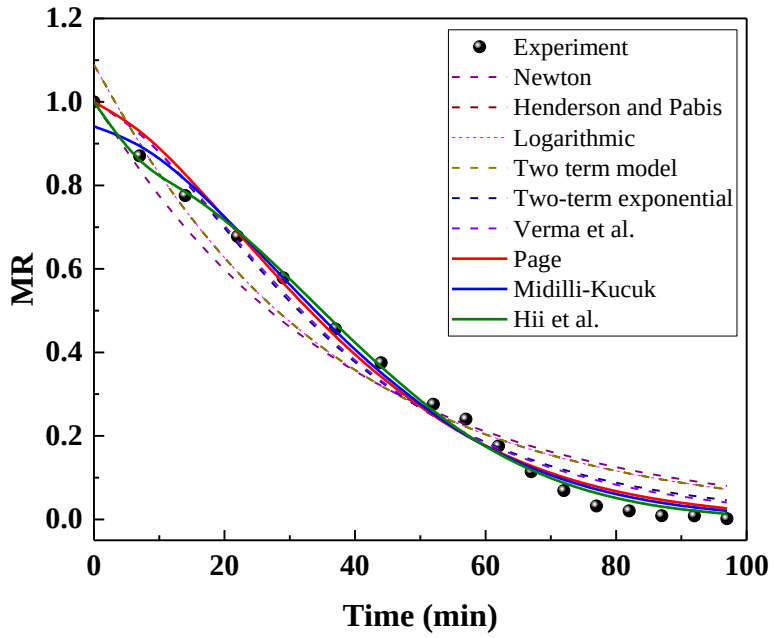
MR
Time (min)
Experiment
Newton
Henderson and Pabis
Logarithmic
Two term model
Two-term exponential
Verma et al.
Page
Midilli-Kucuk
Hii et al.

(b)

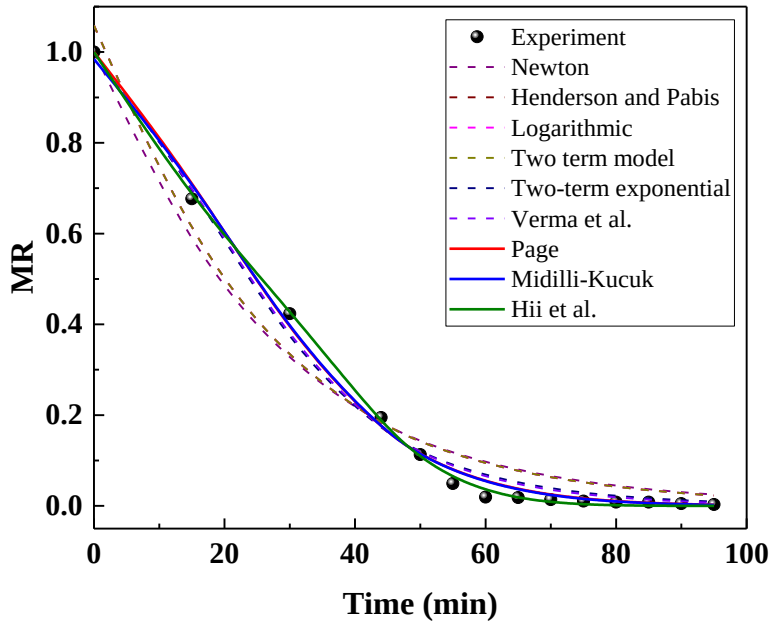
MR
Time (min)
Experiment
Newton
Henderson and Pabis
Logarithmic
Two term model
Two-term exponential
Verma et al.
Page
Midilli-Kucuk
Hii et al.

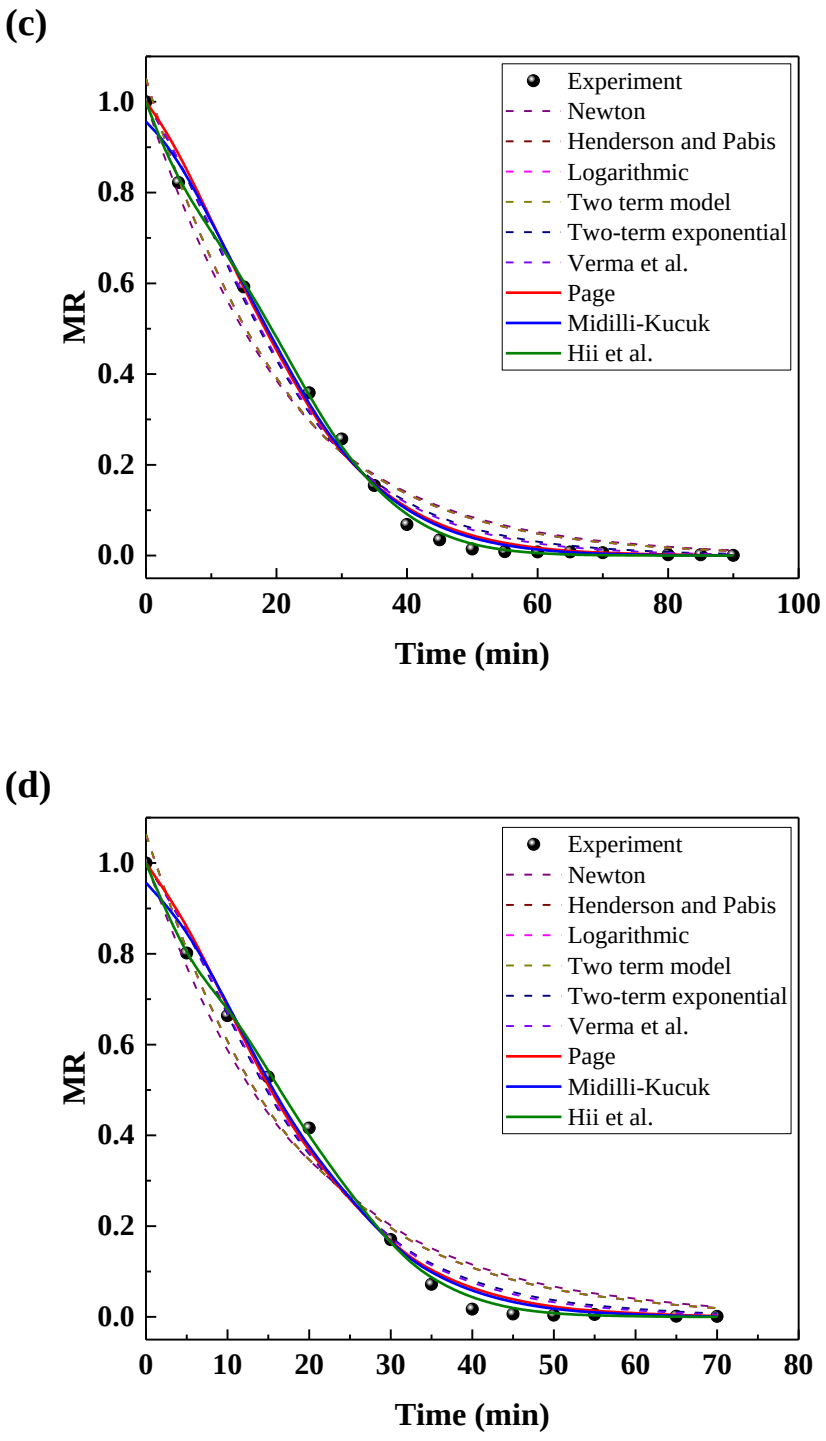

Figure A.3 Comparison between experimental drying data and model predicted data at a drying air velocity of 1.8 m/s: (a) *T*=38 ˚C, (b) *T*=50 ˚C, (c) *T*=65 ˚C, (d) *T*=75 ˚C

References

[1] C.L. Hii, C.L. Law, M. Cloke, Modeling using a new thin layer drying model and product quality of cocoa, J. Food Eng. 90 (2009) 191–198. doi:10.1016/j.jfoodeng.2008.06.022.

[2] D. Chen, Y. Zheng, X. Zhu, Determination of effective moisture diffusivity and drying kinetics for poplar sawdust by thermogravimetric analysis under isothermal condition., Bioresour. Technol. 107 (2012) 451–455. doi:10.1016/j.biortech.2011.12.032.

[3] A. Kaya, O. Aydin, C. Demirtas, M. Akgün, An experimental study on the drying kinetics of quince, Desalination. 212 (2007) 328–343. doi:10.1016/j.desal.2006.10.017.

[4] D.A. Tzempelikos, A.P. Vouros, A. V. Bardakas, A.E. Filios, D.P. Margaris, Case studies on the effect of the air drying conditions on the convective drying of quinces, Case Stud. Therm. Eng. 3 (2014) 79–85. doi:10.1016/j.csite.2014.05.001.

[5] S.M. Tasirin, I. Puspasari, A.W. Lun, P.V. Chai, W.T. Lee, Drying of kaffir lime leaves in a fluidized bed dryer with inert particles: Kinetics and quality determination, Ind. Crops Prod. 61 (2014) 193–201. doi:10.1016/j.indcrop.2014.07.004.

[6] N. Kumar, B.C. Sarkar, H.K. Sharma, Mathematical modelling of thin layer hot air drying of carrot pomace, J. Food Sci. Technol. 49 (2012) 33–41. doi:10.1007/s13197-011-0266-7.

[7] B.A. Fu, M.Q. Chen, Thin-layer drying kinetics of lignite during hot air forced convection, Chem. Eng. Res. Des. 102 (2015) 416–428. doi:10.1016/j.cherd.2015.07.019.

[8] Z. Erbay, F. Icier, A review of thin layer drying of foods: theory, modeling, and experimental results, Crit. Rev. Food Sci. Nutr. 50 (2010) 441–464. doi:10.1080/10408390802437063.

[9] A. Midilli, H. Kucuk, Z. Yapar, A new model for single-layer drying, Dry. Technol. 20 (2002) 1503–1513. doi:10.1081/DRT-120005864.